NTNU
Norwegian University of
Science and Technology

The Morphological Impact of the Proposed Gaza Seaport on the Coast of Gaza

Said Alhaddad

Coastal and Marine Engineering and Management
Submission date: July 2016
Supervisor: Raed Khalil Lubbad, BAT

Norwegian University of Science and Technology
Department of Civil and Transport Engineering

ERASMUS +: ERASMUS MUNDUS MOBILITY PROGRAMME

Master of Science in

COASTAL AND MARINE ENGINEERING AND MANAGEMENT

CoMEM

THE MORPHOLOGICAL IMPACT OF THE PROPOSED GAZA SEAPORT ON THE COAST OF GAZA

Norwegian University of Science and Technology
8 July 2016

Said Alhaddad

The Erasmus+: Erasmus Mundus MSc in Coastal and Marine Engineering and Management is an integrated programme including mobility organized by five European partner institutions, coordinated by Norwegian University of Science and Technology (NTNU).

The joint study programme of 120 ECTS credits (two years full-time) has been obtained at two or three of the five CoMEM partner institutions:

- Norges Teknisk- Naturvitenskapelige Universitet (NTNU) Trondheim, Norway
- Technische Universiteit (TU) Delft, The Netherlands
- Universitat Politècnica de Catalunya (UPC). BarcelonaTech. Barcelona, Spain
- University of Southampton, Southampton, Great Britain
- City University London, London, Great Britain

During the first three semesters of the programme, students study at two or three different universities depending on their track of study. In the fourth and final semester an MSc project and thesis has to be completed. The two-year CoMEM programme leads to a multiple set of officially recognized MSc diploma certificates. These will be issued by the universities that have been attended by the student. The transcripts issued with the MSc Diploma Certificate of each university include grades/marks and credits for each subject.

Information regarding the CoMEM programme can be obtained from the programme coordinator:

Øivind A. Arntsen, Dr.ing.
Associate professor in Marine Civil Engineering
Department of Civil and Transport Engineering
NTNU Norway
Telephone: +4773594625 Cell: +4792650455 Fax: + 4773597021
Email: oivind.arntsen@ntnu.no

CoMEM URL: https://www.ntnu.edu/studies/mscomem

CoMEM Thesis

This thesis was completed by:
Said Alhaddad

Under supervision of:
Prof. Raed Lubbad

As a requirement to attend the degree of
Erasmus+: Erasmus Mundus Master in Coastal and Marine Engineering and Management (CoMEM)

Taught at the following educational institutions:

Norges Teknisk- Naturvitenskapelige Universitet (NTNU)
Trondheim, Norway

Technische Universiteit (TU) Delft
Delft, The Netherlands

At which the student has studied from August 2014 to July 2016.

NORWEGIAN UNIVERSITY OF SCIENCE AND TECHNOLOGY
DEPARTMENT OF CIVIL AND TRANSPORT ENGINEERING

Report Title: The Morphological Impact of the Proposed Gaza Seaport on the coast of Gaza	Date:08/07/2016 Number of pages (incl. appendices):102			
	Master Thesis	X	Project Work	
Name: Said Alhaddad				
Professor in charge/supervisor: Prof. Raed Lubbad				
Other external professional contacts/supervisors:				

Abstract:

Hard engineering works in the coastal zone usually result in adverse impacts on the coastal system, especially on the morphology. When new structures are constructed, longshore sediment transport becomes an issue. The structures interfere with the natural longshore movement of sediments, leading to coastal erosion and accretion, which changes the shape of the coastline. Consequently, maritime structures need to be adequately planned in order to mitigate adverse impacts on coastal morphology. In addition, thorough insight into the morphological change resulting from such interventions on the coast is necessary to enable adequate planning. This study aims to predict the effect of the proposed Gaza Seaport on the morphology of the coast of Gaza. The effect of the Seaport on the morphology shall be investigated with the incorporation of the numerical models, MIKE 21 and LITPACK, developed by DHI.

MIKE 21 is a two-dimensional mathematical modelling system with a wide range of coastal engineering applications. It is used mainly in this study to model flow, waves, sediment transport and morphological change in the vicinity of the seaport. LITPACK is a one-dimensional coastal processes modelling system. It is used mainly in this study to compute littoral sediment transport and predict coastline changes after the construction of the seaport. Results from MIKE 21 ST show that accumulation of sand will take place inside the seaport basin, in the seaport navigation channel and in the sheltered area ahead of the breakwater. In addition, erosion will take place downdrift of the seaport and scour will take place at the tip of the breakwater. Results from LITPACK can be summarized in three points:

-The coastline shape will change considerably in the vicinity of the seaport.

-Accretion will take place updrift of the seaport and erosion will take place downdrift of the seaport which is in agreement with the results obtained from MIKE 21 ST.

-The shadow length of the breakwater is large enough to block the total amount of littoral sediment transport, 1.23×10^6 m^3/year.

The findings of this study provide some implications for the future development of the seaport. Mitigation measures are needed to maintain the existing beach alignment, prior to the seaport construction. One solution could be beach nourishment and/or a sand bypass system, which would transfer accumulated sand updrift of the seaport to the affected areas in the downdrift side. It should be kept in mind that any solution should take into consideration several stakeholder groups that will be affected by the anticipated situation along the coast. The predicted process of sediment transport in the vicinity of the seaport necessitates dredging the seaport navigation channel in the future to maintain its navigable depth. In addition, the breakwater designer should incorporate scour protection into the design to keep the breakwater stable.

Absence of sufficient field data has resulted in this study making several assumptions and performing a sensitivity analysis of longshore sediment transport at the site of interest. The basic concept behind the sensitivity analysis is to provide a starting point for further research that can be continued based on the results obtained in this study. The sensitivity analysis shows that bed roughness is significantly crucial in the calculation of longshore sediment transport. Results show that increased bed roughness results in less longshore sediment transport. However, increased wave height and increased wave period result in more longshore sediment transport.

Keywords:

1. CoMEM
2. Gaza Seaport
3. MIKE 21
4. LITPACK

MASTER THESIS

(TBA4920 Marine Civil Engineering, master thesis)

Spring 2016
for
Said Alhaddad

The Morphological Impact of the Proposed Gaza Seaport on the Coast of Gaza

BACKGROUND

Gaza Strip is an enclave in Palestine, situated on the eastern coast of the Mediterranean Sea. Gaza Strip is one of the most densely populated regions in the world, with 1.8 million people within 365 km2 (BBC, 2014).

Maritime transport is of significant importance for a country's economic and trade success, however currently this mode is not available in Palestine. This lack of maritime transport is due to persistent Israeli occupation. There has been action to improve maritime transport in Gaza Strip, such as a project planned during the 1990s, a European consortium headed by Dutch construction firm (Ballast Nedam) was hired to construct a seaport in the south of Gaza City. In 1996, the design of Gaza seaport was completed by ARCADIS Company. In the summer of 2000, construction of the seaport commenced and by September 2001 it was bombed by Israel. The seaport was destroyed and since then there has been no reconstructed efforts. However, a strong desire to reconstruct the seaport is present amongst Palestinians.

Gaza has a sandy coast, these types of coasts are subject to the dynamics of sediments transport. These types of sediments are largely supplied by rivers or valleys (alluvial sediment), which are then transported alongshore and cross shore by waves, winds and tides. The wave-induced sediment transport induces changes in beach morphology due to cross-shore and longshore sediment transport. Construction of seaports and other maritime engineering works often has adverse impacts on the coastal system and the proposed Gaza Seaport is not an exception. Coastal areas are under great pressure from human activates and developers. Therefore, in order to develop a coastline with minimal possible environmental consequences, it is crucial that the finalized design takes into consideration sound science and research.

Prediction of beach morphological changes is essential for various coastal engineering projects and appropriate management of the coastal zone. Recently, with the development of powerful computers, numerical models are increasingly being utilized to simulate the processes of nature. Numerical modelling provides an opportunity to view and analyze coastal problems and risks. It also has capabilities for sensitivity analysis as there is a possibility to change the input parameters in the model and observe the response.

TASK DESCRIPTION

Description of task

In this study, numerical models, MIKE 21 and LITPACK, will be used to study the morphological impact of the proposed Gaza Seaport on the coast of Gaza. In order to do so, near shore wave climate, tide, wind and bathymetric data should be obtained. MIKE21 will be applied to model flow, waves, sediment transport and morphological change in the vicinity of the seaport. LITPACK will be applied to predict the shoreline evolution for the proposed seaport.

Aims and purpose

Gathering the required data and boundary conditions is a challenging task due to the lack of field measuring tools in Gaza Strip which resulted because of the ongoing Israeli siege. Therefore, gathering the collected data will be the first step. This data could be used in the future for other purposes. In the next stage, the obtained data and boundary conditions will be used as the input in the modelling software to assess the morphological impact of constructing the seaport.

Subtasks and research questions

The subtasks of this research are as follows.

- Review available literature on coastal hydrodynamics and sediment transport modelling.
- Setup a numerical model to simulate the morphological impact of the proposed Gaza seaport on the coast of Gaza.
- Describe the theoretical background for the numerical model used in this thesis.
- Collect available input data from the physical environment of Gaza seaport, e.g. bathymetry, wind, waves, current.
- Calibrate, fine tune and verify the numerical model.
- Run the simulation and discuss the results.
- Conclude, summarise and provide recommendations for future work.

This research aims to answer the following questions:

- What are the processes that should be considered to obtain the results?
- Based on the simulated sediment transports, where it is expected to have a coastline erosion/accretion?
- What is the coastline evolution in the years following the construction of the seaport?
- Will the construction of the proposed seaport cause serious morphological problems on the coastal zone?

General about content, work and presentation
The text for the master thesis is meant as a framework for the work of the candidate. Adjustments might be done as the work progresses. Tentative changes must be done in cooperation and agreement with the professor in charge at the Department.

In the evaluation thoroughness in the work will be emphasized, as will be documentation of independence in assessments and conclusions. Furthermore the presentation (report) should be well organized and edited; providing clear, precise and orderly descriptions without being unnecessary voluminous.

The report shall include:

- Standard report front page (from DAIM, http://daim.idi.ntnu.no/)
- Title page with abstract and keywords.(template on: http://www.ntnu.no/bat/skjemabank) CoMEM students must include CoMEM as one of the keywords.
- CoMEM page (Only CoMEM students)
- Preface
- Summary and acknowledgement. The summary shall include the objectives of the work, explain how the work has been conducted, present the main results achieved and give the main conclusions of the work.
- Table of content including list of figures, tables, enclosures and appendices.
- A list explaining important terms and abbreviations should be included.
- List of symbols should be included
- The main text.
- Clear and complete references to material used, both in text and figures/tables. This also applies for personal and/or oral communication and information.
- Thesis task description (these pages) signed by professor in charge as Attachment 1.
- The report musts have a complete page numbering.

The thesis can as an alternative be made as a scientific article for international publication, when this is agreed upon by the Professor in charge. Such a report will include the main points as given above, but where the main text includes both the scientific article and a process report.

Submission procedure
Procedures relating to the submission of the thesis are described in IVT faculty webpage
http://www.ntnu.edu/ivt/master-s-thesis-regulations

On submission of the thesis the candidate shall submit to the professor in charge a CD/DVD('s) or a link to a net-cloud including the report in digital form as pdf and Word (or other editable form) versions and the underlying material (such as data collection, time series etc.).

Documentation collected during the work, with support from the Department, shall be handed in to the Department together with the report.

According to the current laws and regulations at NTNU, the report is the property of NTNU. The report and associated results can only be used following approval from NTNU (and external cooperation partner if applicable). The Department has the right to make use of the results from the work as if conducted by a Department employee, as long as other arrangements are not agreed upon beforehand.

Start and submission deadlines
The work on the Master Thesis starts on (date) 12th February 2016

The thesis report as described above shall be submitted digitally in DAIM at the latest (date:) 8th July 2016 at 11:59 pm.

Professor in charge: Raed Lubbad

Other supervisors: _____

Trondheim, July 8th, 2016.

_____
Professor in charge (sign)

إلى أمـي وأبـي الحبيبين

To my beloved mother and father

Acknowledgements

First and above all, I would like to thank Allah, the almighty, for granting me opportunity, determination and strength to do my research and for blessing me with great people who have been my support in my personal and professional life.

I would like to express my sincere gratitude to my supervisor, Prof. Raed Lubbad for his encouragement, guidance, academic support, valuable suggestions and insightful comments on my work. My special thanks go to Mr. Mohammad Saud Afzal to support me with his encouragement, meaningful discussions, invaluable advice and rich ideas and to assist me in many different ways during my MSc study. A special acknowledgement is necessary for Prof. Mazen Abualtayef for his guidance and motivation and for providing me with the available data in Gaza to run my simulations.

My deep appreciation goes to the European Union for funding me throughout my MSc study. I am grateful to the secretary Mrs Sonja Marie Ekrann Hammer, for assisting me in many different ways during my MSc study and for her support in administrative issues related to my MSc program. I also would like to thank my friends for their encouragement and sentimental support especially Maysara, Nadir, Ershad, Ayman and Mohammed.

I owe everything to my lovely parents, Abeer and Mousa, who encouraged and helped me at every step of my personal and academic life and longed to see this achievement comes true. My heartfelt gratitude is due to my loving brothers and sisters, for their endless encouragement and well wishes.

I wish to express my deep appreciation to all the members of NTNU and TU-Delft who taught me during my MSc study. Last but not least, I would like to thank all my CoMEM colleagues especially Stuart Pearson, for their support throughout the program.

Said Mousa Alhaddad

Trondheim, July 2, 2016

Abstract

Palestinians in Gaza Strip are in dire need of a commercial seaport to connect Palestine to the World, to enhance the economy and local industry. In 1996, the design of Gaza Seaport was completed, planned to be constructed in the south of the coastal village Elsheikh Ejleen. However, no construction took place to this day due to political issues between Palestine and Israel.

Hard engineering works in the coastal zone usually result in adverse impacts on the coastal system, especially on the morphology. When new structures are constructed, longshore sediment transport becomes an issue. The structures interfere with the natural longshore movement of sediments, leading to coastal erosion and accretion, which changes the shape of the coastline. Consequently, maritime structures need to be adequately planned in order to mitigate adverse impacts on coastal morphology. In addition, thorough insight into the morphological change resulting from such interventions on the coast is necessary to enable adequate planning. This study aims to predict the effect of the proposed Gaza Seaport on the morphology of the coast of Gaza. The effect of the Seaport on the morphology shall be investigated with the incorporation of the numerical models, MIKE 21 and LITPACK, developed by DHI.

MIKE 21 is a two-dimensional mathematical modelling system with a wide range of coastal engineering applications. It is used mainly in this study to model flow, waves, sediment transport and morphological change in the vicinity of the seaport. LITPACK is a one-dimensional coastal processes modelling system. It is used mainly in this study to compute littoral sediment transport and predict coastline changes after the construction of the seaport. Results from MIKE 21 ST show that accumulation of sand will take place inside the seaport basin, in the seaport navigation channel and in the sheltered area ahead of the breakwater. In addition, erosion will take place downdrift of the seaport and scour will take place at the tip of the breakwater. Results from LITPACK can be summarized in three points:

- The coastline shape will change considerably in the vicinity of the seaport.
- Accretion will take place updrift of the seaport and erosion will take place downdrift of the seaport which is in agreement with the results obtained from MIKE 21 ST.

- The shadow length of the breakwater is large enough to block the total amount of littoral sediment transport, 1.23×10^6 m^3/year.

The findings of this study provide some implications for the future development of the seaport. Mitigation measures are needed to maintain the existing beach alignment, prior to the seaport construction. One solution could be beach nourishment and/or a sand bypass system, which would transfer accumulated sand updrift of the seaport to the affected areas in the downdrift side. It should be kept in mind that any solution should take into consideration several stakeholder groups that will be affected by the anticipated situation along the coast. The predicted process of sediment transport in the vicinity of the seaport necessitates dredging the seaport navigation channel in the future to maintain its navigable depth. In addition, the breakwater designer should incorporate scour protection into the design to keep the breakwater stable.

Coastal field measurements are very rare in Gaza Strip due to the poor political situation. Absence of sufficient field data has resulted in this study making several assumptions and performing a sensitivity analysis of longshore sediment transport at the site of interest. The basic concept behind the sensitivity analysis is to provide a starting point for further research that can be continued based on the results obtained in this study. The sensitivity analysis shows that bed roughness is significantly crucial in the calculation of longshore sediment transport and can be considered as the basic calibration parameter in LITDRIFT. Results show that increased bed roughness results in less longshore sediment transport. However, increased wave height and increased wave period result in more longshore sediment transport.

Table of Contents

List of Figures

List of Tables

1 Introduction

1.1 Background

Gaza Strip is an enclave in Palestine, situated on the eastern coast of the Mediterranean Sea. Gaza Strip is one of the most densely populated regions in the world, with 1.8 million people within 365 km^2 (BBC, 2014).

Maritime transport is of significant importance for a country's economic and trade success, however currently this mode is not available in Palestine. This lack of maritime transport is due to persistent Israeli occupation. There has been action to improve maritime transport in Gaza Strip, such as a project planned during the 1990s, a European consortium headed by Dutch construction firm (Ballast Nedam) was hired to construct a seaport in the south of Gaza City. In 1996, the design of Gaza seaport was completed by ARCADIS Company. In the summer of 2000, construction of the seaport commenced and by September 2001 it was bombed by Israel. The seaport was destroyed and since then there has been no reconstructed efforts. However, a strong desire to reconstruct the seaport is present amongst Palestinians.

Gaza has a sandy coast, these types of coasts are subject to the dynamics of sediments transport. These types of sediments are largely supplied by rivers or valleys (alluvial sediment), which are then transported alongshore and cross shore by waves, winds and tides. The wave-induced sediment transport induces changes in beach morphology due to cross-shore and longshore sediment transport. Construction of seaports and other maritime engineering works often has adverse impacts on the coastal system and the proposed Gaza Seaport is not an exception. Coastal areas are under great pressure from human activates and developers. Therefore, in order to develop a coastline with minimal possible environmental consequences, it is crucial that the finalized design takes into consideration sound science and research.

Prediction of beach morphological changes is essential for various coastal engineering projects and appropriate management of the coastal zone. Recently, with the development of powerful computers, numerical models are increasingly being utilized to simulate the processes of nature. Numerical modelling provides an opportunity to view and analyze coastal problems and risks. It also has capabilities for sensitivity analysis as there is a possibility to change the input parameters

in the model and observe the response. In this study, numerical modelling is used to study the morphological impact of the proposed Gaza Seaport on the coast of Gaza.

For this study, the two software types applied are MIKE 21 and LITPACK. MIKE 21 is professional modelling software for two-dimensional free surface flows. MIKE 21 is in a modular form with four main application areas: coastal hydraulics and oceanography, waves, sediment processes and environmental hydraulics. LITPACK is a one-dimensional coastal processes modelling system that is mainly used for the computation of sediment transport and associated beach profile and coastline changes.

Modelling and detailed analysis of waves, sediment transport and morphological conditions in the coastal waters in the vicinity of Gaza Seaport have been completed. MIKE 21 is mainly used to study the tendency of sediment transport in the vicinity of the sea port and bed level changes. LITPACK modelling is undertaken to predict coastline evolution during the years following seaport construction.

1.2 Thesis Structure

This report is divided into seven chapters. Chapter 2 discusses the important coastal processes with emphasis on their formulations and numerical modelling. The area selected for study, Gaza Strip, is described in Chapter 3 with focus on the proposed Gaza Seaport. Chapter 4 describes the numerical models used in this study, MIKE 21 and LITPACK.

Chapter 5 firstly outlines the data available for the area of interest with a brief discussion on the source and reliability of data. Then, it discusses the model setups for the simulations conducted during this study. The results obtained from each model run during the study are presented and discussed in Chapter 6. Finally, Chapter 7 draws the important conclusions from this work and presents the limitations of the current study with some recommendations for further work in the future.

2 Coastal Morphodynamics

Coastal morphodynamics is defined as “the mutual adjustment of topography and fluid dynamics involving sediment transport” (Wright and Thom, 1977). It is dependent on the interaction of multiple variables, such as fluid dynamics, sediment characteristics and human interventions. Fluid dynamics drive sediment transport resulting in morphological change over time. This morphological change alters boundary conditions for the fluid dynamics, which results in changes in sediment transport patterns. Human interventions usually lead to morphological problems like erosion. Therefore, good thorough should be gained into the morphological change resulting from new hard structure on the coast.

There are many formulations to describe the complex processes in the coastal zone. This chapter introduces these formulations of hydrodynamics and sediment transport with more focus on their application in numerical models. One should keep in mind that most of these formulations were obtained empirically based on experiments and laboratory results. This means that they have considerable inaccuracy and one should calibrate and validate the results of the models for each site.

2.1 Coastal Hydrodynamics

The dynamic processes in the nearshore zone are driven by external forces, e.g. gravitational force of the moon and sun and wind. Under the influence of these external forces, the fluid motion appears as coastal currents, tides and tidal currents, internal and surface waves, storm surges, tsunamis and others (Horikawa, 1988). Coastal hydrodynamics concerns with wave propagation, transformation and dissipation, wave-induced water level changes and longshore and cross-shore currents due to wave, wind and tidal actions.

The waves transform when they propagate from deep to shallow water depths. Wave transformation means that wave characteristics, wave height, wave length and wave direction, change until the waves break and lose their energy. In order to model waves approaching the shoreline, various transformations have to be taken into account, such as refraction, shoaling and wave breaking. There are various software packages that translate offshore wave conditions toward the nearshore, such as MIKE, SWAN, HISWA and WAMTECH. Using these numerical models require input data, such as wave height, wave period and wind speed and direction. An overview of the method used to analyze the input data is described in the next section.

2.1.1 Spectral Analysis

Spectral Analysis is a widely used statistical method for data analysis in engineering. There are different methods to determine the spectral density function from a discrete time record. The Fast Fourier Transform (FFT), which is an algorithm for calculating the Discrete Fourier Transform (DFT), is the most widely used one.

The surface elevation at one location can be unraveled into a number of sine waves with different frequencies. The amplitude and phases of these waves can be determined by Fourier analysis. According to Fourier any signal can be represented by a sum of harmonic components which is called Fourier-series. Assuming a stationary record, these sine waves have a constant amplitude and phase per component in time. The Fourier series can be written in terms of sine or cosine functions for a time-record with specific duration (Bosboom & Stive, 2015). The surface elevation can be written as a Fourier series as follows:

$$\eta = \sum_{n=1}^{N} a_n \cos(2\pi f_n t + \alpha_n) \qquad (1)$$

where η is the surface elevation, $f_n = \frac{n}{T_r}$ for n = 1,2,3..., a is the wave amplitude, t is the time, T_r is the record duration and α is the phase.

Wave energy spectrum represents the distribution of waves in frequency domain. It makes understanding the characteristics of the sea state much easier. The narrower the spectrum the more regular the waves are. In the case of large long waves, the spectrum will be shifted towards the lower frequencies and contain more energy. On the other hand, the spectrum will be shifted towards the higher frequencies and be lower in the case of small short waves. Figure 2.1 shows energy spectra for sea with the corresponding time series.

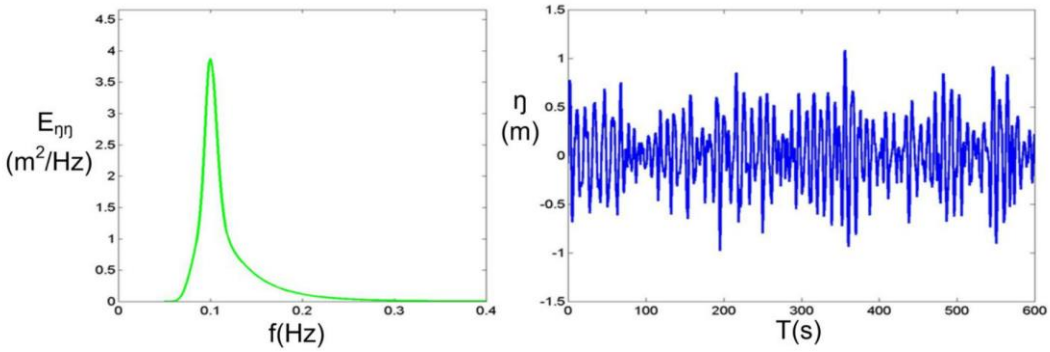

Figure 2.1: Surface elevation time series (right) and the corresponding spectra (left) (Source: Bosboom & Stive, 2015)

Wave energy at a point has an angular distribution and a distribution over a range of frequencies. The angular distribution of wave energy is called "directional spreading". Spectral representations which include both the frequency distribution and the angular spreading of wave energy are known as "directional spectra". Knowing the evolution of directional spectra in shallow water is very important in coastal engineering since it leads to accurate wave predictions.

Assuming the random surface is represented by a normal distribution, various essential characteristics of seas state can be determined from the spectrum. The zeroth moment, for instance, is determined by calculating the area under the spectrum. This parameter can be used with the second moment to determine the zero-crossing period from the spectrum, see Holthuijsen (2007).

2.1.2 Energy Balance

Applying the law of energy conservation gives information on the transformation of waves approaching the shoreline, such as the change in wave height (*H*), wave length (*L*), celerity (*c*), and wave direction (*θ)*. Therefore, the energy balance is solved numerically by the model.

The total energy of a wave propagating across a wave field can be represented as:

$$E = \frac{1}{8}\rho g H_{rms}^2 \tag{2}$$

where *E* is the wave energy, ρ is the density of the fluid and H_{rms} is the root mean square wave height.

Energy is not conserved in the case of current presence since energy transfer between currents and waves takes place. However, energy is conserved in the absence of current. Energy conservation equation reads as (Holthuijsen, 2007):

$$\frac{\partial E}{\partial t} + \frac{\partial}{\partial x}(E c_g \cos\theta)\frac{\partial}{\partial y}(E c_g \sin\theta) = S - D \tag{3}$$

where θ represents the wave direction with respect to X-axis which is aligned normal to the shoreline, S is the generation source term, D is the dissipation term and c_g is the wave group celerity.

The energy generation term, S represents the superposition of source functions describing various physical phenomena such as the generation of energy by wind. The energy dissipation term, D

represents the dissipative processes, such as the dissipation of wave energy due to white capping, the dissipation of energy due to bottom friction and the dissipation of wave energy due to depth-induced breaking.

Usually currents are present in the oceans and should be taken into consideration in the model. The energy transfer between the waves and the currents is not easily determined. Additional terms to the energy balance equation are needed to represent the effect of work done by the current against the radiation stresses. However, a simpler approach is to consider the action balance of the waves instead of energy balance. In the presence of currents a wave quantity called wave action is conserved. Wave action density (N) reads as:

$$N = \frac{E}{\sigma_r} \tag{4}$$

where E is the energy density and σ_r is the relative angular frequency ($\sigma_r = 2\pi f_r$).

Wave action balance equation reads as:

$$\frac{\partial N}{\partial t} + \nabla.(\vec{v}N) = \frac{S}{\sigma} \tag{5}$$

where N (x, σ, θ, t) is the action density, t is the time, $\vec{v}$ = (c_x, c_y, c_σ, c_θ) is propagation velocity of a wave group in four dimensional phase space and ∇ is the four dimensional differential operator (Komen et al. 1994).

2.1.3 Wave Transformation

Many theories have been developed in order to describe wave transformation processes and thus to improve the capabilities of wave models. The most important processes affecting nearshore wave transformations are described in this section.

The change of water depth plays an important role in wave transformations. When ocean waves enter coastal waters, their amplitude and direction will be affected by the limited water depth. The waves start to feel the bottom and slowdown in shallow water (water depth is less than about half the wave length). The phenomenon of wave height increase near the coast, due to the variations in the wave group velocity in the propagation direction, is called shoaling. The phenomenon of the change of wave direction due to depth-induced variations in the phase speed along the wave crest is called refraction. This makes obliquely incident wave to bend toward normal incidence.

Wave breaking takes place when waves propagate into very shallow areas, and the wave height can no longer be supported by the water depth. The waves start breaking when the particle velocity exceeds the velocity of the wave crest. Miche (1994) expressed the limiting wave steepness based on Stokes wave theory:

$$\left(\frac{H}{L}\right)_{max} = 0.142 \tanh(kh) \quad (6)$$

where *H/L* is wave steepness, *k* is the wave number and *h* is the water depth.

In deep water the previous equation reduces to:

$$\left(\frac{H}{L}\right)_{max} = 0.142 \approx \frac{1}{7} \quad (7)$$

This is the maximum possible steepness for an individual wave. White capping occurs when the deep water steepness exceeds this limit. The mathematical development of a white capping model can be traced to Hasselmann (1974). These days, the model proposed by Komen et al. (1994) is usually preferred as it includes the adjustment for the dissipation source function (Janssen et al. 1989) in order to obtain a proper balance between wind input and dissipation at higher frequencies.

Depth-induced breaking dissipates most of the wave energy. It occurs when the wave height becomes greater than a certain fraction of the water depth. Most of formulations suggest a breaker index which has different values based on calibrations and experiments. Laboratory and field data have also shown that the breaker index varies significantly depending on the wave conditions and the bathymetry. Based on solitary wave theory the breaker index has approximately a value of 0.78 ($\gamma = H_b/h_b$), where γ is the breaker index, H_b is the breaking wave height and h_b is the water depth at the breaking point. Kaminsky and Kraus (1993) found that breaker index is in the range between 0.6 and 1.59 with an average of 0.79. Recently, Ruessink et al. (2003) have presented a new empirical form for γ, where γ is determined as a function of the product of the local wave number *k* and the water depth *d*.

$$\gamma = 0.76kd + 0.29 \quad (8)$$

Bottom friction is an important parameter in the modelling of wave transformations. There are different mechanisms for wave energy dissipation at the bottom, such as energy dissipation through percolation, friction, motion of a soft muddy bottom and bottom scattering. The energy

dissipation by bottom friction has been a subject of investigation and different theories have been formulated to model it. Nowadays, models have an option to determine the formulation to calibrate the model by bottom friction parameters depending on grain size diameter.

2.1.4 Wave-induced Set-up and Currents

Propagating waves across the ocean transfer energy as well as momentum which points in the direction of wave propagation. Momentum transfer is equivalent to a stress and horizontal variations in this stress work as forces on the water and may thus tilt the mean sea level or generate currents. Wave momentum is the product of the mass and the wave-induced velocity of the water particles. It can also be interpreted as a net flux of mass between wave trough and wave crest associates with wave propagation (Holthuijsen, 2007).

Radiation stress is defined as the depth-integrated and wave-averaged flow of momentum due to waves. Longuet-Higgins and Stewart (1964) defined it as the excess momentum flux due to presence of waves. When there is a change in radiation stress from one position to another, wave forces will act on the fluid. These forces affect mean water motion and levels. Radiation stresses are responsible for set-down, set-up and driving a longshore current in the nearshore zone in the case of obliquely incident waves.

Wave-induced set-up is the increase in mean water level above the still water level due to momentum transfer to the water column by waves that are breaking and dissipating their energy. On the other hand, wave-induced set-down is the decrease in mean water level below the still water level to balance the excess momentum flux, see Figure 2.2.

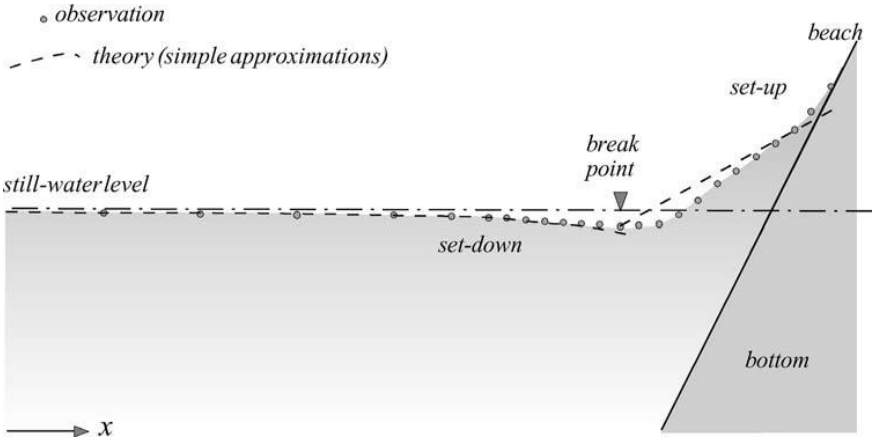

Figure 2.2: The set-down and set-up induced by waves approaching a very steep beach (Source: Holthuijsen, 2007)

Time and wave averaged equations of the radiation stresses read as follows:

$$S_{xx} = \overline{\int_{-h_0}^{\eta} (\rho u_x) u_x dz} + \overline{\int_{-h_0}^{\eta} p_{wave} dz} \tag{9}$$

$$S_{yy} = \overline{\int_{-h_0}^{\eta} (\rho u_y) u_y dz} + \overline{\int_{-h_0}^{\eta} p_{wave} dz} \tag{10}$$

$$S_{xy} = \overline{\int_{-h_0}^{\eta} (\rho u_x) u_y + \tau_{xy} dz} = \overline{\int_{-h_0}^{\eta} (\rho u_x) u_y dz} \tag{11}$$

$$S_{yx} = \overline{\int_{-h_0}^{\eta} (\rho u_y) u_x dz} \tag{12}$$

where u_x and u_y are the water particle velocities in x and y direction respectively, p_{wave} is the hydrostatic pressure component of the wave, z is the vertical coordinate directed upward with its origin at the still water level, S_{xx} and S_{yy} are the normal stresses that include the hydrostatic pressure in the water column, τ_{xy} & τ_{yx} are the shear stress components of the wave and the over bar indicates averaging over the wind wave period. The shear stress due to waves (τ_{xy}) is considered as zero because of the assumption of an irrotational ideal fluid (Longuet-Higgins and Stewart, 1964).

2.1.5 Shallow Water Equations

Flow models are usually based on the solution of the three-dimensional incompressible Reynolds averaged Navier-Stokes equations, subject to the assumptions of Boussinesq and of hydrostatic pressure. The local two-dimensional continuity equation can be written as:

$$\frac{\partial h}{\partial t} + \frac{\partial h\bar{u}}{\partial x} + \frac{\partial h\bar{v}}{\partial y} = hS \tag{13}$$

where h is the water depth and u and v are water particle velocities in x and y direction respectively, S is the energy source-dissipation term.

The horizontal momentum equation for x-component is written as:

$$\frac{\partial h\bar{u}}{\partial t}+\frac{\partial h\overline{u^2}}{\partial x}+\frac{\partial h\overline{vu}}{\partial y} = fh\bar{v}-gh\frac{\partial \eta}{\partial x}-\frac{h}{\rho_0}\frac{\partial p_a}{\partial x}-\frac{gh^2}{2\rho_0}\frac{\partial \rho}{\partial x}+\frac{\tau_{sx}}{\rho_0}-\frac{\tau_{bx}}{\rho_0} -\frac{1}{\rho_0}\left(\frac{\partial S_{xx}}{\partial x}+\frac{\partial S_{xy}}{\partial y}\right)+\frac{\partial}{\partial x}hT_{xx}+\frac{\partial}{\partial y}hT_{xy}+hu_sS \quad (14)$$

The horizontal momentum equation for y-component is written as:

$$\frac{\partial h\bar{v}}{\partial t}+\frac{\partial h\overline{v^2}}{\partial y}+\frac{\partial h\overline{vu}}{\partial x} = fh\bar{u}-gh\frac{\partial \eta}{\partial y}-\frac{h}{\rho_0}\frac{\partial p_a}{\partial y}-\frac{gh^2}{2\rho_0}\frac{\partial \rho}{\partial y}+\frac{\tau_{sy}}{\rho_0}-\frac{\tau_{by}}{\rho_0} -\frac{1}{\rho_0}\left(\frac{\partial S_{yx}}{\partial x}+\frac{\partial S_{yy}}{\partial y}\right)+\frac{\partial}{\partial y}hT_{xy}+\frac{\partial}{\partial y}hT_{yy}+hu_sS \quad (15)$$

where t is the time; x and y are the Cartesian coordinates; η is the surface elevation; d is the still water depth; $h = \eta+d$ is the total water depth; u and v are velocity components in x and y direction; f is the Coriolis parameter; g is gravitational acceleration; ρ is the density of water; τ_{sx}, τ_{sy} are the x and y components of surface wind and τ_{bx} and τ_{by} are the components of bottom stress; T_{ij} includes viscous friction, turbulent friction and differential advection estimated using eddy viscosity formulation based on depth averaged velocity gradients.

The inputs and boundary conditions required for any model to calculate the current components and water particle velocities are included in the right-hand side of Equation 14 and 15. Each model applies different schemes and assumptions to solve these equations. The calculated current and water particle velocities are in charge of sediment transport taking place in the nearshore coastal zone.

Momentum equations usually include the effect of turbulence in the terms having laminar stresses and Reynolds stresses. Turbulence can be represented as a constant in the horizontal stress terms or by using the Smagorinsky's formulation (1963) to express sub-grid scale transports using an effective eddy viscosity related to characteristic length scale, see Lilly (1989).

2.2 Sediment Transport

The interaction between hydrodynamics and sediments results in sediment transport and thus bed level change. Sediment transport is the movement of sediment particles through a well-defined plane over a certain period of time. It plays an important role in determining the shape of the coast. Sediment transport is induced by the interaction of winds, waves, currents, tides and sediments.

The movement of sediments in shallow water is more than in deep water because waves can feel the bottom more in shallow water and influence the seabed. Furthermore, tidal currents are stronger in shelf seas than in the open ocean. When water flows over a surface fast enough, sediment particles on the surface are stirred up and transported to be deposited again when the flow slows down. Heavy particles may be rolled or bounced along the surface by water flow. In general, the movement of sediment particles depends on the properties of the transported sediments. Important properties of sediments are grain size diameter, porosity, relative density, bulk density and fall velocity.

The modeling of sediment transport depends on empirical formulations because the interaction between hydrodynamics and sediments is poorly understood to this day. Many formulations have been developed to model sediment transport, such as Engelund and Hansen (1967), Engelund and Fredsøe (1976) and Van Rijn (1984). These formulations usually have different processes and are developed based on specific situations. Therefore, calibration and validation of the numerical model is very important to obtain robust results. Calibration should be performed using representative data for the hydrodynamic condition and the considered site.

2.2.1 Sediment Properties

Sediment properties influence the sediment transport taking place at any site. Based on the particle size, sediments are classified into clay, sand, gravel and cobbles. The most important sediment properties are briefly described in the following paragraphs.

The most two crucial parameters for sediment transport are the median particle diameter D_{50} and the grading D_{90}/D_{10}. The D_x is the value of the particle diameter at x% in the cumulative grain size distribution. Sediments are classified based on the grading into well sorted if D_{90}/D_{10} is smaller than 1.5 and poorly sorted or well-graded sediment if D_{90}/D_{10} is larger than 3. One should keep in mind that this classification is not formal and these ranges might be different.

Grain density depends on the degree of compaction of the sediments and on the mineral composition. The mass density of sand is usually 2650 kg/m^3 since it consists of quartz. Relative density is the ratio of the density of sediment over the density of water. It is usually around 2.65 for natural sediments. Porosity is the ratio of the volume of openings (voids) to the total volume of sediment. Usually porosity of 40% is used for sand in modelling.

The fall velocity of grains depends on the grain size, grain shape, specific density and the density and viscosity of the water. It also depends on whether the flow is laminar or turbulent. This velocity can be determined from the balance between downward directed force and upward directed force. The upward directed force on the particle is caused by the frictional drag of the water. The downward directed force is caused by the difference between the particle density and the water density. The fall velocity ω_s is given by:

$$\omega_s = \sqrt{\frac{4(s-1)gD}{3C_D}} \tag{16}$$

where s is the relative density of the sediment, D is the sediment grain size, C_D is the drag coefficient and g is the acceleration of gravity. The drag coefficient depends on the particle Reynolds number and the shape and roughness of the particle. Reynolds number *Re* is given by:

$$Re = \frac{\omega_s D}{v} \tag{17}$$

where v is the kinematic viscosity coefficient. Figure 2.3 shows the drag coefficient of spheres as a function of Reynolds Number.

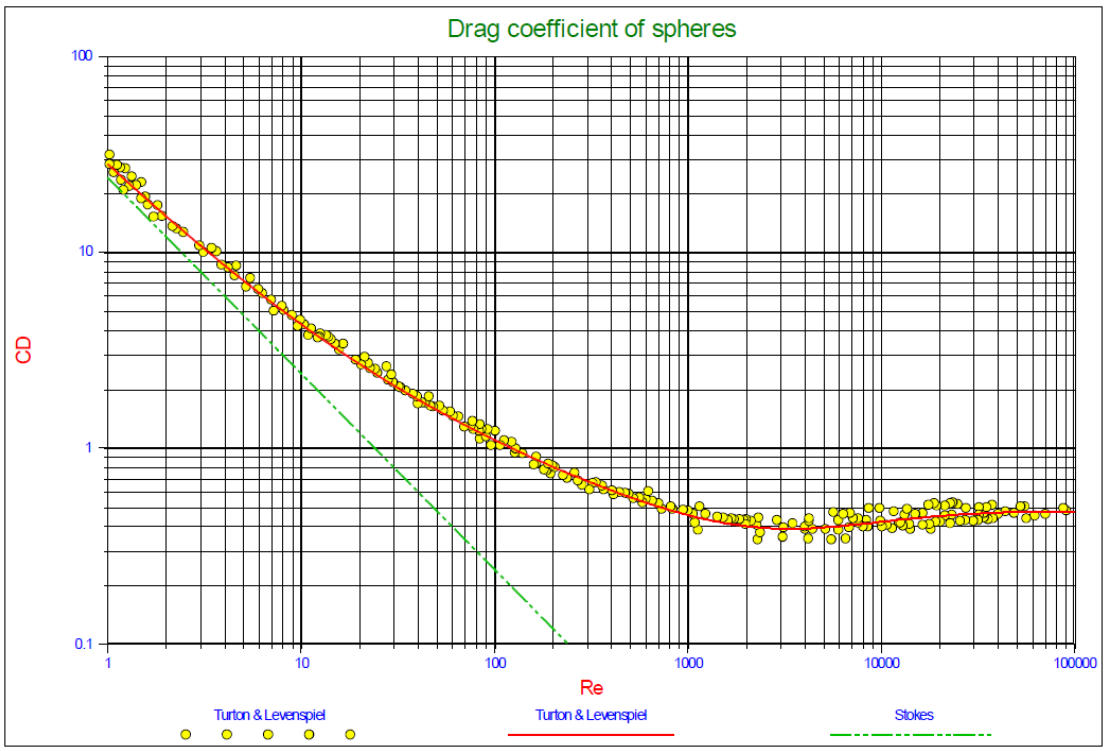

Figure 2.3: Drag coefficient of spheres as a function of Reynolds Number (Source: Miedema, 2015)

Critical Shields parameter θ_{cr}, is a dimensionless number used to calculate the initiation of motion of sediments in a fluid flow. It is the main parameter in models for sediment movement. It reads as follows:

$$\theta_{cr} = \frac{\tau_{b,cr}}{(\rho_s - \rho)gD} = C \tag{18}$$

where ρ_s is the density of sediments, ρ is the density of fluid, $\tau_{b,cr}$ is the critical bottom shear stress and C is a constant which is determined experimentally. The value of C was found to be around 0.05 for sand positioned smoothly on a flat bed. Figure 2.4 shows the critical Shields parameter as a function of the particle Reynolds number (R_e). Shields did not observe sediment movement in the zone below Shields curve, whereas he observed sediment movement in the zone above Shields curve. One should keep in mind that Shields diagram is only valid in the case of uniform permeant flow in a horizontal flat bed.

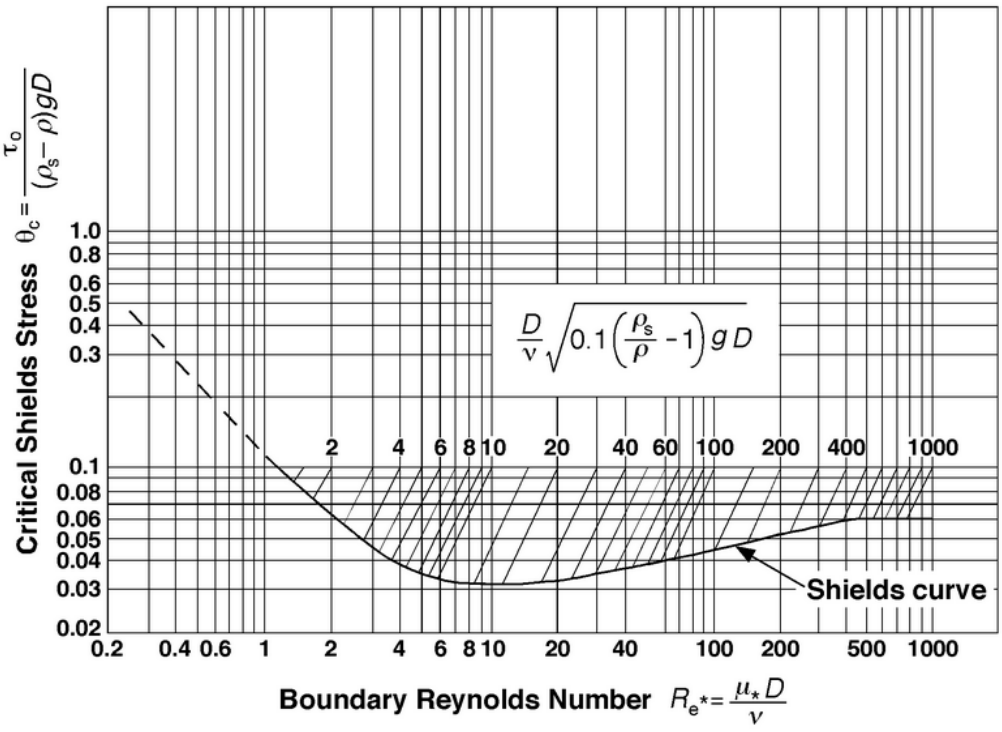

Figure 2.4: Shields Diagram for incipient motion (Source: Shields, 1936)

2.2.2 Transport Modes

Sediment transport is usually divided into two types: bed load transport and suspended load transport. Bed load is the part of the total load which has continuous contact with the bed. Therefore, the bed load has to be determined in terms of the effective shear stress which acts on the grain surface. On the other hand, suspended load is the part of the total load which moves without continuous contact with the bed due to the agitation of the fluid turbulence. The suspended load is related to the total bed shear stress.

Bed load transport takes place when the bed shear stress exceeds a critical value. Many formulations have been developed in order to determine the bed load transport, such as Kalinske-Frijlink (1952), Meyer-Peter and Muller (1948), Einstein (1962), Rottner (1959), Ackers-White (1973). Bed-load transport is usually expressed in the dimensionless form:

$$\Phi_b(t) = \frac{S_b(t)}{\sqrt{(s-1)gD_{50}^3}} \tag{19}$$

where Φ_b is a dimensionless parameter, s is the relative density of sediments and D_{50} is the sediment mean grain diameter.

Kalinske-Frijlink (1952) formula was developed by curve fitting using all data available at that time:

$$\Phi_b(t) = 2D_{50}\sqrt{\frac{\tau_b}{\rho}}\exp\left(\frac{-0.27\ (s-1)D_{50}\rho g}{{\tau_b}'}\right) \tag{20}$$

where τ_b is the bottom shear stress and ${\tau_b}'$is the effective shear stress.

Meyer-Peter (1948) used large amount of experimental data for curve fitting:

$$\Phi_b(t) = 8(\theta' - \theta_c)^{1.5} \tag{21}$$

where θ' is the effective Shields parameter $\theta' = \frac{{\tau_b}'/\rho}{(s-1)gD_{50}}$, ${\tau_b}'$is the effective shear stress and θ_c is the critical Shields parameter.

The principle of Einstein's analysis is that the number of deposited grains in a unit area depends on the number of moving grains and the probability that the hydrodynamic forces allow the grains to settle down. Experimental data fitting gives:

$$\Phi_b(t) = 40\,K(\theta')^3 \tag{22}$$

$$K = \sqrt{\frac{2}{3} + \frac{36\ v^2}{(s-1)g{D_{50}}^3}} - \sqrt{\frac{36\ v^2}{(s-1)g{D_{50}}^3}} \tag{23}$$

Figure 2.5 shows a comparison between various bed load transport formulas developed for rivers. X-axis represents Shields parameter based on skin friction and Y-axis represents the dimensionless transport Φ in the case of steady flow. One can see in the figure that the transport rates for a specific value of Shields parameter vary considerably between the formulas. Therefore, model calibration for sediment transport is very crucial.

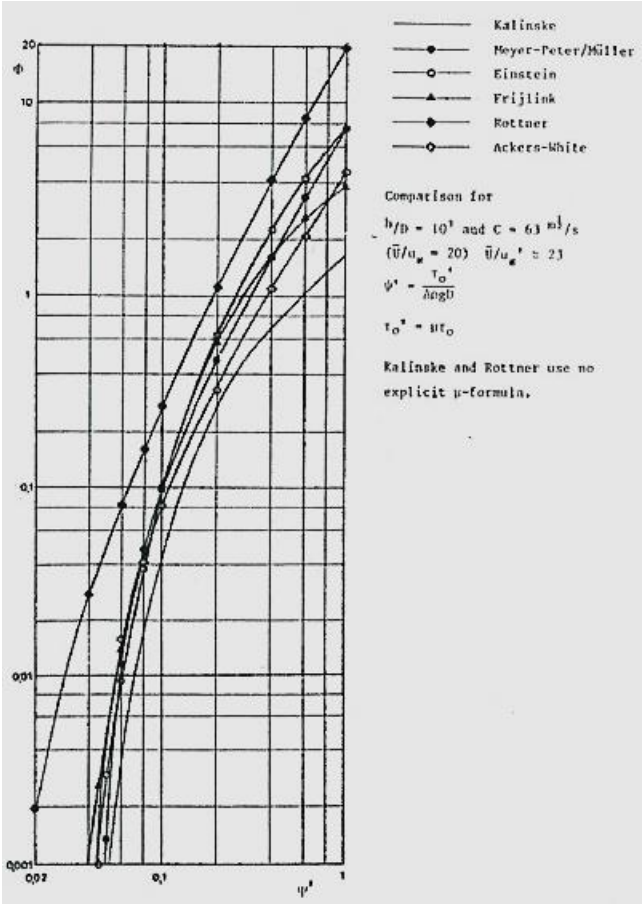

Figure 2.5: Comparison of various bed load transport formulas developed for rivers (Source: Bosboom & Stive, 2015)

Suspended load transport is defined as the irregular motion of the particles through the water column induced by turbulence-induced drag forces on the particles. The particles on the bed are lifted up when the actual bed shear stress is much larger than the critical bed shear stress. The particles lose their contact with the bed and go into suspension when the turbulent upward forces are larger than the submerged weight of the particles.

The instantaneous suspended transport rate S_s can be determined by integrating the sediment flux from the top of the bed later to the instantaneous water level (see Figure 2.6):

$$S_s(t) = \int_{z=a}^{h} c(z,t)u(z,t)dz \tag{24}$$

where c is the local instantaneous sediment concentration at height z above the bed and u is the local instantaneous fluid velocity at height z above the bed.

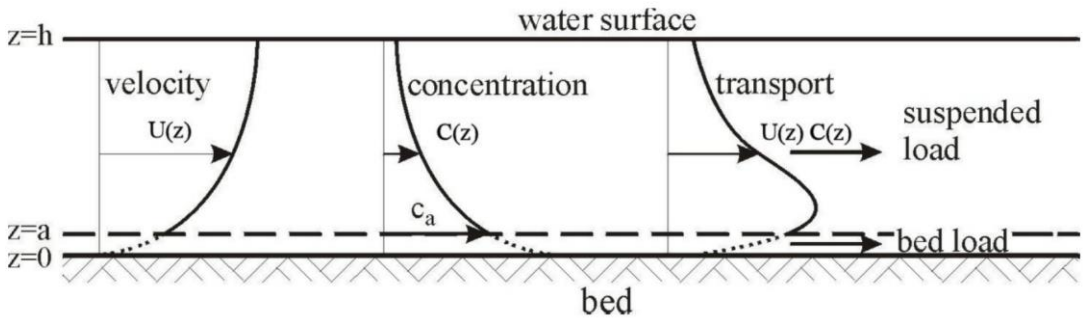

Figure 2.6: Sediment Transport Modes (Source: Bosboom & Stive, 2015)

The instantaneous concentration and velocity at any height can be represented by a mean part and an oscillatory part:

$$c = C + \tilde{c} \tag{25}$$

$$u = U + \tilde{u} \tag{26}$$

where C is the time-averaged concentration at height z, U is the time-averaged fluid velocity at height z, $\tilde{c}$ is the oscillating concentration component and $\tilde{u}$ is the oscillating fluid component.

The time averaged suspended sediment transport rate consists of current-related part (the first part of the right-hand-side of Eq. 27) and wave-related part (the second part of the right-hand-side of Eq. 27):

$$\langle S_s \rangle = \int_a^h UC dz + \int_a^h \overline{\tilde{u}\tilde{c}}\, dz \tag{27}$$

A mass balance equation for sediment has to be solved in order to get the sediment concentration (Bagnold, 1966):

$$\frac{\partial c}{\partial t} + \frac{\partial uc}{\partial x} + \frac{\partial vc}{\partial y} + \frac{\partial wc}{\partial z} - \frac{\partial w_s c}{\partial z} = 0 \tag{28}$$

The first part of the previous equation represents the change in sediment concentration, the second and third parts together represent the net import of sediment by the horizontal fluid velocity, the fourth part represents the net upward transport of sediment by the vertical fluid velocity and the fifth part represents the net downward transport with the fall velocity.

The horizontal advective terms can be neglected in Eq. 28 since they are usually smaller than the vertical advective terms. This reduces Eq. 28 to:

$$\frac{\partial c}{\partial t} + \frac{\partial wc}{\partial z} + \frac{\partial w_s c}{\partial z} = 0 \tag{29}$$

Assuming that the fall velocity is constant, the advection-diffusion equation reads:

$$\frac{\partial c}{\partial t} - w_s \frac{\partial c}{\partial z} + \frac{\partial \langle c'w' \rangle}{\partial z} = 0 \tag{30}$$

where c' and w' are the concentration turbulent part and vertical-velocity turbulent part respectively. The second part of the previous equations represents the sediment net going downward with its fall velocity and the third part represents the sediment net going upward with fluid turbulence.

With the assumption of upward transport due to turbulent diffusion, sediment flux due to turbulence can be modeled. The damping of turbulence due to high sediment concentration is usually taken into consideration in the empirical formulations. The general non-steady advection-diffusion equation used to model sediment transport reads:

$$\frac{\partial c}{\partial t} - w_s \frac{\partial c}{\partial z} - \frac{\partial}{\partial z} \nu_{t,s} \frac{\partial c}{\partial z} = 0 \tag{31}$$

where $\nu_{t,s}$ is the turbulent diffusivity of sediment mass.

2.2.3 Longshore Sediment Transport

Longshore sediment transport is the total transport along a coast in the entire active zone. Two important factors for wave-driven longshore sediment transport are the hydrodynamics in the breaker zone and the sediment properties. The longshore current is driven primarily by breaking waves and is concentrated in the surf zone.

Waves generate the longshore current and increase the amount of suspended sediments due to the turbulence generated in the wave boundary layer and at the surface under breaking waves. Wave-induced longshore current is the main reason for the net movement of sediment parallel to the shoreline. Thus, the time-averaged longshore sediment transport per unit width is given by:

$$\langle S_y \rangle = \underbrace{m_2 \langle u^2 + V^2 \rangle}_{1} \underbrace{V}_{2} \tag{32}$$

where V is the depth-mean longshore current velocity, m_2 is a dimensional coefficient and u is the cross-shore time-varying orbital motion. The first part of the previous equation represents the sediment load stirred by wave-current motion and the second part represents the longshore current which is responsible for longshore transport.

Based on field studies, many formulas to predict the longshore sediment transport have been developed, such as CERC formula (Shore Protection Manual, 1984), Kamphuis (1991), Komar and Inman (1970), Inman et al. (1981), Kraus et al. (1982), Miller (1999) and Bayram et al. (2007). The differences between these formulas are that they take the influence of waves into consideration in different ways and the sensitivities to certain parameters vary between them. The resulting total transport from these formulas varies so much and can be up to a factor of ten (Bosboom & Stive, 2015). Therefore, calibration of the formulation is very important before using the results of numerical modelling.

The Coastal Engineering Research Center (CERC) formula is one of the oldest longshore transport formulations but it is widely used to this day. It has been developed in the late 1940's before the development of the longshore current theory. Thus, the longshore current is not considered in this formula. It includes only the effect of the wave-generated longshore current. Accuracy of the CERC formula is believed to be ± 30-50 percent since some parameters that might influence longshore sediment transport are not included in the formula, such as breaker type and grain size (Wang, et al., 2002). The general CERC formula reads:

$$S = \frac{K}{\rho g(s-1)(1-p)} (Enc)_b \cos \emptyset_b \sin \emptyset_b \tag{33}$$

where S is the deposited volume of transported sediment, K is a coefficient, s is the relative density of sediment, ρ is the water density, p is the porosity, g is the gravitational acceleration, E is wave energy, n is the ratio between group and phase velocity, c is the wave phase velocity, $\emptyset$ is the wave angle of incidence and b is a subscript referring to conditions determined at the outer edge of the breaker zone.

Due to the limitations of the CERC formula, there was a need for developing a new formula that accounts for the influential parameters absent in the CERC formula. Kamphuis (1991) suggested an empirical formula that includes the effect of grain size, beach slope and wave steepness:

$$I_m = 2.27\, H_{s,b}^2 T_p^{1.5} (tan\alpha_b)^{0.75}\, \mathrm{D}^{-0.25}\, (\sin 2\emptyset_b)^{0.6} \tag{34}$$

where I is the immersed mass of transported sediment and $tan\alpha_b$ is the beach slope at the breaker point.

With the assumption that suspension is the prominent mode of transport for longshore sediment transport in the surf zone, Bayram et al. (2007) suggested a new formula to predict longshore sediment transport. They developed the formula on the basis that the breaking waves mobilize the bed sediments and subsequently the sediment particles are moved by a mean current in nearshore zone:

$$Q_{lst} = \frac{\varepsilon}{(\rho_s - \rho)(1-p) g w_s} F \bar{V} \tag{35}$$

where Q_{lst} is the longshore sediment transport rate, F is the energy flux of the incident wave, $\bar{V}$ is the average longshore current velocity, p is a sediment porosity to convert sand weight to volume and ε is the longshore sediment transport coefficient and given by:

$$\varepsilon = \left(9 + 4\frac{H_{s,b}}{w_s T_p}\right).10^{-5} \tag{36}$$

Based on field and laboratory data, Bayram et al. (2007) deduced that their formula predicts higher longshore sediment transport than the CERC and Kamahis formula.

3 Gaza Seaport

Gaza Strip is an enclave in Palestine, situated on the eastern coast of the Mediterranean Sea. It is located at 34.20°E, 31.25°N with a total surface area of 365 km^2 (Worldabc, 2015). Its width varies between 9 and 10 kilometers in the north to 12 and 13 km in the south, with a minimum width of 5.7 km (Ali, 2002).

Gaza Strip is one of the most densely populated regions all over the world since it is a home to about 1.8 million Palestinians. According to BBC News (2014), it is expected that the total population will grow to 2.13 million inhabitants by the end of the current decade.

The execution of Gaza Seaport project is essential to enhance the political and economic situation in Gaza Strip. It emphasizes the concept of independence and utilization of natural regional resources in international waters. Gaza Seaport will effectively connect the Palestinian economy to the world and will enhance the local industry, the export and commercial services (Ward, 2014).

These days Palestinians rely totally on Israeli ports for all import and export operations. Gaza Seaport will reduce and possibly end the economic dependence on the Israeli economy and enable free trade of Palestinian imports and exports. The seaport will offer a free access road from Palestine to the world and will open the maritime window for dealing with the world directly without any constraints on either import or export (Ward, 2014).

3.1 Historical Background of Gaza Seaport

Gaza Seaport was mentioned in the Oslo Accords in 1993. The Oslo Accords are a set of agreements between the government of Israel and the Palestine Liberation Organization to fulfill the right of Palestinians to self-determination. In the 1990s, the Dutch government was approached regarding funding and constructing the seaport. The Dutch government was selected because it had good relations with Israel and that would increase the probability that Israel would allow the seaport to be built. Dutch and French companies, Ballast Nedam and Spie Batignolles, were hired to construct the seaport. In 1994, the contract between the construction companies and the Palestinian Authority was signed (Alternativenews, 2010).

During the first years after signing the construction contract, no construction work took place. The Palestinian Authority negotiated with Israel about the start of construction, but there were no results. The Dutch government even hired security experts from the port of Rotterdam in the Netherlands to offer advice but Israel continued to delay construction, citing security concerns. Israel prevented construction materials from reaching the construction site. Raw materials were kept months before they were cleared through customs. During these months they were stored in Israeli warehouses for which storage fees had to be paid. It then took long time to get these materials to get through the checkpoints between Israel and Gaza. Finally, when the raw materials reached the construction place, workers were held for long time at checkpoints while they were paid to sit in their cars. In the summer of 2000, construction of the seaport finally commenced.

In September 2001, Israel bombed the Gaza Seaport. Israel did not pay back anything to the European donors for its destruction of the nascent Gaza Seaport. After the destruction, donor funds were withdrawn and no rehabilitation/construction has taken place (Alternativenews, 2010).

3.2 Geological Background of the Coast of Gaza

The coastline of Gaza Strip forms a small section of a larger concave system which extends from Alexandria at the west side of the Nile Delta, via Port Said, Bardawil Lagoon, El Arish, Gaza, Ashqelon, and Tel Aviv to the Bay of Haifa. This coastal cell forms the southeastern corner of the Levantine Basin (Figure 3.1). This entire coastline, including the coastline of Gaza Strip, has been shaped over 15 thousand years ago by the Nile River and especially its sediment yield originating from Africa's mountains. The Nile sand moves along the entire concave coastline in the anti-clockwise direction, generally in a northeast direction. In this concave of the Mediterranean, the relatively short 42 km Gaza coastline is almost straight (Palestinian National Authority, 2001).

The Low Aswan dam and the High Aswan dam have almost completely blocked the Nile river sediment discharge to the sea. Fortunately, the Bardawil Lagoon sandbar continues to act as a significant source of sand to the coast of Gaza. As a result, any mitigation measures to prevent

the current erosion at Bardawil could affect the sand supply to the Gaza and Sinai coast (Perlin and Kit, 1999).

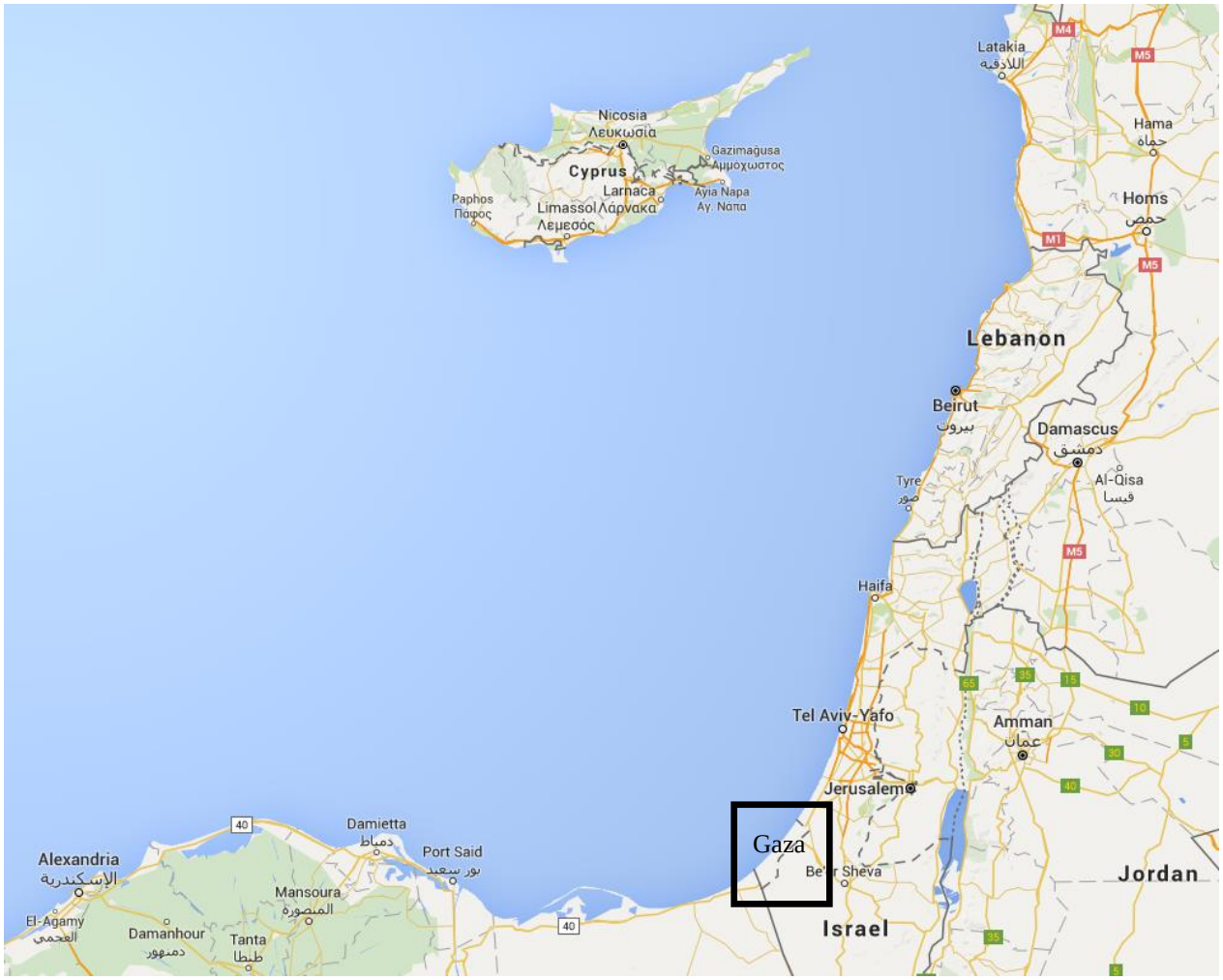

Figure 3.1: Gaza coastline in The Mediterranean context (Source: Google Maps, 2016)

3.3 Location of the Proposed Gaza Seaport

A site selection study of the proposed Gaza Seaport has been done by a Dutch engineering firm (Grabowsky & Poort). The results of this study showed that the most convenient location of the seaport is in the south of the coastal village Elsheikh Ejleen (Smaling, 1996), see Figure 3.2. The location was chosen for the following reasons:

- Very close to an industrial area
- Flexible for expansion
- The government is the main land ownership
- No hinder to urban settlements
- In the center of Gaza Strip
- Excellent transport corridor

On the other hand, the location has some drawbacks, such as minor negative effect on Wadi Gaza (one of the most important coastal wetlands located on the Eastern Mediterranean Basin) and loss of recreational beaches (Smaling, 1996).

Figure 3.2: Proposed location of Gaza Seaport (Source: Ward, 2014)

3.4 Proposed layout of Gaza Seaport

The design of Gaza Seaport shows that the project will be done in three phases. Each phase is described briefly in the following paragraphs.

3.4.1 Phase I

Two Ro-Ro berths and a general cargo berth with a length of 200 m will be constructed. The water depth will be limited to 11 m. A breakwater of 730 m will be constructed to limit downtime due to wave penetration. An additional 400 m of berth with a design water depth of MSL 15.25m will be provided. An additional berth for containers, a berth close to the small craft harbor for cement and other dry bulk will also be provided. The water depth will be increased to 12m to allow the use of large and more economical sizes of bulk vessels.

A new berth for bulk cargo will be provided. This berth is suitable for the most economical grain vessels and has a design water depth of 12m. About 20% of the traffic relates to liquid oil products. Therefore, a dedicated terminal including berth and bank farm will be required. Figure 3.3 shows the layout of Gaza Seaport by the end of phase I.

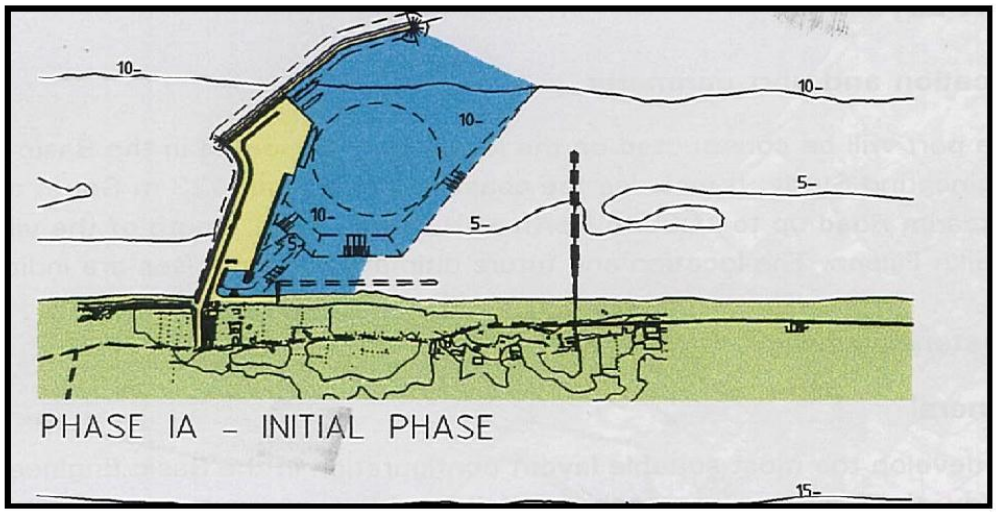

Figure 3.3: Phase I of development of Gaza Seaport, breakwater and berths (Source: Ward, 2014)

3.4.2 Phase II

In this phase a full container terminal is planned which will have a maximum capacity of 500,000 TEU (twenty-foot equivalent unit). Total berth length is 600m, suitable to accommodate vessels with a draft up to 14m. Protection of the terminal will be provided by extension of the existing breakwater.

3.4.3 Phase III

In this phase, a central terminal is planned. The terminal is planned mainly to be used for bulk, suitable to accommodate ships with a draft up to 14m. Figure 3.4 shows the layout of Gaza Seaport by the end of phase III.

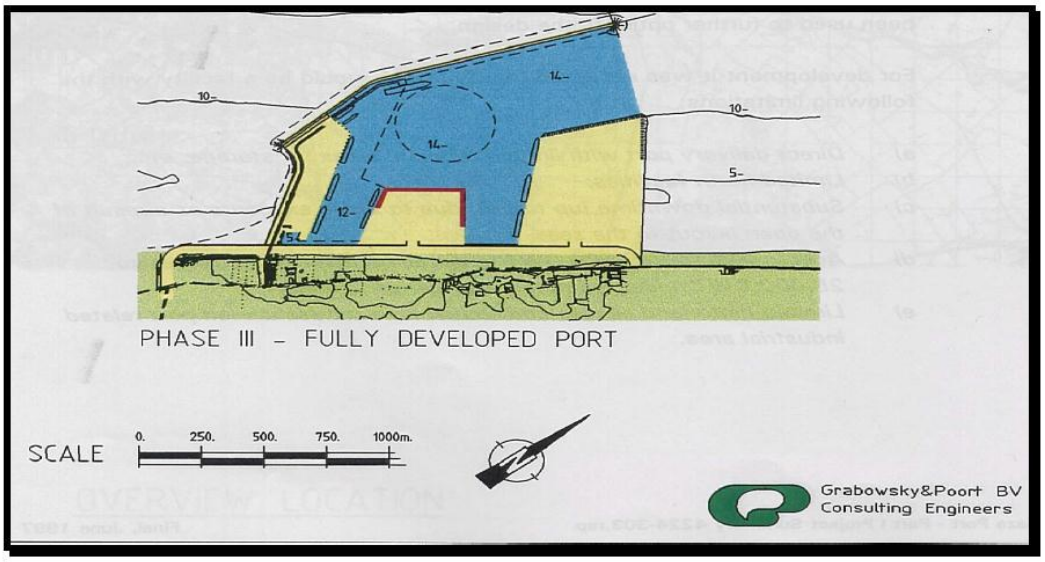

Figure 3.4: Phase III of development of Gaza Seaport, the breakwater has been extended and container terminal and bulk terminal have been added (Source: Ward, 2014)

The construction of the seaport will be done by the end of phase III. Usually such maritime engineering works have an adverse impact on the morphology in the vicinity of the structure. This study aims primarily at predicting the possible morphological effects of the proposed Gaza Seaport on the coast of Gaza by answering the following questions:

- What is the coastline evolution during the years following the seaport construction?
- Where it is expected to have a coastline erosion/accretion?
- Will the construction of the seaport cause morphological problems on the coastal zone?

This prediction is done with the incorporation of the numerical models, MIKE 21 and LITPACK, which are described in the next chapter.

4 Numerical Models

4.1 Numerical Model – MIKE 21

Numerical models are commonly used to simulate the processes of nature. MIKE 21 is one example of the numerous commercially available hydrodynamic modeling software packages. MIKE 21 is used here to study the tendency of sediment transport in the vicinity of the sea port and bed level changes. This chapter describes the numerical model MIKE 21 and presents a brief description of its different modules.

MIKE 21, developed by DHI, is a two-dimensional simulation package used for coastal, offshore and inland modeling. It has the required tools to simulate physical, chemical and biological processes in coastal and marine areas. Therefore, it is the most used package for coastal and marine engineering projects all over the world (DHI, 2016).

Among the different products of MIKE 21, MIKE 21 Flow Model was used in the current study. MIKE 21 Flow Model is a modelling system for two-dimensional free surface flows based on a flexible mesh approach. It is applicable for the simulation of hydraulic and environmental phenomena in lakes, estuaries, bays, coastal areas and seas. It could be applied wherever stratification is neglected.

MIKE 21 Flow Model consists of different modules as follows:

- Hydrodynamic Module (HD)
- Sand Transport Module (ST)
- Mud Transport Module (MT)
- Transport Module
- ECO Lab/Oil Spill Module
- Particle Tracking Module

In this study, Hydrodynamic Module and Sand Transport Module were used to run the simulations. Therefore, they are briefly described in this chapter.

4.1.1 Hydrodynamic Module (HD) with Flexible Mesh (FM)

The Hydrodynamic Module simulates water level variations and flows in response to a variety of forcing functions in lakes, estuaries and coastal regions. The effects and facilities incorporated in the model include: bottom shear stress, wind shear stress, barometric pressure gradients, Coriolis force, momentum dispersion, sources and sinks, evaporation, flooding and drying and wave radiation stresses (DHI, 2013).

All other modules require at least the Hydrodynamic Module to be run. Therefore, it is the fundamental computational component of the entire MIKE 21 Flow Model. Moreover, setup of the hydrodynamic model is the most important task for any study. The Hydrodynamic Module is based on the numerical solution of the two dimensional shallow water equations; the depth-integrated incompressible Reynolds averaged Navier-Stokes equations. Therefore, the model has continuity, momentum, temperature, salinity and density equations (DHI, 2012a).

A wide range of hydraulic and related phenomena can be modelled by the Module. This includes modelling of tidal hydraulics, wind and wave generated currents and storm surges. It simulates the propagation of flows in the time domain and takes the effects of the tidal variations and wave driven currents into consideration. The wave-tide interaction is also taken into account (DHI, 2013).

The model requires the following inputs:

- A digitized bathymetry.
- Basic model parameters describing the extent of the model area, the grid spacing of the computational model grid, the time step and the duration of the simulation.

Boundary conditions in MIKE 21 hydrodynamic model could be either the surface elevation or flux (the total amount of discharge passing the open boundary) at all open boundary points specified on the boundary.

4.1.2 MIKE 21 Sand Sediment Transport (ST)

The Sand Transport module of MIKE21 Flow Model describes erosion, transport and deposition of sand under the action of currents and waves or pure current. The module computes the rates of non-cohesive sediment transport at each point of a triangular grid covering the area of interest. The initial rates of bed level change associated with the time-averaged, over the user-defined simulation period, transport field are also output from a MIKE 21 ST simulation. Wind, wave, tide and current can be all taken into account for the best precision in the simulations.

MIKE 21 ST has the ability to simulate sand transport rates in various areas, including natural environments like tidal inlets, estuaries and coast lines, and man-made constructions like harbors and bridges (DHI, 2007).

One should keep in mind that the simulation is performed on the basis of the hydrodynamic conditions that correspond to the given bathymetry. There is no feedback of the rates of bed level change on the waves and the hydrodynamics, as in the case for a full morphological model. Consequently, the results provided by MIKE 21 ST can be used to identify potential areas of erosion or deposition and to get an indication of the initial rate at which bed level changes will take place, but not to determine an updated bathymetry at the end of the simulation period.

Sand Transport module calculates the sediment transport rates using two different model types: pure current and combined current and waves.

In the 'pure current' type the sediment transport rates are calculated directly during the simulation based on the actual conditions. There are five different sand transport theories in MIKE 21 ST for the calculation of transport rates in pure current conditions:

- The Engelund and Hansen total-load transport theory.
- The Engelund and Fredsøe total-load (determined as bed load + suspended load) transport theory.
- The Zyserman and Fredsøe total-load (bed load + suspended load) transport formulation
- The Meyer-Peter and Müller bed-load transport theory.
- The Ackers and White total-load transport formulation.

In the 'combined current and waves' type the sediment transport rates are found by linear interpolation in a sediment transport table. There are two methods available for the calculation of the sediment transport rates in combined current and waves:

- Application of DHI's deterministic intra-wave sediment transport program (STP). It is an advanced sediment transport model which accounts for the influence of several processes on the sediment transport rates, such as waves propagating at an angle with respect to the current, breaking/unbroken waves, plane/ripple-covered bed and others (DHI, 2007).
- Bijker's total load transport method (the total load sediment transport is calculated as the sum of bed load transport and suspended load transport).

On the computed sediment transport rates, Sand Transport module accounts for the influence of the following phenomena:

- Geometric properties of bed material described by a single grain size or a grain size distribution curve.
- Plane/ripple-covered bed.
- Finite differences technique on space-staggered rectangular grid.
- Courant-Friedrichs-Lewy stability criterion.

4.2 MIKE 21 Spectral Waves (SW)

MIKE 21 SW includes a new third generation spectral wind-wave model depending on unstructured meshes. The model simulates the growth, decay and transformation of wind-generated waves and swells in offshore and coastal areas. It includes two different formulations: fully spectral formulation and directional decoupled parametric formulation. The fully spectral formulation is based on the wave action conservation equation. It includes the following physical phenomena:

- Wave growth by action of wind
- Non-linear wave-wave interaction
- Dissipation by white-capping
- Dissipation due to bottom friction
- Dissipation due to depth-induced wave breaking
- Refraction and shoaling due to depth variations
- Wave-current interaction
- Effect of time-varying water depth
- Effect of ice coverage on the wave field

On the other hand, the directional decoupled parametric formulation is based on a parameterization of the wave action conservation equation. The parameterization is made in the frequency domain by introducing the zeroth and the first moment of the wave action spectrum (DHI, 2015).

The MIKE 21 SW model uses a triangular mesh grid so the size of the grid could be varied according to the desired accuracy of the output. In general, a coarser mesh is used in offshore areas and a much finer mesh is used in the areas of interest.

4.3 Numerical Model - LITPACK

LITPACK is used here to study the long term evolution of the coastline of Gaza after the construction of Gaza Seaport. LITPACK is a software package for the modelling of non-cohesive sediment transport in waves and currents, littoral drift, coastline evolution and profile development along quasi-uniform beaches. Each individual module of LITPACK simulates particular coastal processes. There is a link between the modules performed by an automatic control module. This results in a rapid simulation of complex coastal problems, without loss of detail in the individual modules (DHI, 2012b).

All LITPACK modules apply a fully deterministic approach which accounts for more factors than the semi-empirical approach. The main modules of the LITPACK are as follows:

- Non-cohesive sediment transport (LIST)
- Longshore current and littoral drift (LITDRIFT)
- Coastline evolution (LITLINE)
- Cross-shore profile evolution (LITPROF)
- Sedimentation in trenches (LITTREN)

In this research, LITLINE module and LITDRIFT module were used to run the simulations. Therefore, they are briefly described in this chapter.

4.3.1 The LITLINE Module

LITLINE calculates the coastline position based on input of the wave climate as a time series data. The model is based on a one-line theory, in which the cross-shore profile is assumed to remain unchanged during erosion/accretion. Therefore, the coastal morphology is solely described by the coastline position (cross-shore direction) and the coastal profile at a given longshore position.

The influence of structures, sources and sinks are included in the module. It accounts for the following:

- Structures (groins, jetties, revetments and offshore breakwaters)
- Sources and sinks
- Diffraction of waves
- Depth contours
- Active depth and dunes

Appropriate internal boundary conditions are introduced in order to model the changes to the transport conditions caused by coastal structures. Besides blocking the transport, large structures change the transport relations close to the structure due to the sheltering effect from the structure itself. This effect is automatically included by introducing modified transport relations close to the structure. The influence of diffraction on the wave climate is included with jetties and breakwaters (DHI, 2012c).

LITLINE calculates the coastline evolution by solving a continuity equation for the sediment in the littoral zone:

$$\frac{\partial y_c}{\partial t} = -\frac{I}{h_{act}}\frac{\partial Q}{\partial x} + \frac{Q_{sou}}{h_{act}\Delta x} \tag{37}$$

in which

y_c: distance from the baseline to the coastline

t: time

h_{act}: height of the active cross-shore profile

Q: longshore transport of sediment expressed in volumes

x: longshore position

Δx: longshore discretization step

Q_{sou}: source/sink term expressed in volume/Δx.

The continuity equation for sediment volumes is solved using an implicit Crank-Nicholson scheme, giving the development of the coastline position in time.

The following basic inputs are required in LITLINE:

- Longshore relative coastline alignment together with dune properties, profile description, active depth and depth contour angles at each grid point
- Cross-shore profile bathymetries
- Data base with wave properties (wave height, wave period and wave angle), tidal current and water levels
- Position and size of structures
- Position and magnitudes of sources/sinks
- Database of transport rates which should be generated in advance
- Sediment characteristics (mean diameter of sediment d_{50}, geometrical spreading)

The basic output data of the model are as follows:

- Coastline position in time series (m);
- Depth of the topographic bed (m);
- Sediment transport rate (m^3/day);
- Accumulation of sediment transport rate (m^3);
- Sediment transport rate unit (m^3/m).

4.3.2 The LITDRIFT Module

LITDRIFT is a part of the software package LITPACK developed by DHI. It simulates the cross-shore distribution of wave height and longshore current for a coastal profile. It also simulates the littoral drift or shore parallel sediment transport. The software package is based on a sediment transport module. LITDRIFT could be used to study the wave driven currents and longshore sediment transport of non-cohesive sediment a long uniform beach. The assessment of the wave conditions is vital for the estimation of the wave forces at a shoreline.

Sediment parameters used for the computation of littoral drift include specific gravity, mean grain diameter, fall velocity, bed roughness, critical shield parameter, sediment spreading and the nearshore wave climate. The output from this model is the littoral drift for the individual wave situations and the total sediment budget. The model has the ability to calculate the net/gross littoral transport over a certain design period (DHI, 2012d). The structure of LITDRIFT is illustrated in Figure 4.1.

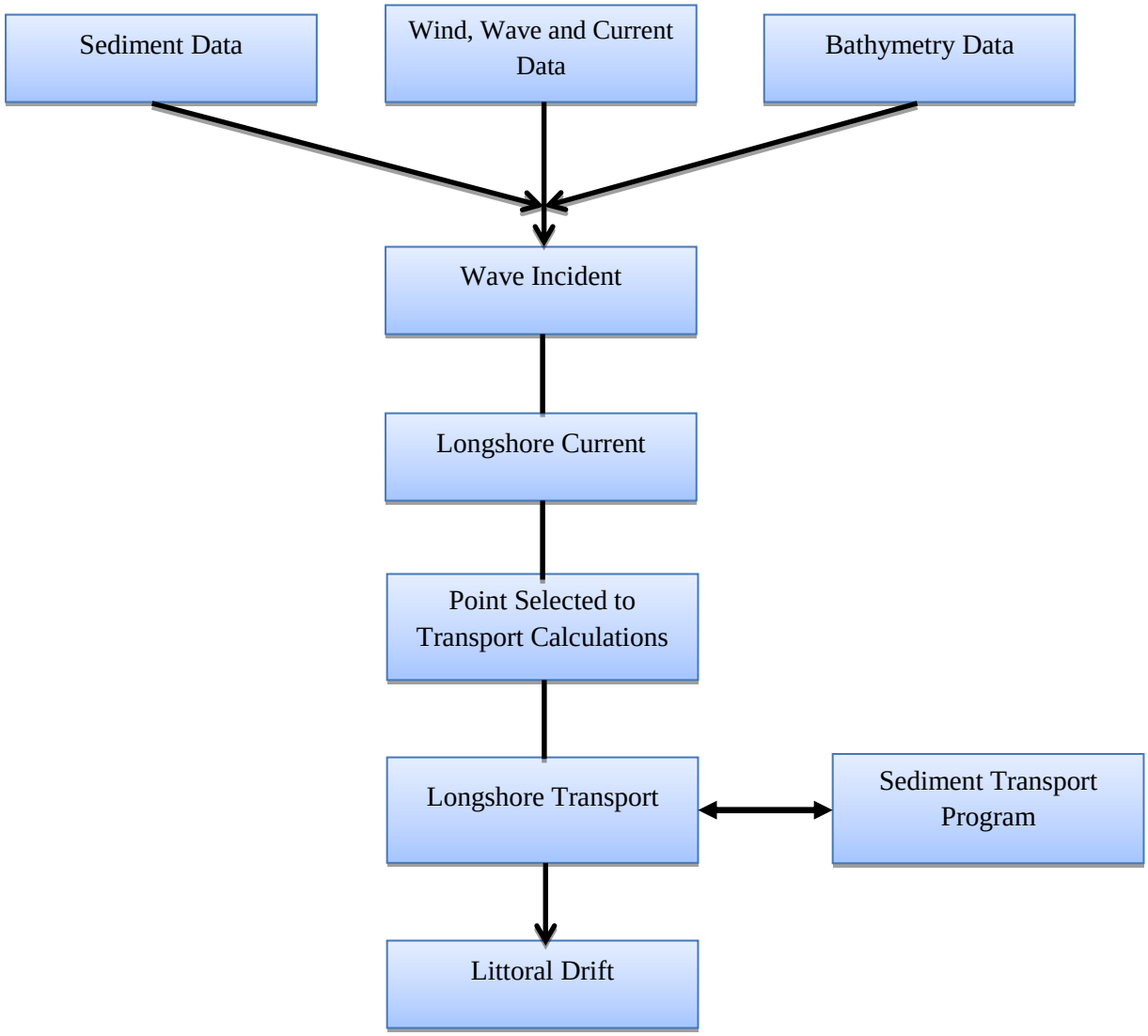

Figure 4.1: The Structure of LITDRIFT

5 Gaza Seaport: Case Study

5.1 Data

The most important step of numerical modeling is to choose representative data for the area of interest. This is because numerical models have different sensitivity to each kind of data. The most relevant data for the purpose of the current study is bathymetry, wave conditions, water level and tides, wind and sediment properties. This section outlines the data used in setting up the model with brief discussion on the source and reliability of data.

5.1.1 Bathymetry

The term "bathymetry" is referred to the ocean's depth relative to sea level. The seabed of the coast of Gaza follows depth contours which are almost parallel to the coast (Palestinian National Authority, 2001). Using accurate bathymetry is very crucial to obtain correct prediction of wave climate and sediment transport at the area of interest. As very limited field measurements for the bathymetry in front of the coast of Gaza are available, bathymetric data was obtained from Jeppesen charts using MIKE C-MAP. This software works on the Global Electronic Chart Database Professional and (CM-93 Edition 3.0 technology) provided by Jeppesen Marine, Norway. MIKE C-MAP provides bathymetric data for the whole world with a good resolution comparing with open sources (DHI, 2012e).

The digitized bathymetry for Gaza Strip is shown in Figure 5.1. A closer view of bathymetry for the area marked in Figure 5.1 is shown in Figure 5.2. The 10-m and 15-m water depth are located at 860m and 1160m seaward from the shoreline respectively.

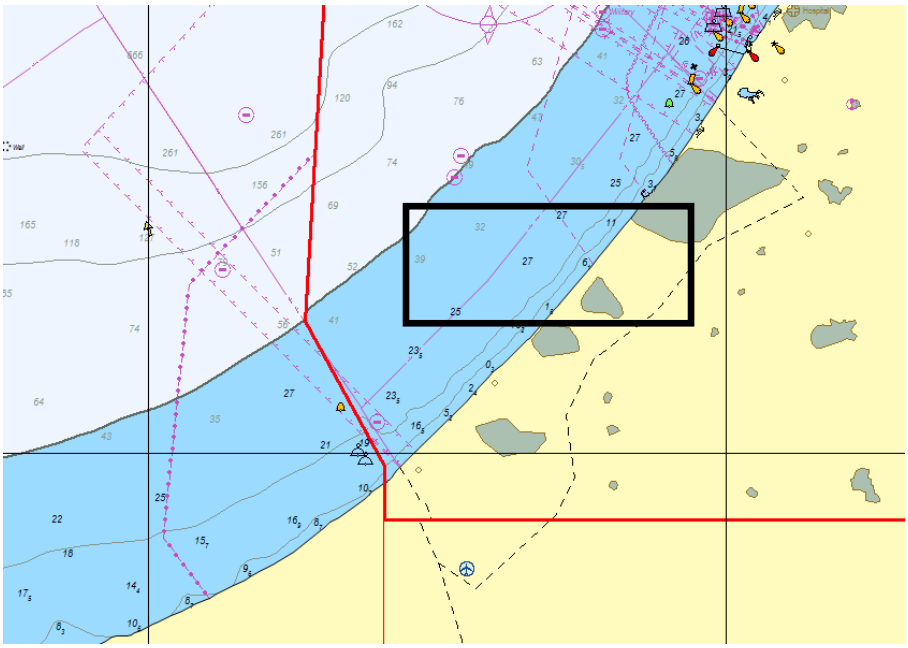

Figure 5.1: Bathymetry – Gaza Strip (Source: MIKE C-MAP)

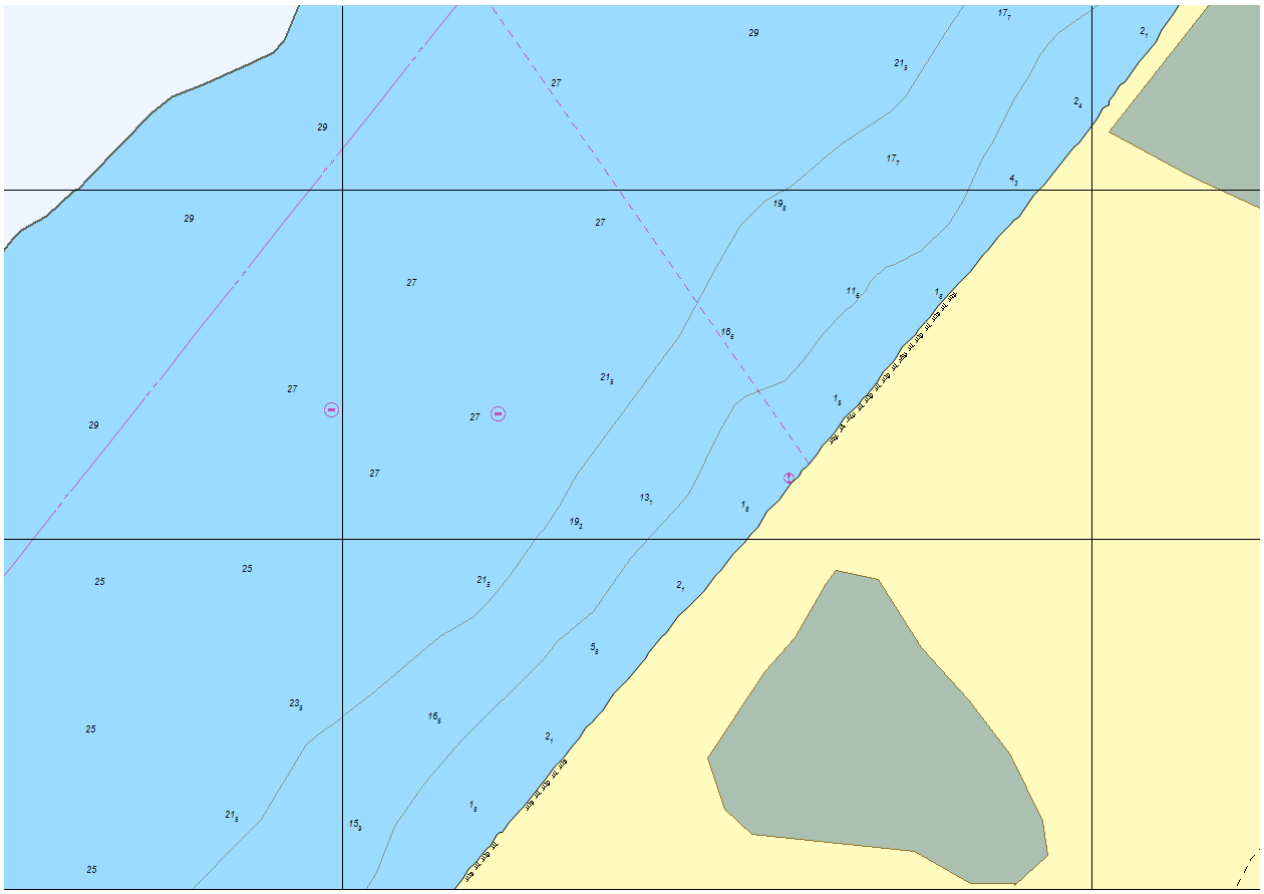

Figure 5.2: Closer view of bathymetry – Gaza Strip (Source: MIKE C-MAP)

5.1.2 Wave Data

Unfortunately, there are no field measurements of the wave climate for the coast of Gaza. The basic reason behind this is that there are no measuring facilities in Gaza Strip since the Israeli occupation bans them from entering Gaza Strip. Therefore, various open sources were checked to look for wave data for the coast of Gaza or any neighboring coasts.

Some examples of the open sources which were investigated:

- DHI Water forecast for Mediterranean
- European Centre for Medium-Range Weather Forecasts (ECMWF)
- Global altimeter SWH data set (Remote sensing)
- National Centers for Environmental Prediction
- Marine Environment Monitoring Service
- World Wave Atlas (WWA)

Unfortunately, no complete wave dataset was found in the all previously mentioned open sources. Consequently, the Italian office of DHI was contacted since it has obtained wind and wave hindcast database for all the Mediterranean Sea. Nevertheless, they could not provide this data for free.

Israel Marine Data Center (ISRAMAR) was contacted and new field measurements taken every hour for wave climate were found at Ashkelon station which is 20-kilometer apart from the proposed Gaza Seaport. These measurements include just the significant wave height (H_s) and the peak period (T_p) for the year 2015, see Figure 5.3.

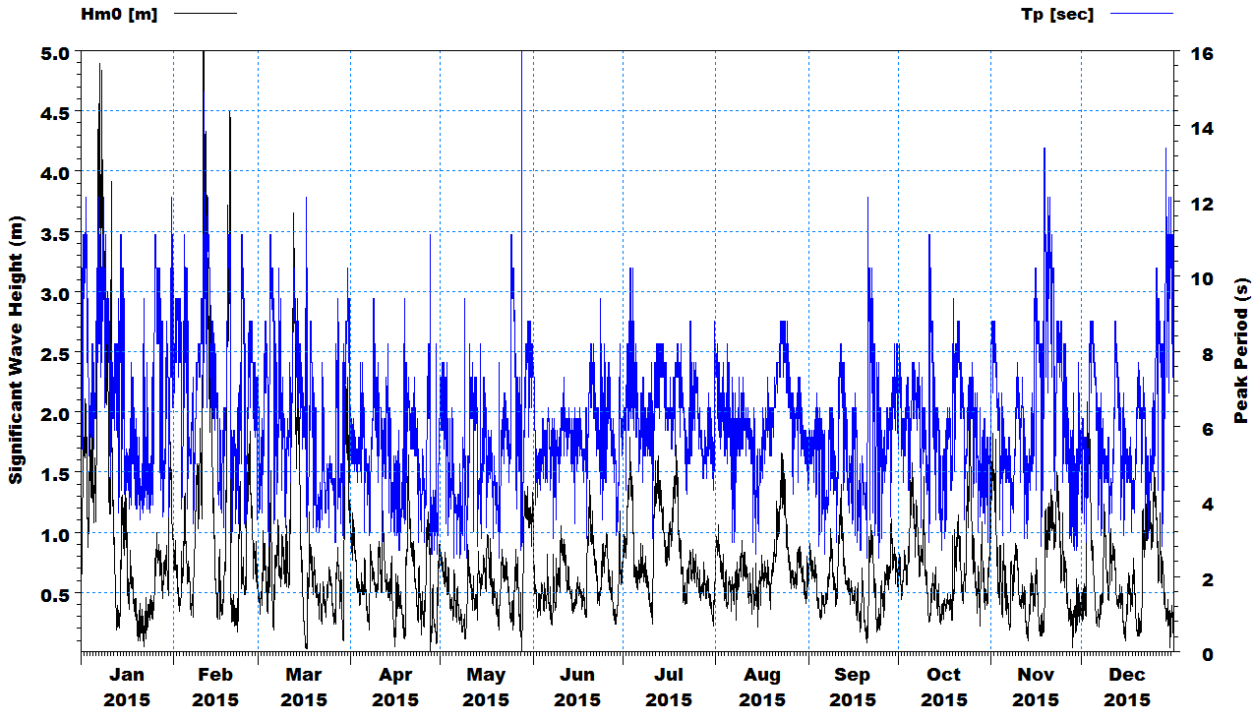

Figure 5.3: Significant wave heights and the peak periods at Ashkelon station

This means that this data lacks the mean wave direction in order to be used in numerical modeling. However, old wave data is available for two stations along the coast of the Mediterranean Sea namely Alexandria and Ashdod (see Figure 5.4). A statistical analysis was performed to study the mean wave direction in the eastern coast of the Mediterranean Sea.

Figure 5.4: Alexandria and Ashdod stations (Source: Google Earth, 2016)

In order to visualize the mean wave direction, wave rose was plotted for each available year as shown in the figures below.

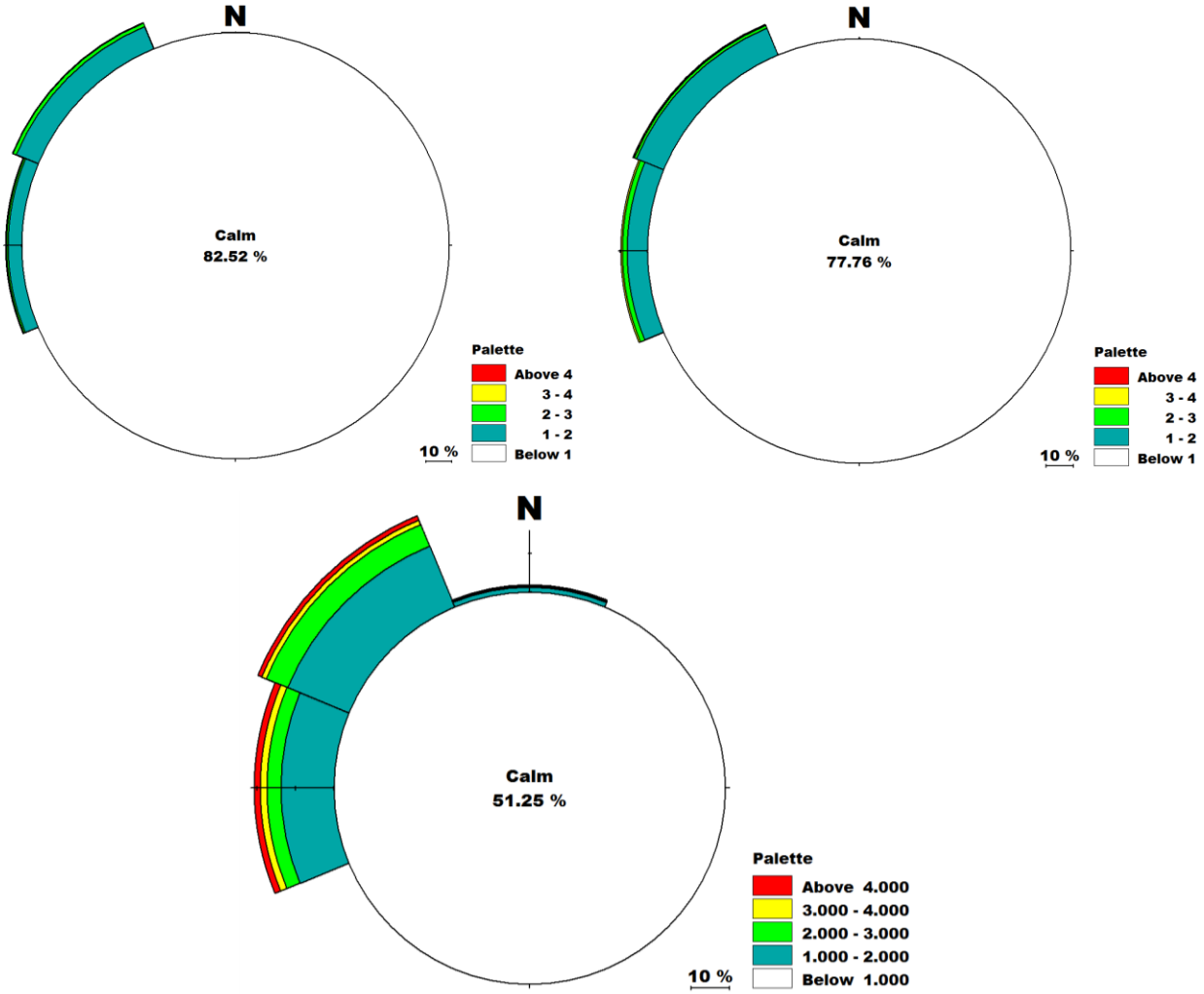

Figure 5.5: Alexandria wave rose, Top left: 2005, Top right: 2004, Bottom: 1989.

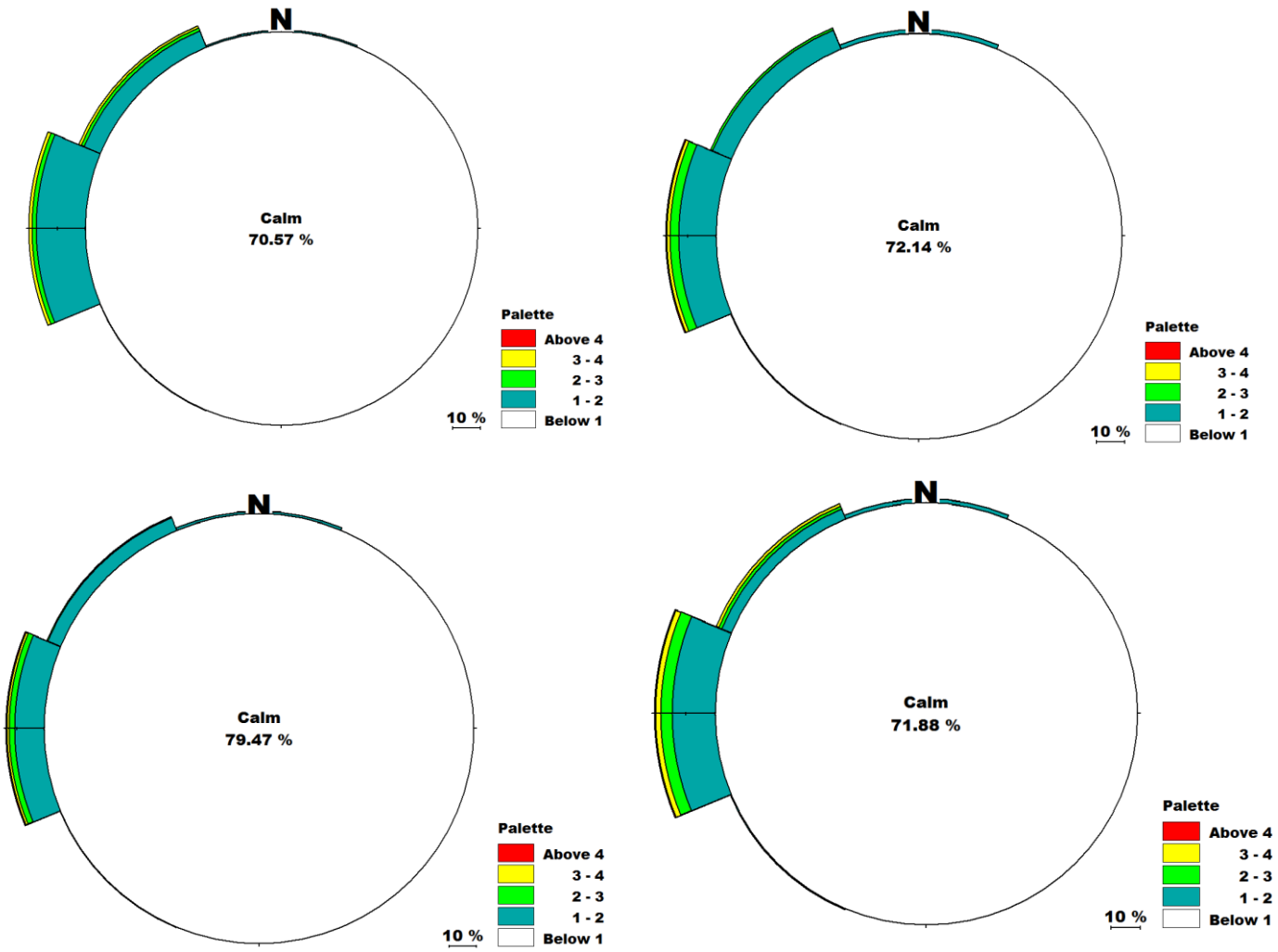

Figure 5.6 Ashdod wave rose. Top left: 1997, Top right: 1996, Bottom left: 1995, Bottom right: 1994

It is clear from the figures above that the mean wave direction is consistent during the three years in Alexandria and the four years in Ashdod. The prominent mean wave directions are North West and West which are the very similar in the two areas even though they are much far away from each other. This indicates that the mean wave direction from Ashdod, which is 24-kilometer far from Ashkelon, can be used in this study. Table 5.1 compares the mean H_s values and the mean T_p values during winter at Ashkelon in 2015 and at Ashdod in 1994. The values are very close indicating again that the wave data at Ashkelon in 2015 can be supplemented with the data from Ashdod in 1994 on mean wave direction. This approach was considered in this study to run the numerical models.

Table 5.1: Mean values of H_s and T_p at Ashdod 1994 and Ashkelon 2015

	Ashdod, 1994		Ashkelon, 2015	
Month	**Mean Hs**	**Mean T_p**	**Mean Hs**	**Mean T_p**
December	0.6	6.7	0.6	6.0
January	1.2	7.0	1.1	7.2
February	1.4	7.9	1.4	7.7

Figure 5.7 and Figure 5.8 show the trend of the mean H_s value and the mean T_p value respectively during the winter period (December to February) in Ashdod. All significant wave heights and peak periods have been considered for the analysis that shows a negative trend in the computed linear fits. Since the negative slope is very mild, one conservatively may assume that the wave climate obtained in a certain year is constant along the upcoming years for predicting the morphological changes due to constructing Gaza Seaport.

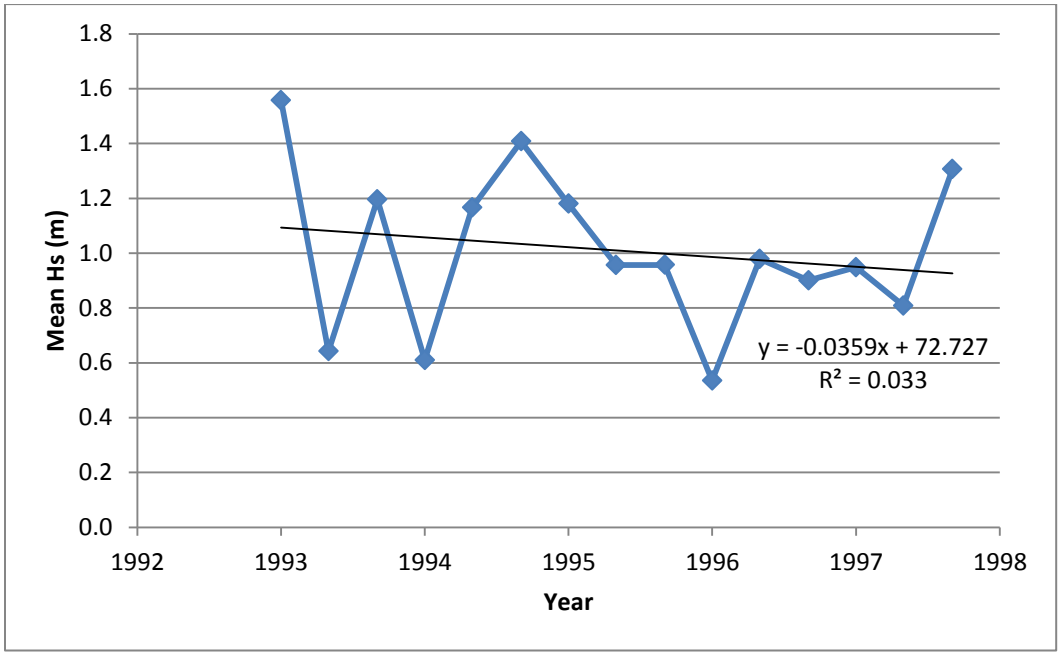

Figure 5.7: Average significant wave height for winter season in Ashdod (1993-1997)

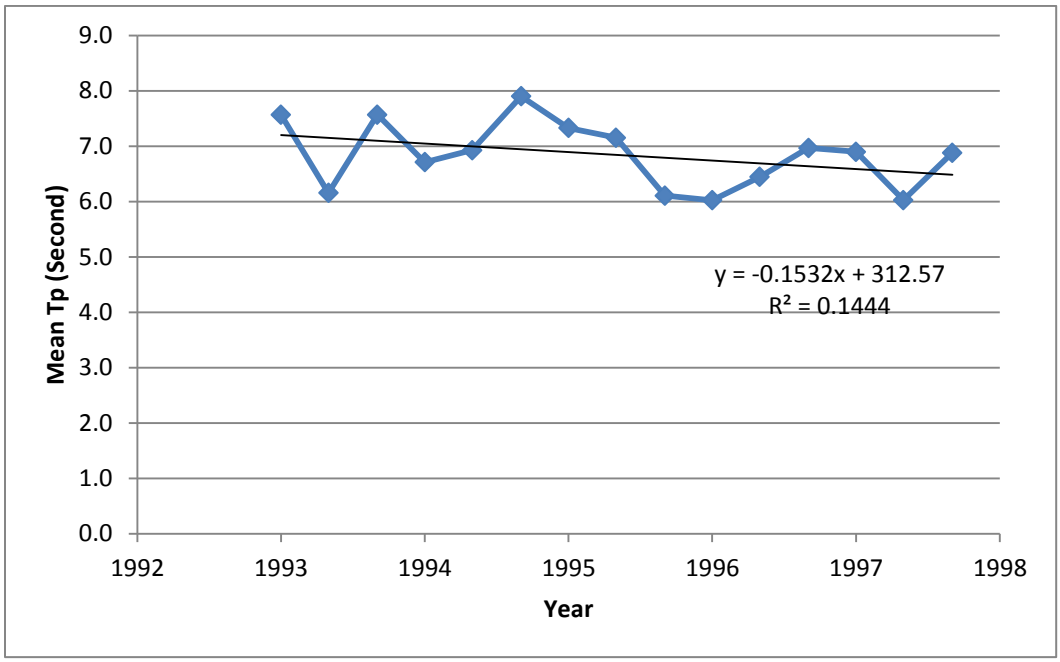

Figure 5.8: Average peak period for winter season in Ashdod (1993-1997)

5.1.3 Water Level and Tides

Tidal data at the boundaries were obtained from MIKE C-MAP tidal stations. Figure 5.9 shows the closest two tidal stations to Gaza Seaport namely: Port Said and Sour. As it appears in the figure below, these two stations are too far away from the site of interest. Therefore, the tidal data obtained from these two stations was used as boundary conditions for a large model in order to obtain the water level at the boundaries of a smaller model around the site of interest. Further in this study, it is referred to the large model as the regional model and to the small model as the local model, see Figure 5.10.

Figure 5.11 and Figure 5.12 show the tidal level variation for the first two months in 2015 at Port Said and Sour respectively. The tide at Port Said station has a semi-diurnal characteristic whereas the tide at Sour station has a mixed semi-diurnal characteristic. The maximum tidal range for the two stations in February is 0.46 m.

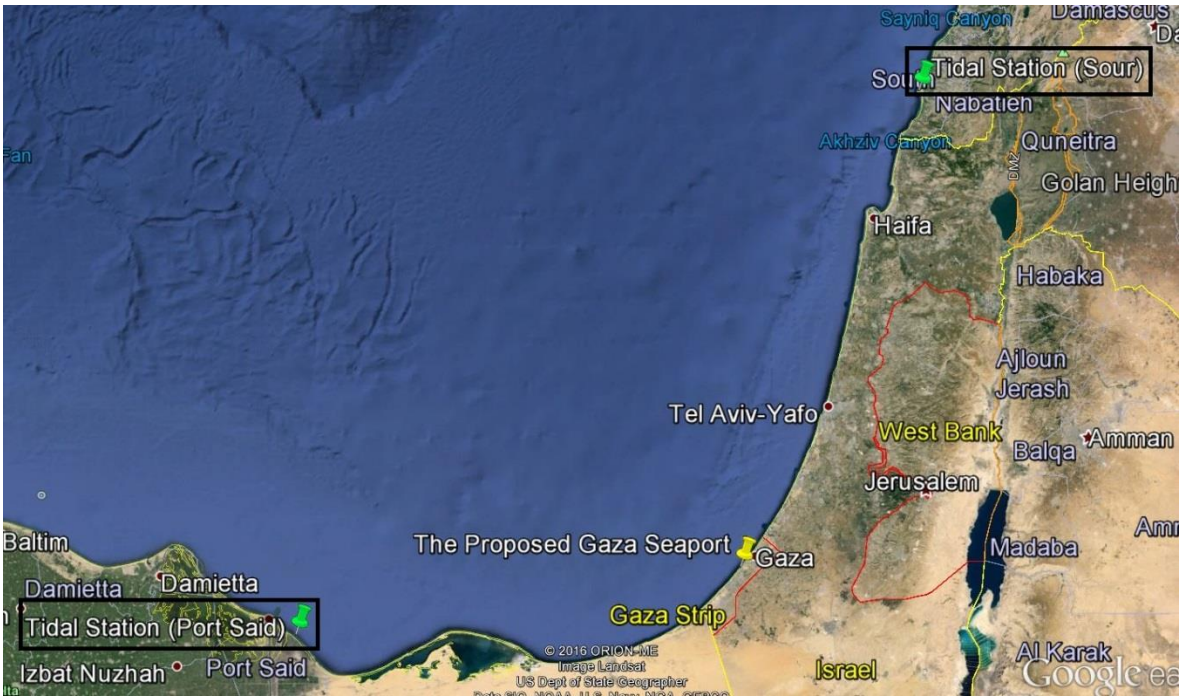

Figure 5.9: Available tidal stations (Source: Google Earth, 2016)

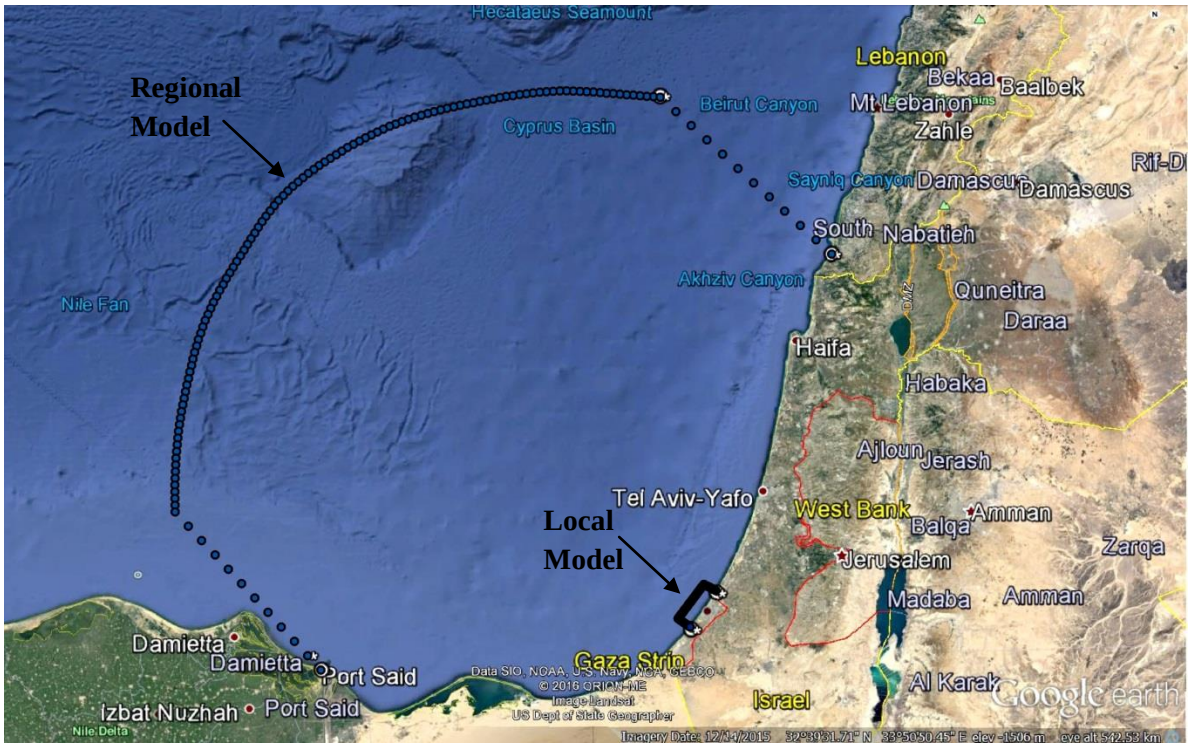

Figure 5.10: Regional and local models (Source: Google Earth, 2016)

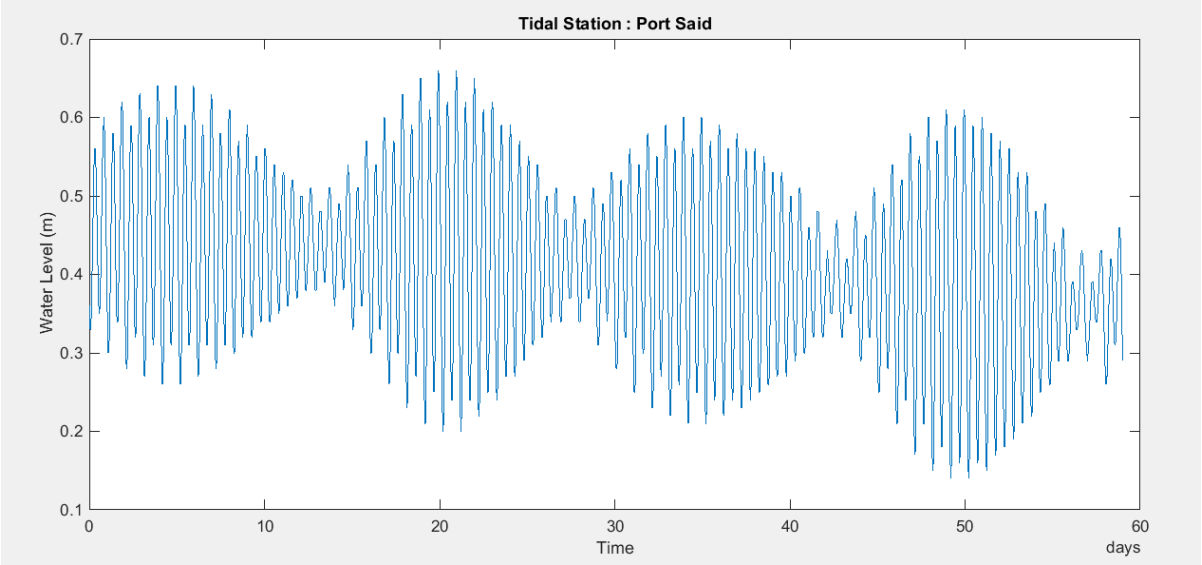

Figure 5.11: Tidal Elevation at Port Said in January and February 2015 (Source: MIKE C-MAP)

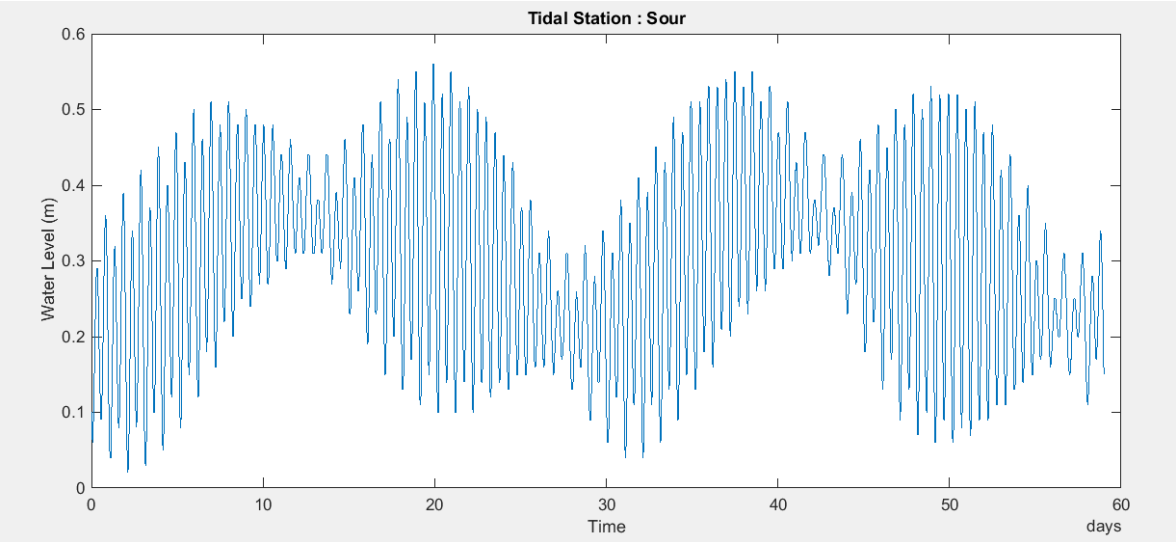

Figure 5.12: Tidal Elevation at Sour in January and February 2015 (Source: MIKE C-MAP)

5.1.4 Wind

The Hydrodynamic Module of MIKE 21 FM was run for the regional model in order to get the water levels at the boundaries of the local model. Wind data is required as an input for this simulation and as the area of the model is quite large, wind grid series was used. Wind data used in the simulation is extracted from ECMWF database. It is available in the form of resolved wind velocity components in east and north direction. Figure 5.13 shows the locations of wind data found from ECMWF database.

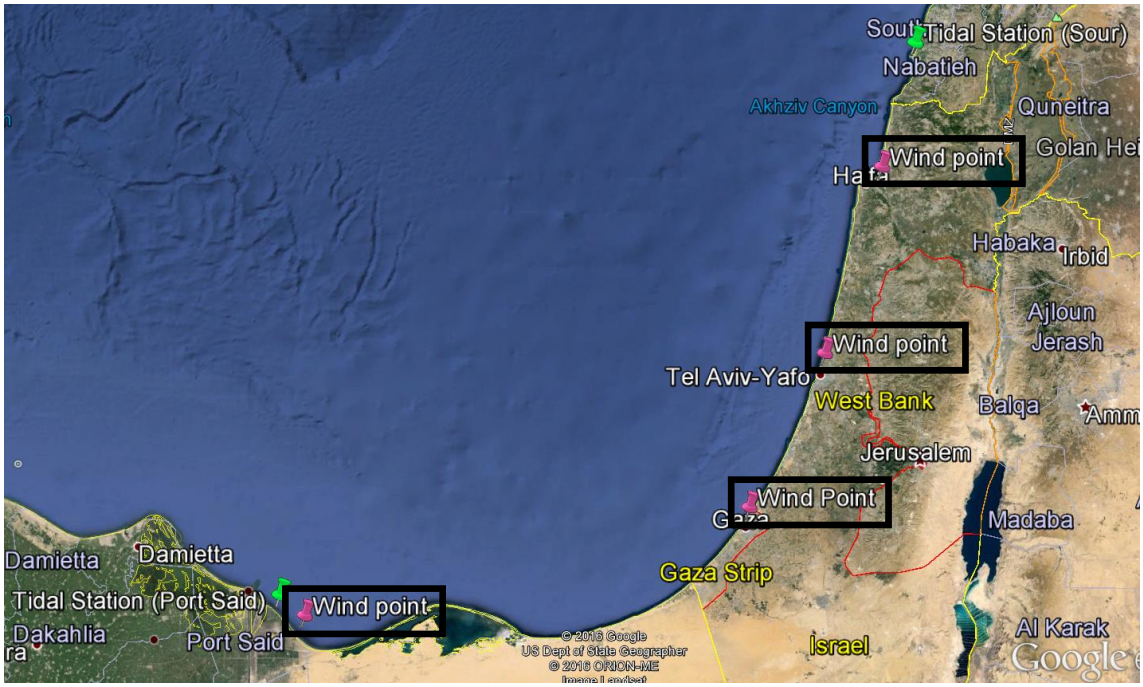

Figure 5.13: Locations of wind data found from ECMWF database

Field measurements of wind speed and wind direction at the coast of Gaza are available from the wind gauge shown in Figure 5.14 for the year 2015. This data was used in the simulation of the local model to predict sediment transport around the proposed Gaza Seaport.

Figure 5.14: Location of the wind gauge (Source: Google Earth)

The measured wind data is used to generate a wind rose diagram over the year 2015 as shown in Figure 5.15. Wind distribution demonstrates that the prominent wind direction is North West and West with an average wind speed of 1.96 m/s. The time series of wind speeds measured hourly at the coast of Gaza is given in Figure 5.16.

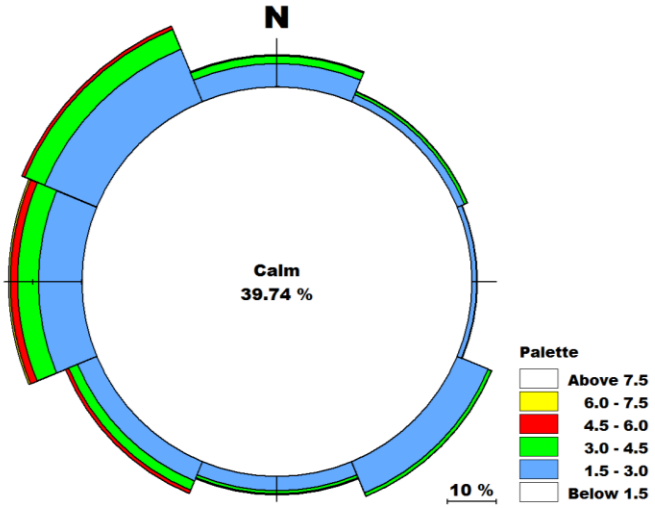

Figure 5.15: Wind rose at the coast of Gaza

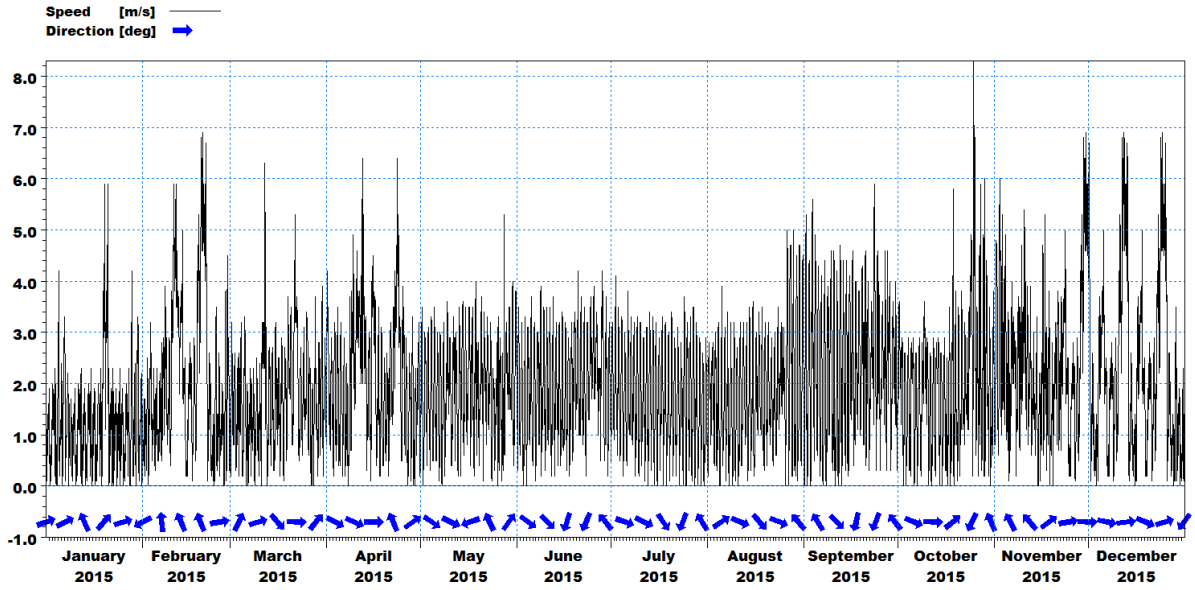

Figure 5.16: Time series of wind speed (wind direction indicated with blue arrows) for 2015 at Gaza wind gauge

Figure 5.17 shows that there is a considerable difference between the wind speeds obtained from field measurements at the coast of Gaza and the wind speeds obtained from global modelling (ECMWF database). The filed measurements are much lower and that is questionable. Nevertheless, wind speeds measured at the coast of Gaza are used further in the local model simulations since they are the only available wind data for the area of interest, ECMWF database has wind data at positions outside the domain of the local model.

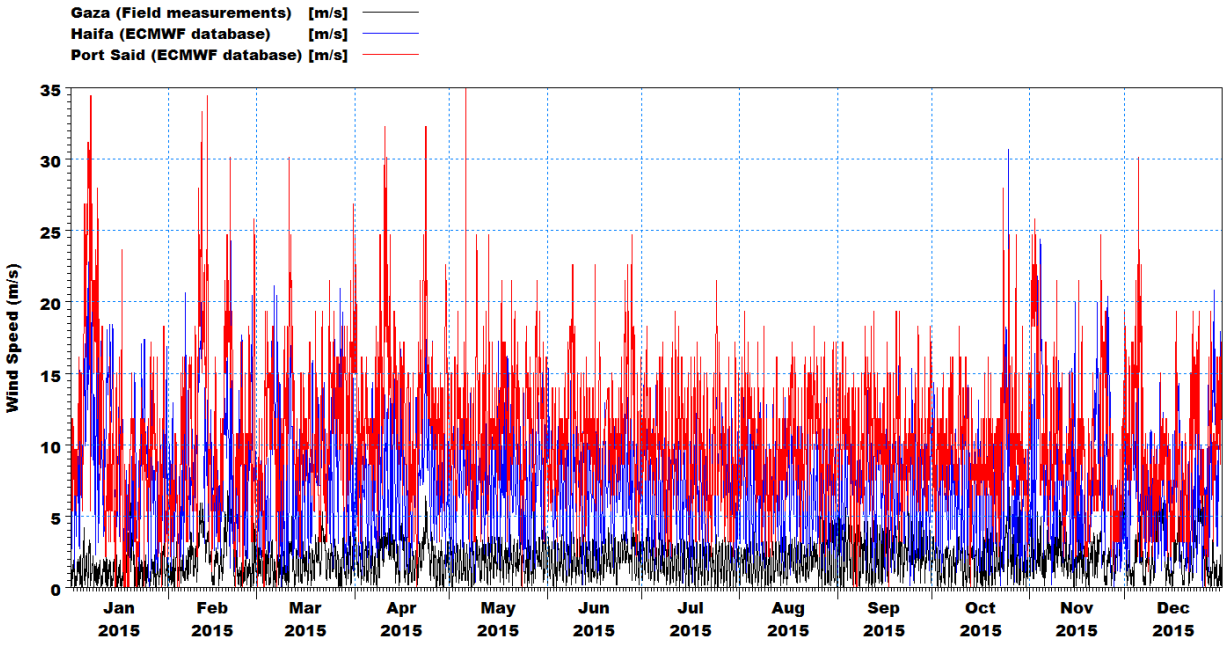

Figure 5.17: Comparison between wind speeds obtained from field measurements and ECMWF database

5.1.5 Sediment Properties

The coastal profile at the coast of Gaza can be divided into the seabed, the beach, the dune face, and the adjacent body of the dune. The coastal profile consists mainly of sand with an average grain size of 0.27mm diameter. Nonetheless, it has also erosion-resistant formations of rock and kurkar (the regional name of aeolian quartz sandstone with carbonate cement) protrude on the seabed, on the beach, and in the cliffs. A geophysical survey for the proposed seaport showed the presence of non-erodible layers at a mean distance of about 3m below the alluvial seabed. Moreover, a detailed bathymetric survey of the area of interest showed that between the shoreline and 10 m depth the seabed is characterized by areas of rock outcrops and linear features of sand bars (Sogreah, 1996).

Figure 5.18 and Figure 5.19 show the results of sieve analysis tests performed at a distance of 70m and 150m from the shoreline respectively at Deir Al-Balah City. The site of the tests is 7 km far away from the proposed seaport. These tests were performed at the Soil Laboratory in the Islamic University of Gaza (IUG) and the results were obtained by personal communications. The results were analyzed and plotted to be used further in this study. Figure 5.20 shows the characteristics of the seabed of Gaza strip.

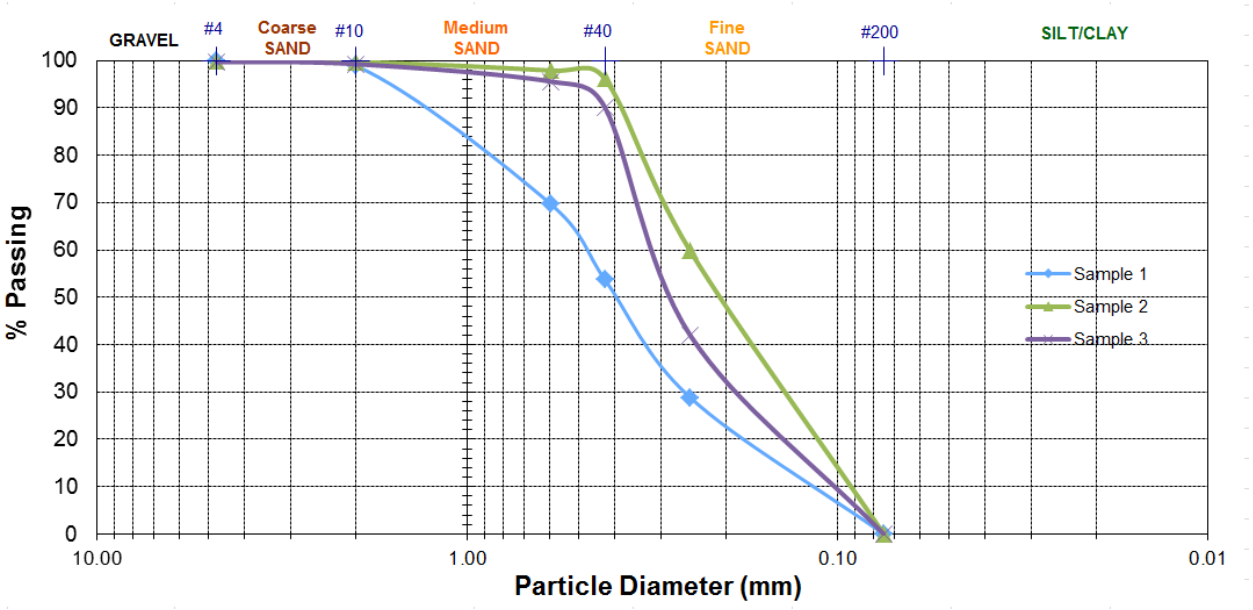

Figure 5.18: Sieve Analysis test for Gaza seabed at a distance of 70 m from the shoreline

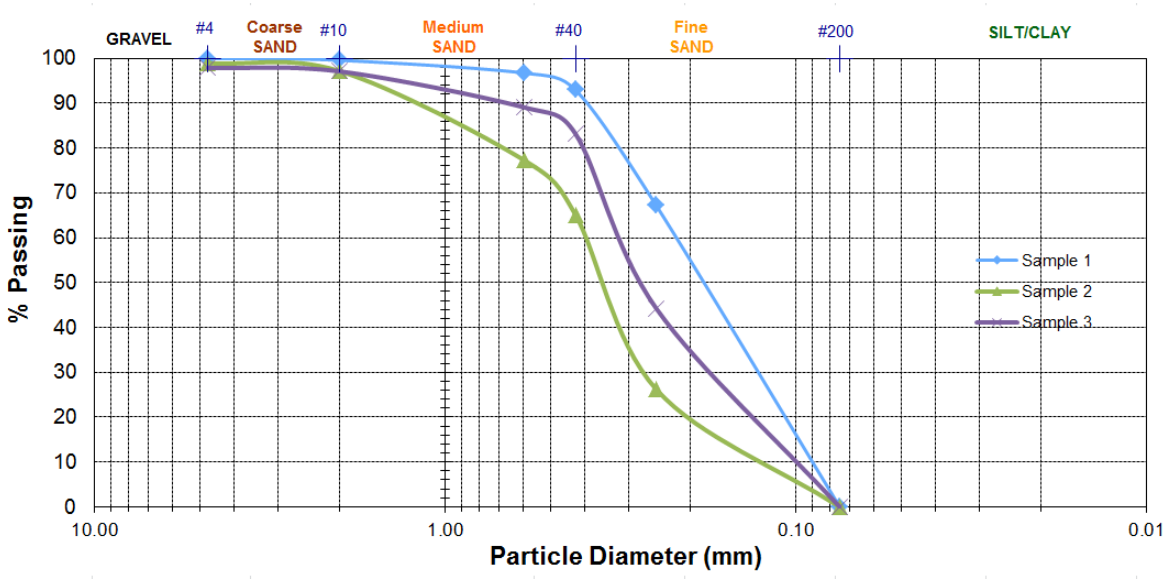

Figure 5.19: Sieve Analysis test for Gaza seabed at a distance of 150 m from the shoreline

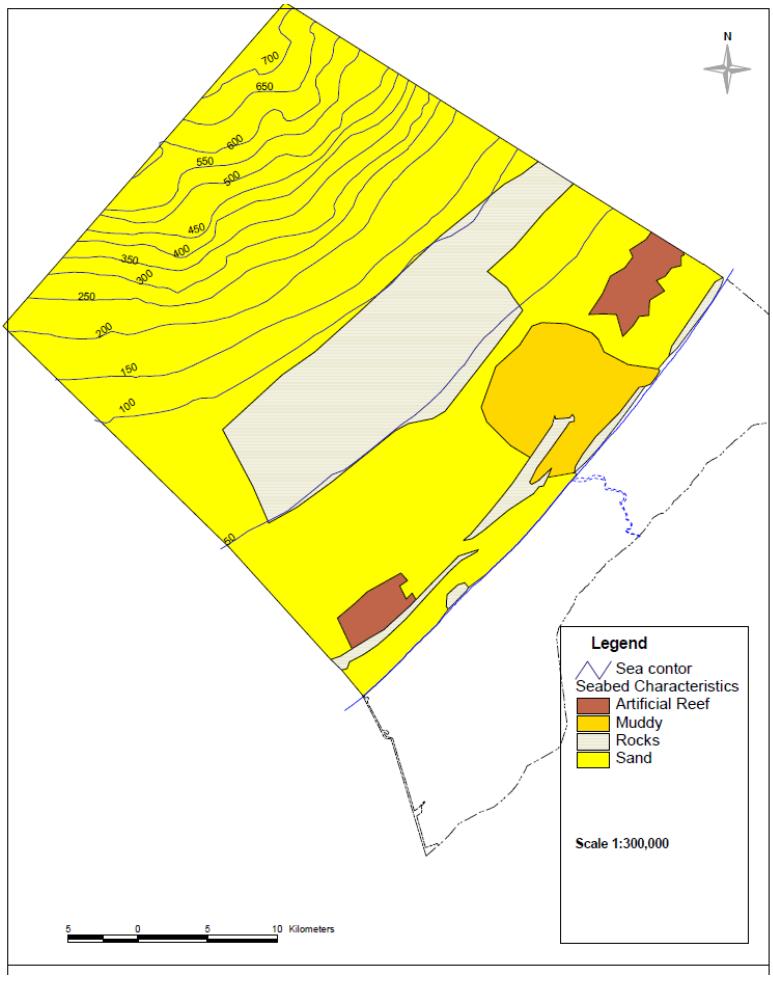

Figure 5.20: Seabed characteristics of Gaza Strip (Source: Palestinian National Authority, 2001)

5.2 Model Set-up (MIKE 21)

The modelling of flow, waves, sediment transport and morphological change is done using the MIKE 21 FM model. The model calculates waves (MIKE 21 SW), flow (MIKE 21 HD), sediment transport and morphological evolution (MIKE 21 ST) on an unstructured mesh and in a sequential and fully integrated manner.

5.2.1 Regional Model

The regional model area covers 350 km in the alongshore direction and 125 km in the cross shore direction. The MIKE 21 HD model was run using the water levels of two tidal stations namely: Port Said and Sour. Zero flux was selected at the offshore boundary condition. This model was run using gird series of wind data obtained from ECMWF database as was discussed in Paragraph 5.1.4. The MIKE 21 HD was used to calculate the water levels at the boundaries of the local model. Figure 5.21 shows the unstructured mesh used in the regional model. This mesh was generated with a maximum element area of 1×10^6 m^2. A fine mesh could be used to improve the results but it would be expensive since the model area is very large.

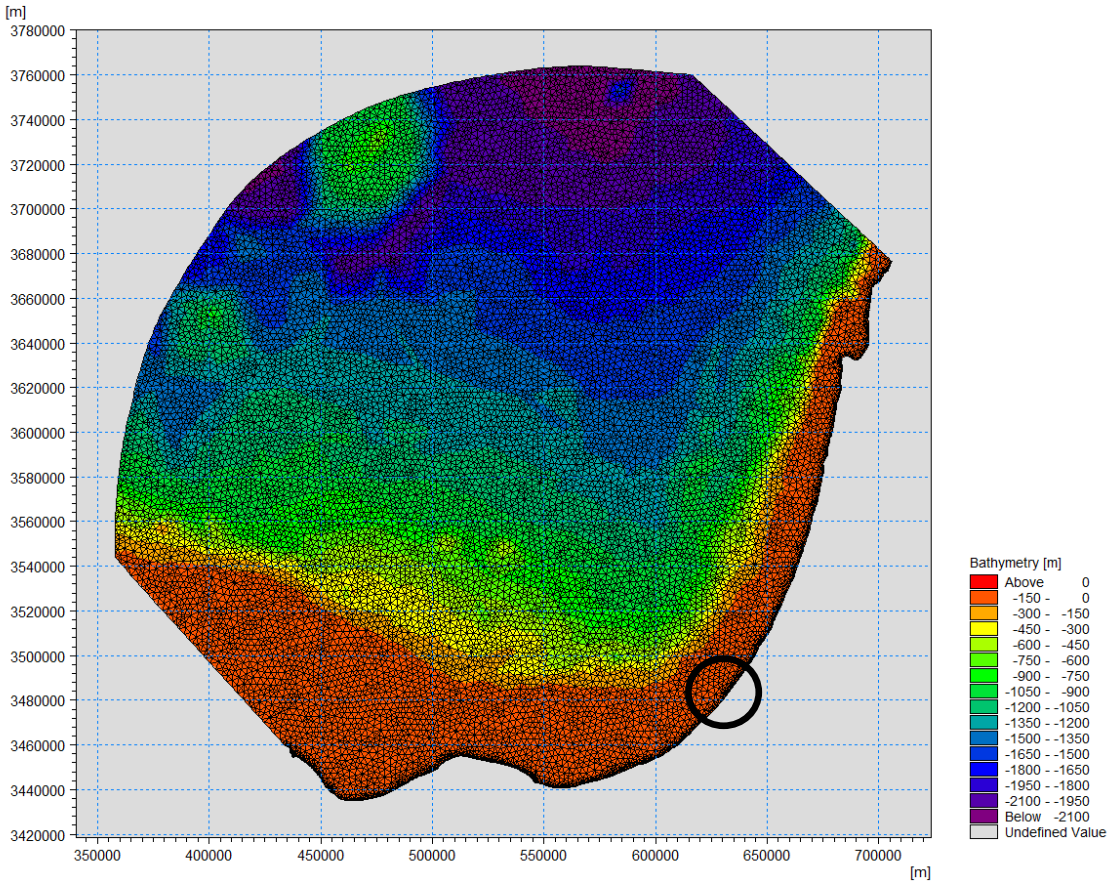

Figure 5.21: Mesh used in the model run to obtain the water levels

5.2.2 Local Model

The local model area covers 22.6 km in the alongshore direction and 7.8 km in the cross shore direction.

5.2.2.1 Bathymetry and Seaport Layout

Figure 5.22 shows the model bathymetry with the proposed Gaza Seaport. The wave, flow and sediment transport description is refined towards the area of interest. In the vicinity of the seaport the resolution of the bathymetry is increased in order to enhance the results. The unstructured offshore mesh was generated with a maximum element area of 5×10^3 m^2, whereas the unstructured mesh in the vicinity of the seaport was generated with a maximum element area of 0.5×10^3 m^2, see Figure 5.23.

Gaza Seaport with its all facilities including terminals and a breakwater is imposed as shown in Figure 5.22. A closer view of the area marked by the black box is shown in Figure 5.23. The width of the entrance, from the foot of the breakwater to the edge of the terminal, is 450 m.

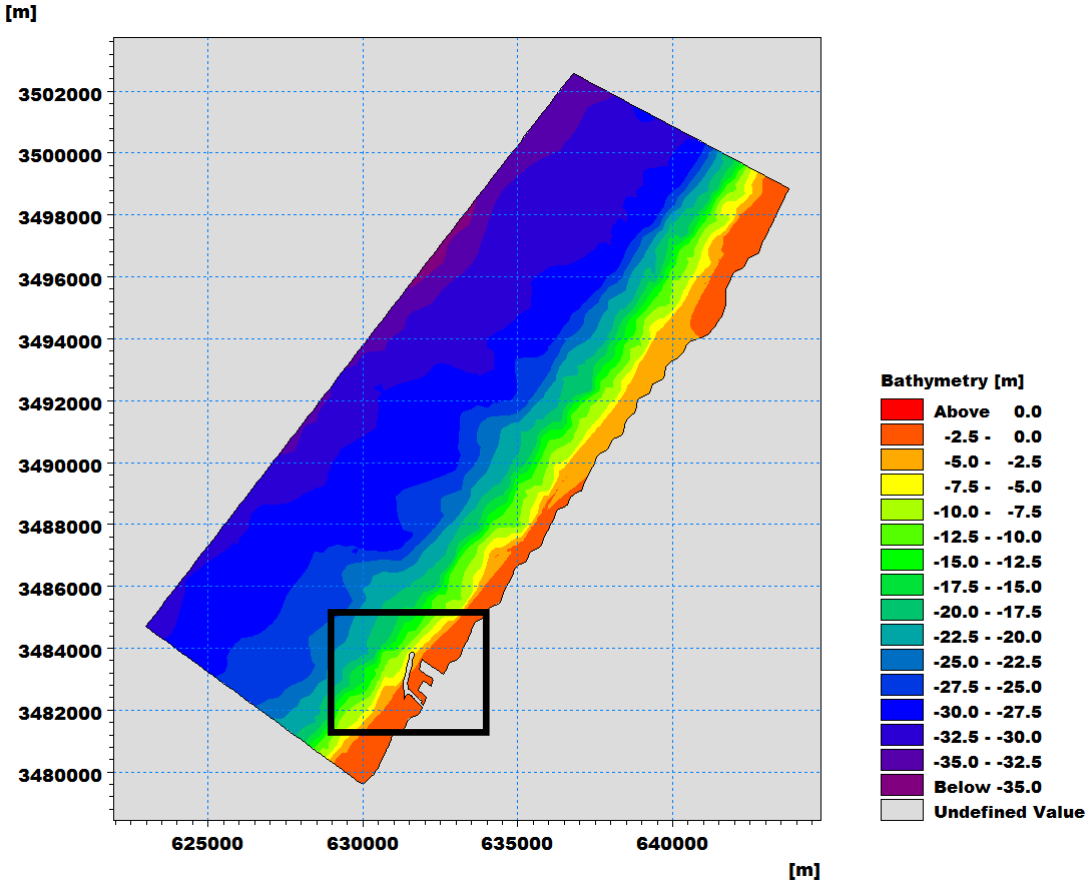

Figure 5.22: Model bathymetry with the proposed Gaza Seaport

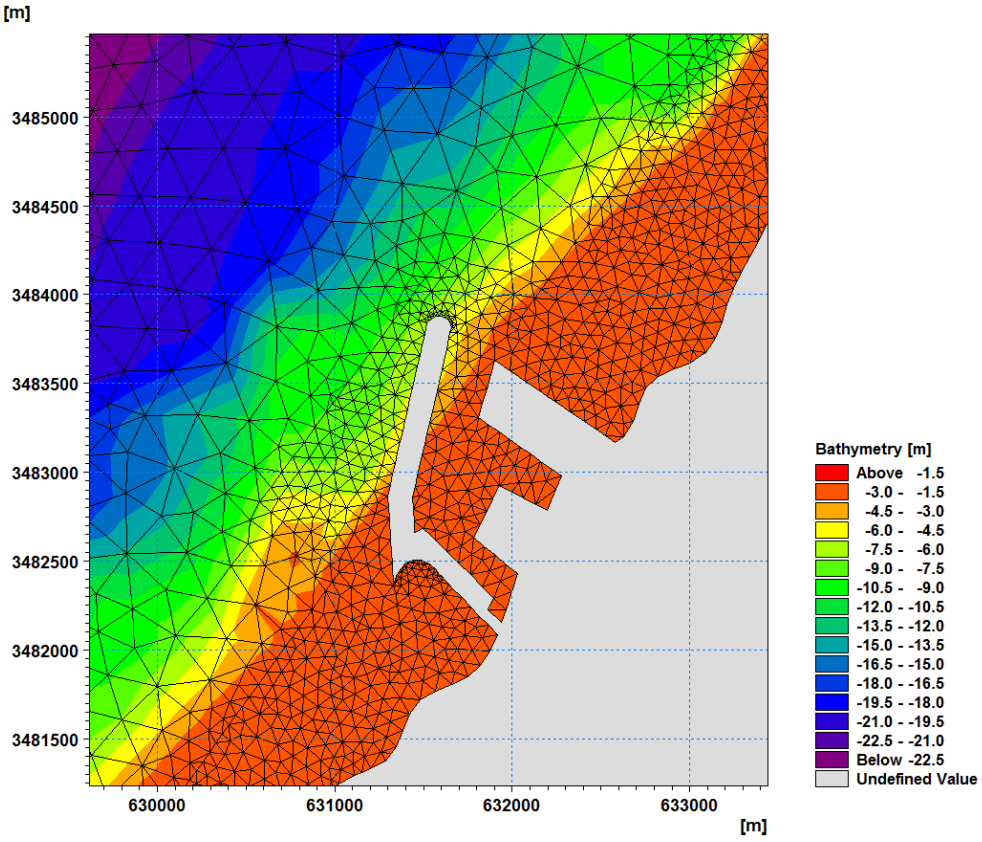

Figure 5.23: Model bathymetry with the proposed Gaza Seaport (Closer view)

5.2.2.2 Flow

The MIKE 21 HD was also run for the local model to calculate the flow which is necessary for sediment transport calculations. The black circle plotted in Figure 5.21 indicates where the smaller model was nested.

5.2.2.3 Waves

A fully spectral wave model, MIKE 21 SW, was used to simulate the propagation of waves. The model includes all relevant wave phenomena, such as shoaling, breaking, refraction, and local wind generation. The simulation period of this model was a year; from January 2015 to December 2015.

The wave parameters (significant wave height (H_s), peak period (T_p), wave direction and directional spreading) were specified at the boundaries. Measurements obtained at Ashkelon station were used at the northern boundary. As there is no wave data available in the southern direction, it was assumed that southern boundary has the same wave data as the northern boundary in order to run the simulation. A lateral boundary condition is used along the offshore boundary. This type of boundary condition is a good approximation when the boundary line is almost straight (DHI, 2012f). This information of the incoming waves in the start point and the end point of the offshore boundary are obtained from the connected boundary lines. Figure 5.24 shows the domain boundaries. The corresponding time series of waves for the two boundaries are given in Figure 5.25 and wave rose are represented in Figure 5.26.

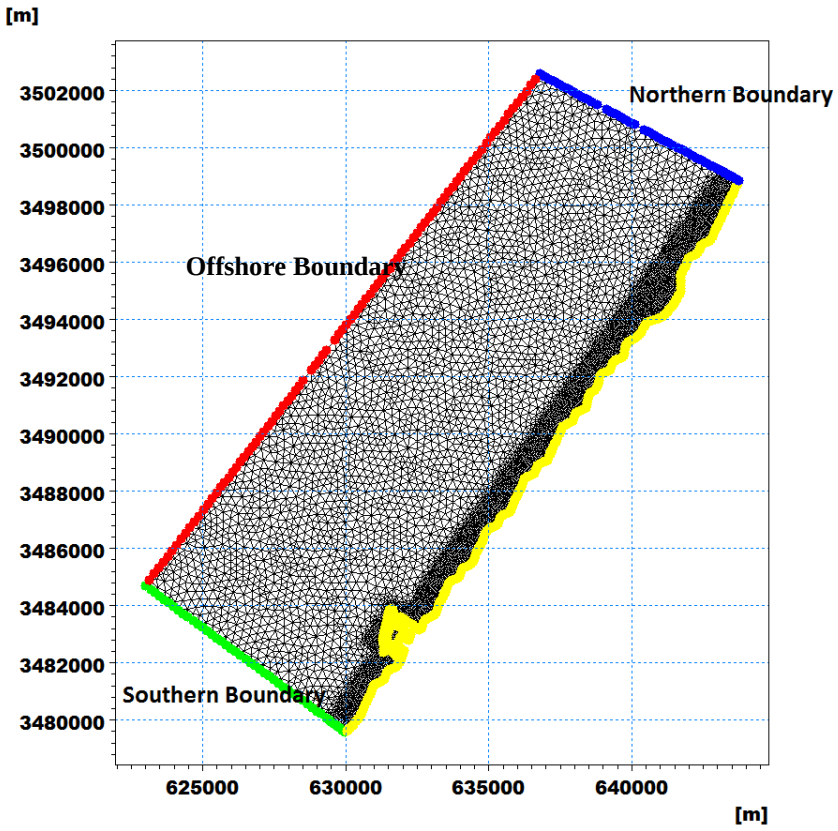

Figure 5.24: Domain boundaries

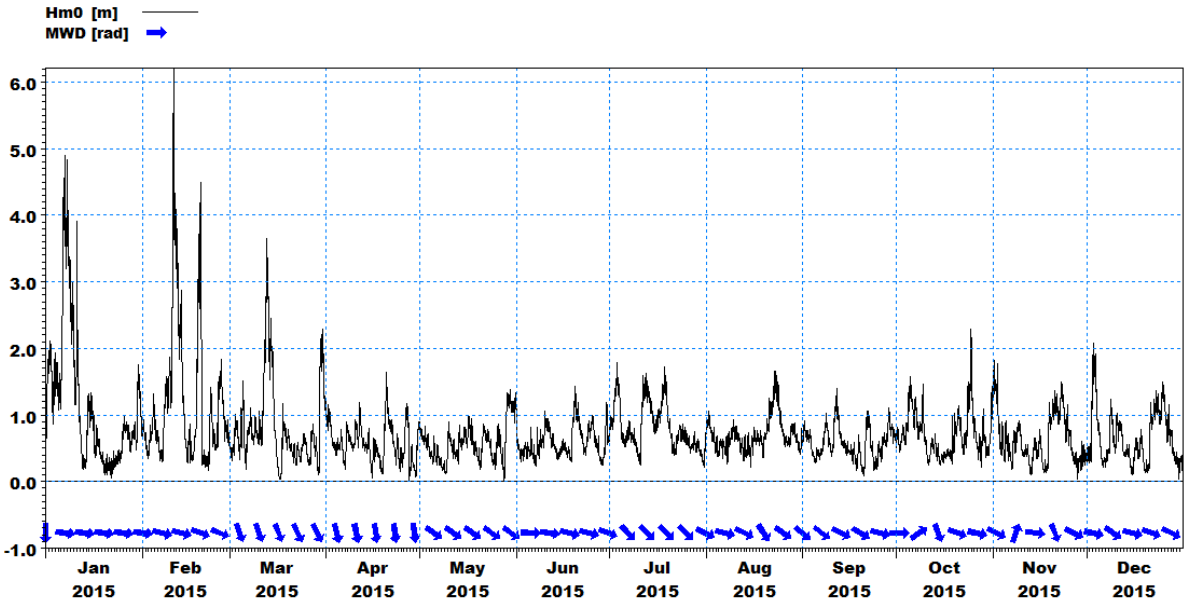

Figure 5.25: Time series of significant wave heights (wave direction indicated with blue arrows) for 2015 at Ashkelon station

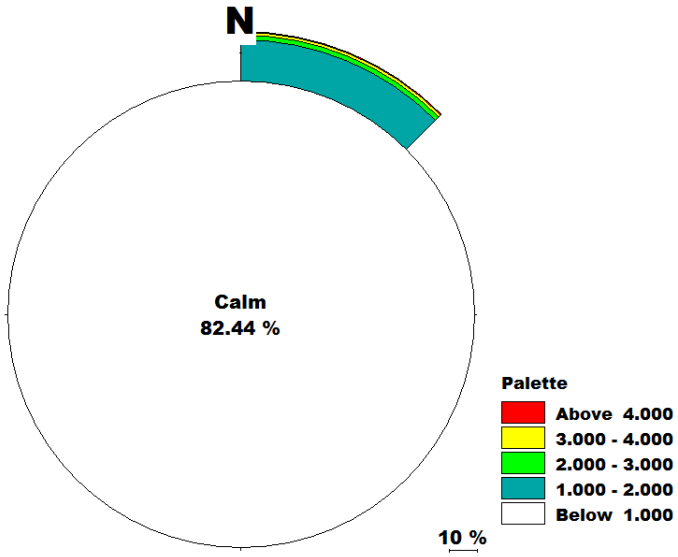

Figure 5.26: Wave rose at Ashkelon Station

Several parameters have to be determined before the simulation starts (see Table 5.2). MIKE uses Newton-Raphson iteration to calculate the wave parameters at each point from the original one.

Table 5.2: Parameters used to run MIKE-SW

Parameters	Value
Wave height	From Ashkelon Station
Wave period	From Ashkelon Station
Wave direction	From Ashdod Station
Wind force	From Gaza Station
Wave breaking constant	$H_b = 0.8*H_S$
Water level	Obtained from regional model simulation results
Bottom friction	Estimated 0.005 m
Current	Obtained from MIKE 21 HD results for the local model
Ice	No ice
Diffraction	Soothing factor=1
Fetch	Jonswap formula

5.2.2.4 Sediment Transport

The wave/current induced sediment transport and the associated morphological evolution in the study area were obtained by MIKE 21 ST. The sediment transport is calculated every time step using the information from MIKE 21 SW (wave height, wave period, mean wave direction and directional spreading) and MIKE 21 HD (water levels and currents).

The transport rates and the morphological evolution are calculated on the flexible mesh presented in Figure 5.27.

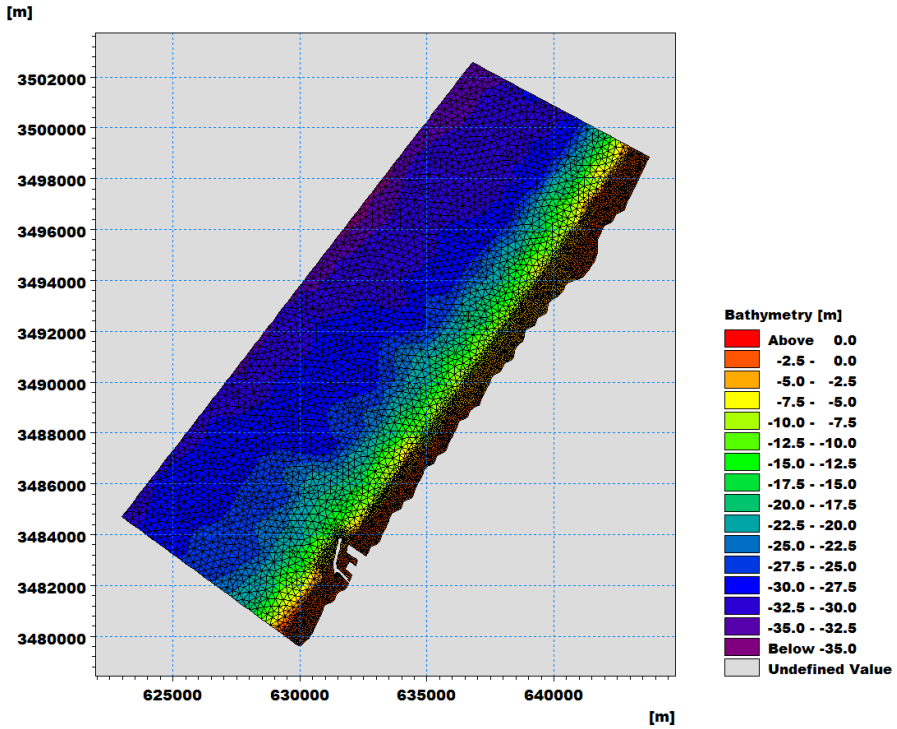

Figure 5.27: Flexible mesh used to run the model MIKE ST

The model requires information on the mean grain size, the relative density of the sand and porosity of the bed. As there are no sediment samples collected in the vicinity of the proposed seaport, the results from the experiments performed at Deir Al-Balah City are used and analyzed. As it is mentioned before, the site of these experiments is 7 km far away from the propose seaport. The mean grain size typically varies between 0.2 mm to 0.4 mm while the average grain size is 0.27 mm. The relative density of sand, *s*, is found to be close to 2.65. The porosity of the bed, *n*, is assumed to be 0.4.

The morphological modelling was done with a constant set of sediment parameters as follows:

d_{50} = 0.27 mm, s= 2.65 and n=0.4.

5.2.3 Summary

The flowchart below summarises the input data and the simulations run by MIKE 21.

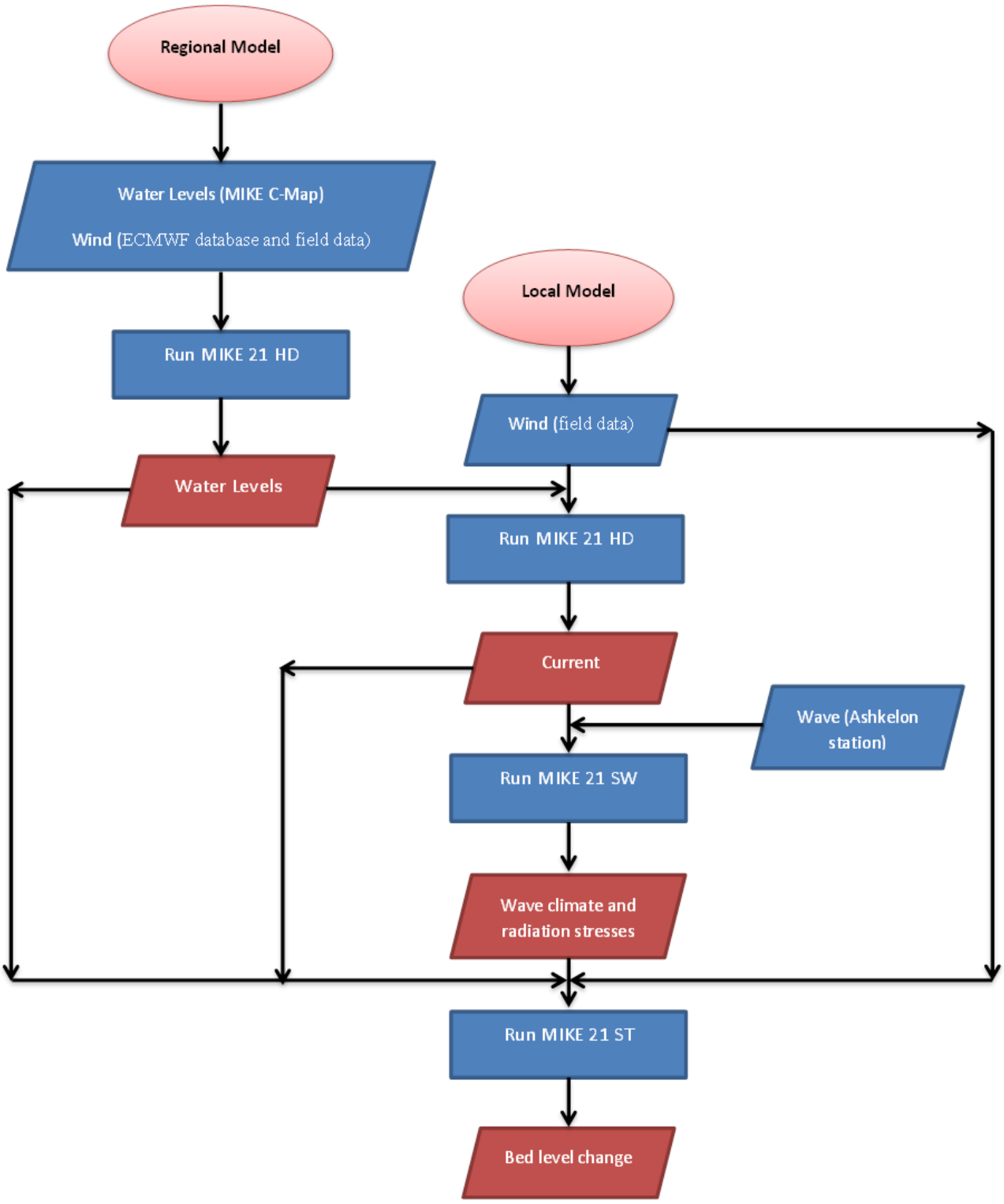

Figure 5.28: Summary of simulations run by MIKE 21

5.3 Model Set-up (LITPACK)

In this study, the mathematical modeling LITPACK is applied in order to predict the shoreline evolution in response to the proposed Gaza Seaport. The LITDRIFT model of the LITPACK software shows the annual shoreline sediment transport by adjustment of the cross-section profile. The LITLINE model of the LITPACK software predicts the shoreline morphological evolution. Input data required for both LITLINE and LITPACK models is described in the following paragraphs.

5.3.1 Cross-shore Profile

The cross-shore distribution of the transport within the surf zone is highly dependent on the shape of the cross-shore profile. For given wave conditions, the shape of the cross-shore profile determines the surf-zone properties, such as where and how violent the waves break and the width of the breaking zone. A steeper beach profile, for instance, results in a quicker loss of energy due to wave breaking and also larger driving forces for sediment transport. The main parameters that determine the shape of the cross-shore profile are wave climate, tidal variation and sediment properties.

The cross-shore profile extracted from MIKE C-MAP has inaccuracy in the first 200m seaward from the shoreline (see Figure 5.29). A nearshore coastal profile surveyed in 1986 at a location about 1 km south of the Gaza Fishing Port was used to correct the nearshore profile (see Table 5.3) (Palestinian National Authority, 2001). Consequently, the nearshore bathometry is obtained from the surveyed coastal profile and the bathymetry in deep water is obtained from MIKE C-MAP. Figure 5.30 shows the cross-shore profile used in the simulations. Note that the zero of the X-axis is at the shoreline in Table 5.3, but it is offshore at -10m depth in Figure 5.29 and Figure 5.30.

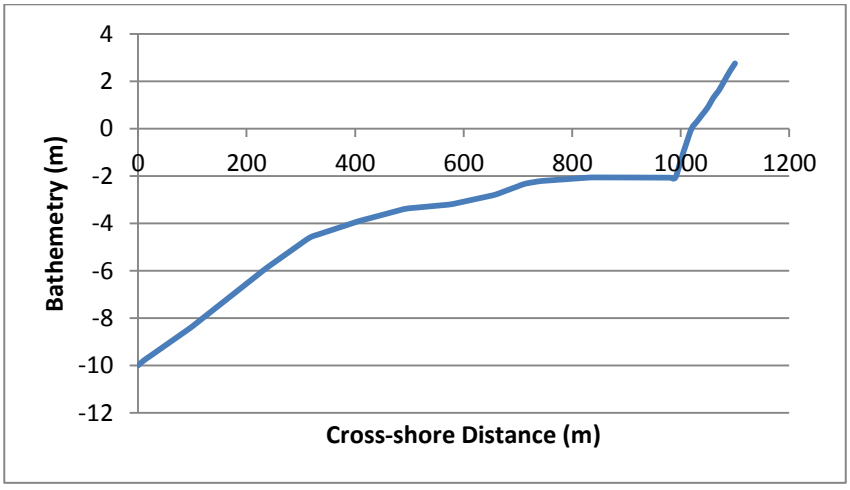

Figure 5.29: Cross-shore profile obtained from MIKE C-MAP

Table 5.3: Bathymetry of the sea of Gaza strip (Source: Palestinian National Authority, 2001)

Distance from shoreline (m)	Depth (m) below MSL
0	0
100	-2
200	-4
350	-6
500	-8
670	-10
870	-12
1070	-14
1260	-16
1460	-18
1660	-20

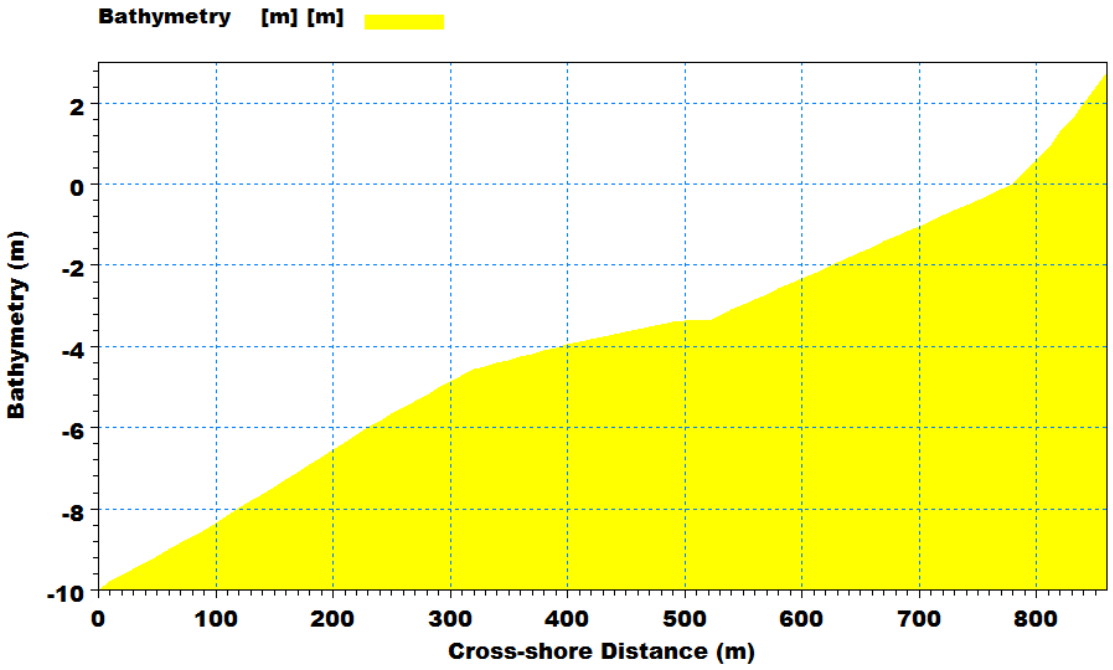

Figure 5.30: Representative cross-shore profile applied in LITLINE and LITPACK models

5.3.2 Coastline and Dune Position

Figure 5.31 shows that the coastline is almost straight around the proposed seaport. Therefore, the coastline and dunes are considered to be alongshore uniform in the model.

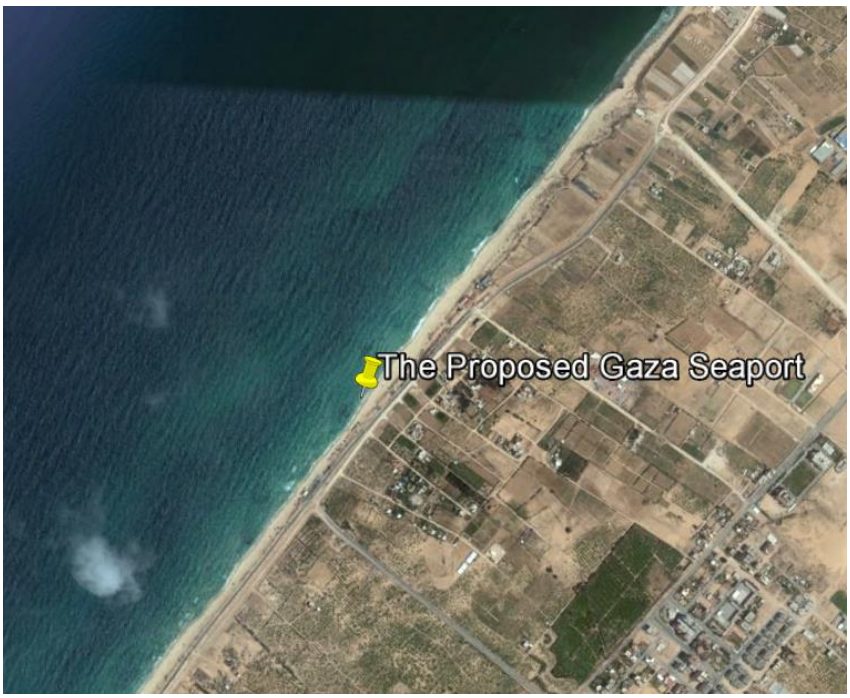

Figure 5.31: The shape of the coastline around the proposed seaport (Source: Google Earth, 2016)

The beach width is 80 m on average around the seaport (see Figure 5.32). The position of the coastline and dune are defined in the model at 0m and -80m respectively.

Figure 5.32: Beach width around the proposed seaport (Source: Google Earth, 2016)

Figure 5.33 presents various beach elements used in LITDRIFT and LITLINE model studies.

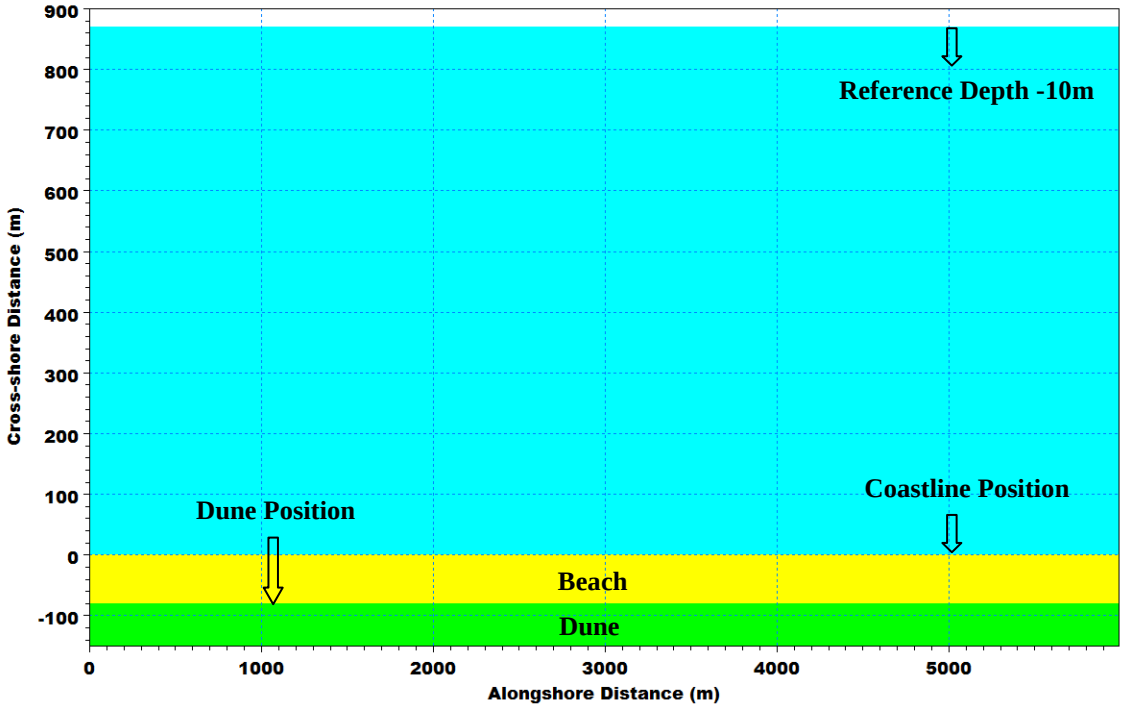

Figure 5.33: Representation of beach elements

5.3.3 Sediment Properties

Sediment transport is highly dependent on the sediment properties. The mean sediment properties in LITPACK include mean grain size distribution and density of sediment. The mean grain size distribution is represented by the mean grain diameter, d_{50}, and the spreading factor for grain sizes, $\sigma = \sqrt{\frac{d_{84}}{d_{16}}}$ (DHI, 2012b).

The hydraulic bed roughness K is one of the most important calibration parameters in LITDRIFT. It represents the roughness of the bottom faced by the longshore current.

For information about the sediment properties, some bed samples obtained at Deir Al-Balah City are used in this study. This investigation provided information as given below in Table 5.4. The numbers as mentioned in the table below show a similarity throughout the tested area. The modelling results are of course dependent on these numbers. The hydraulic bed roughness was chosen after performing sensitivity analysis, see Paragraph 6.4.2.

Table 5.4: Bed parameters applied for the profile

Parameter	Value
Mean grain diameter (d_{50})	0.27 mm
Spreading factor for grain sizes ($\sigma = \sqrt{\frac{d_{84}}{d_{16}}}$)	2
Hydraulic bed roughness (k)	30×d_{50} (see Paragraph 6.4.2)

5.3.3.1 Ripples

When ripples are present, their roughness dominates the bed roughness and has a major effect on the sediment transport. In LITDRIFT, the user has three approaches with regards to considering ripples:

1. Enable ripple dimensions to be calculated based on the hydrodynamics in the model LITSTP. They are calculated based on formulations from (Nielsen, 1979).
2. Account for ripples by re-calculating the bed roughness where they are assumed to be present.
3. Do not explicitly consider ripples in the model setup.

The LITSTP model considers wave-generated ripples to exist when the effective shields parameter is less than one (DHI, 2012g). They are considered as large roughness elements. Their effect on sediment transport is mainly considered by calculating the increased roughness.

It is important to note that LITDRIFT does not take into account effects on the vertical velocity profile. When ripples are calculated to be present, the velocity profile is not corrected. This results in an unrealistically large velocity where there are ripples, which contributes to a larger sediment transport than what would be calculated with a corrected velocity profile.

The second approach is to account for ripples in the assignment of bed roughness along the beach profile. This approach requires a lot of assumptions. First, it is not feasible to make a time-varying roughness to account for sweeps and formation of new ripples, so a constant rippled condition has to be assumed. This may be fine for certain wave conditions but not for high energy conditions closer to shore. In practice, the third approach is often used, since a constant bed roughness is used as the main calibration parameter in LITDRIFT (DHI, 2012g). Ultimately, the third approach was used in this study.

5.3.4 Wave Climate

The results from MIKE 21 SW Model at a selected reference point of 10m depth are used as input data to LITPACK model, see Figure 5.34. A summary of the percentage of each significant wave height with respect to a certain wave direction is given in Table 5.5.

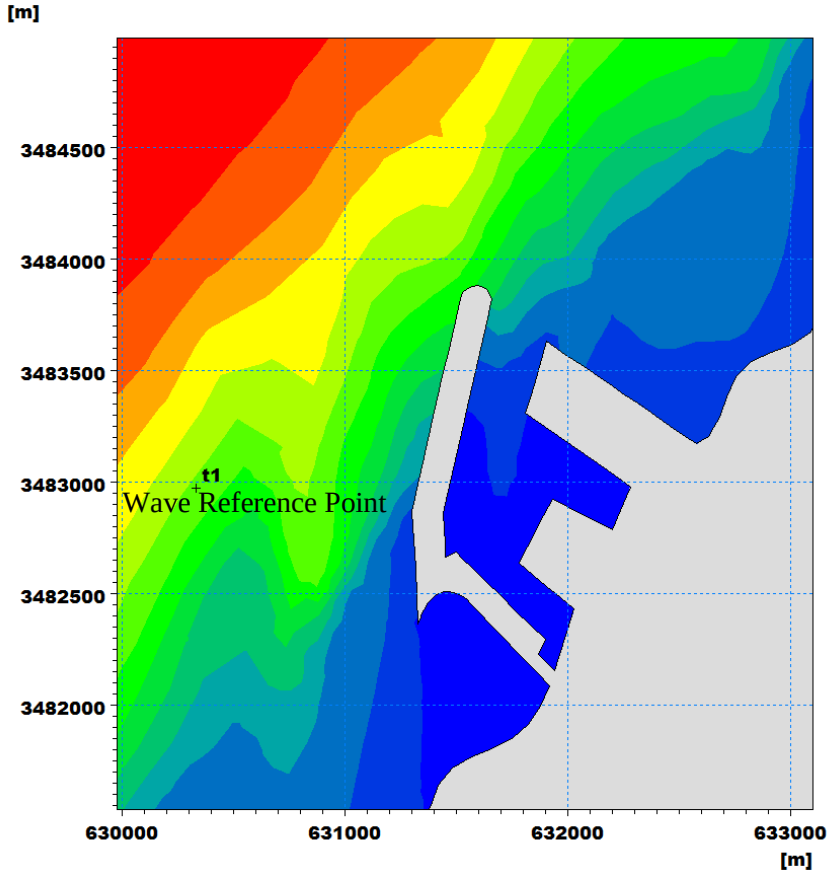

Figure 5.34: Results of MIKE 21 SW with the location of the wave reference point indicated.

Table 5.5: Wave percentages at the wave reference point in the study area

Hs/Direction	220-240	240-260	260-280	280-300	300-320	320-340	340-360
0-0.4	0.08	0.06	4.87	6.06	5.42	3.41	3.98
0.4-0.8	0.52	0.34	9.23	17.38	13.69	5.73	7.81
1.2-1.6	0.04	0.04	2.32	3.09	3.62	1.64	1.24
1.6-2.0	0	0	0	0	0	0	2.16
2.0-2.4	0	0	0	0	0	0	0.86
2.4-2.8	0	0	0	0	0	0	0.63
2.8-3.2	0	0	0	0	0	0	0.47

5.3.5 LITDRIFT Set-up Characteristics

All the input data described in the previous paragraphs was used to run the LITDRIFT model. The model was set up based on the characteristics given in Table 5.6. A single sediment description was used to represent the gradation curve. The critical shields parameter, the relation between destabilizing and stabilizing forces on a grain at the bed, is set to 0.045 taken from the literature (Engelund & Hansen, 1972). Sediment porosity of 0.4 was used. The wave theory used in the model was chosen to be the Stokes approach with a wave spreading factor of 0.6. The wave spreading factor is a reduction factor on the wave radiation stresses to account for directional waves. The factor 0.6 is typical for wind waves on a sandy beach.

It should be kept in mind that the model deals with transport capacities and does not consider the amount of available sediment.

Table 5.6: Set-up characteristics for the LITDRIFT model

Parameter	Value
Wave set-up calculation included	Yes
Currents included	Yes
Wind included	No
Sediment description	Single
Ripples included	No
Sediment density	2.65 g/cm^3
Critical Shields parameter	0.045
Sediment porosity	0.4
Wave theory	Stokes
Wave spreading factor	0.6
Description of bed concentrations	Deterministic

5.3.6 LITLINE Set-up Characteristics

Before simulating the coastline evolution by the LITLINE model, it is necessary to generate a transport table to use as input. For this purpose, program LINTABL was applied based on the characteristics given in Table 5.7.

Table 5.7: Set-up characteristics for the LINTABL program

Parameter	Value
Spectral distribution of waves	Rayleigh distribution
Sediment density	2.65 g/cm^3
Critical Shields parameter	0.045
Sediment porosity	0.4
Sediment description	Single
Ripples included	No
Reference depth	10m
Wave theory	Stokes
Description of bed concentrations	Deterministic
Water level included	Yes
Currents included	Yes

The input data required to run the LITLINE model was descripted in the previous paragraphs. The model was set up based on the characteristics given in Table 5.8.

Table 5.8: Set-up characteristics for the LITLINE model

Parameter	Value
Height of active beach	1.5m
Angle of normal to baseline	90
Limiting depth for off-shore contours	10m
Maximum active length	860m
Climatic description	Based on wave percentages at the reference point (Table 5.5)
Morphological update scheme	Update continuously
Modify transport tables	No

6 Results and Discussion

This chapter presents and discusses the results obtained from each model run in this study.

6.1 MIKE 21 HD

Water levels required to run the local model were obtained from the regional model as discussed earlier. Three profile series of water levels were extracted from the results of MIKE 21 HD in order to be used further in the simulations. Figure 6.1 shows the boundaries where the profile series were obtained.

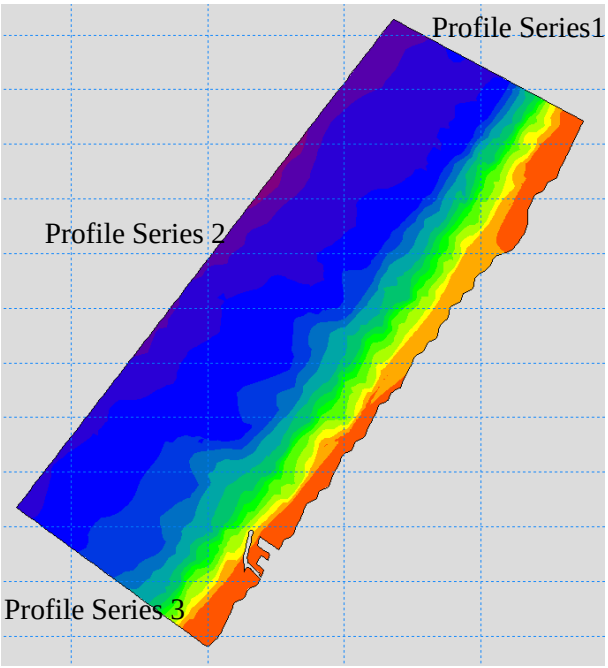

Figure 6.1: Location of the obtained profile series

To show a sample of the results, the water level at Ashkelon wave station was extracted and plotted. Figure 6.2 shows the water level at Ashkelon station in January and February 2015 resulted from the simulation. It appears from the figure that the tide at Ashkelon wave station has a semi-diurnal characteristic with a tidal range of 0.45m which is almost in line with the value found online (Tide-forecast, 2016).

The flow around the seaport was simulated using MIKE 21 HD with the three water level profiles. Figure 6.3 shows a snapshot of the current fields. The colours indicate depth-averaged speed whereas the vectors show the direction of the current (length of vector is proportional to the speed). It is clear that the current flows to the North direction which will carry sediments from south to north as it will be presented later.

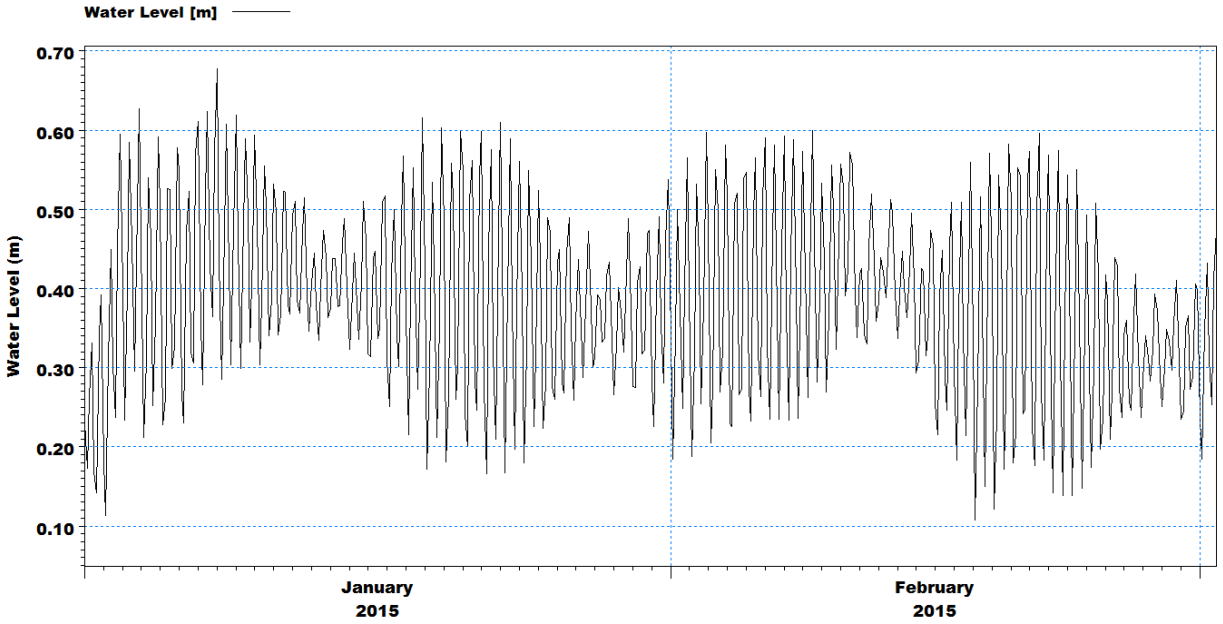

Figure 6.2: Water level at Ashkelon Station in January and February 2015 resulted from the simulation

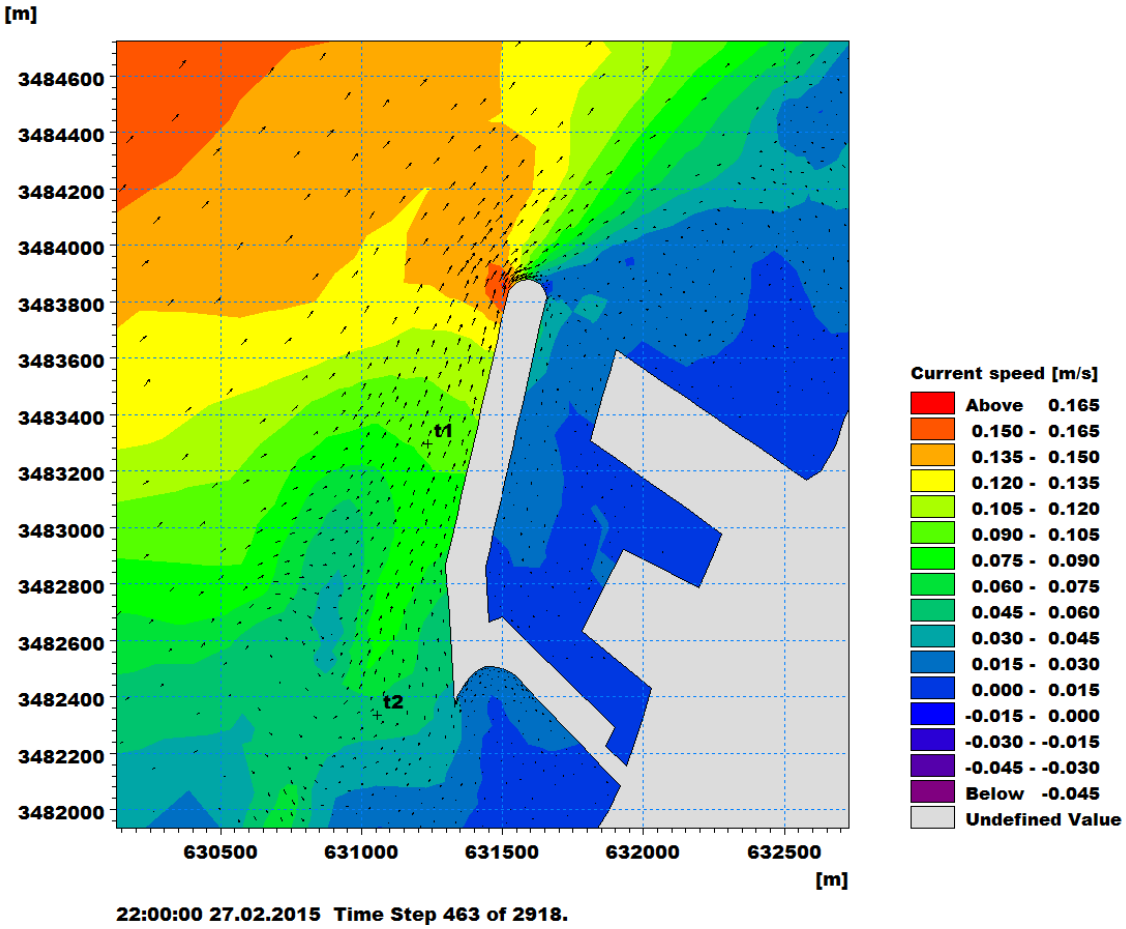

Figure 6.3: Snapshot of typical current fields

Results and Discussion

In order to check the variation of the current speeds and directions in front of the seaport, time series was extracted at two points, t1 and t2, marked at Figure 6.3. Time series plot of currents at point t1 is presented in Figure 6.4 with an average current speed of 0.095 m/s. Time series plot of currents at point t2 is presented in Figure 6.5 with an average current speed of 0.054 m/s. Average values of current are used for many purposes such as, port planning, ships mooring, estimation of longshore sediment transport and design of migratory fish cages.

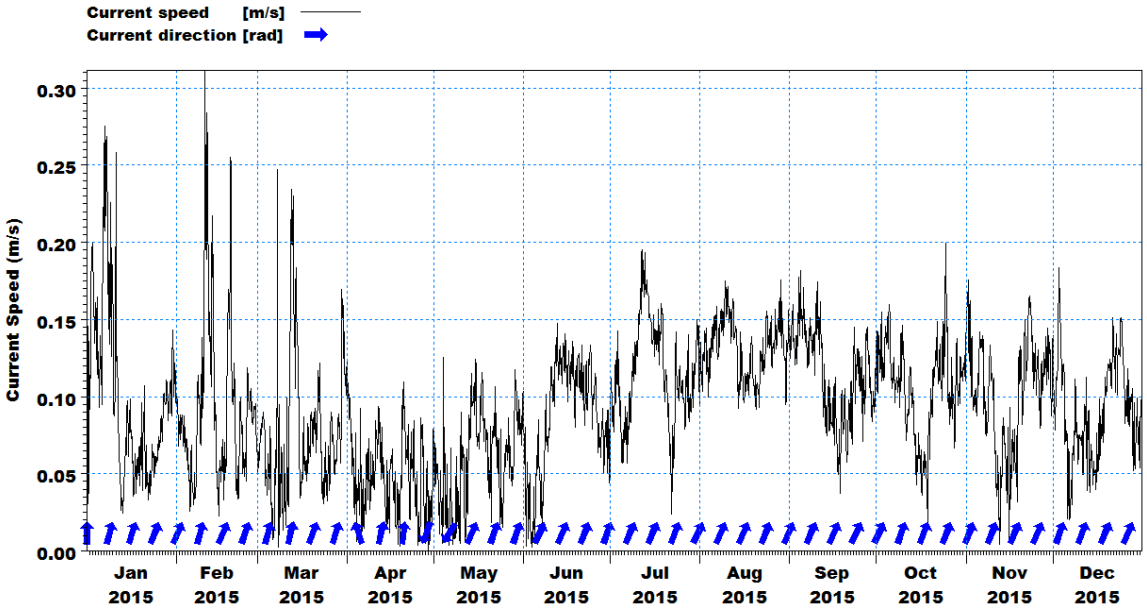

Figure 6.4: Time series of current speeds at point t1 marked at Figure 6.4

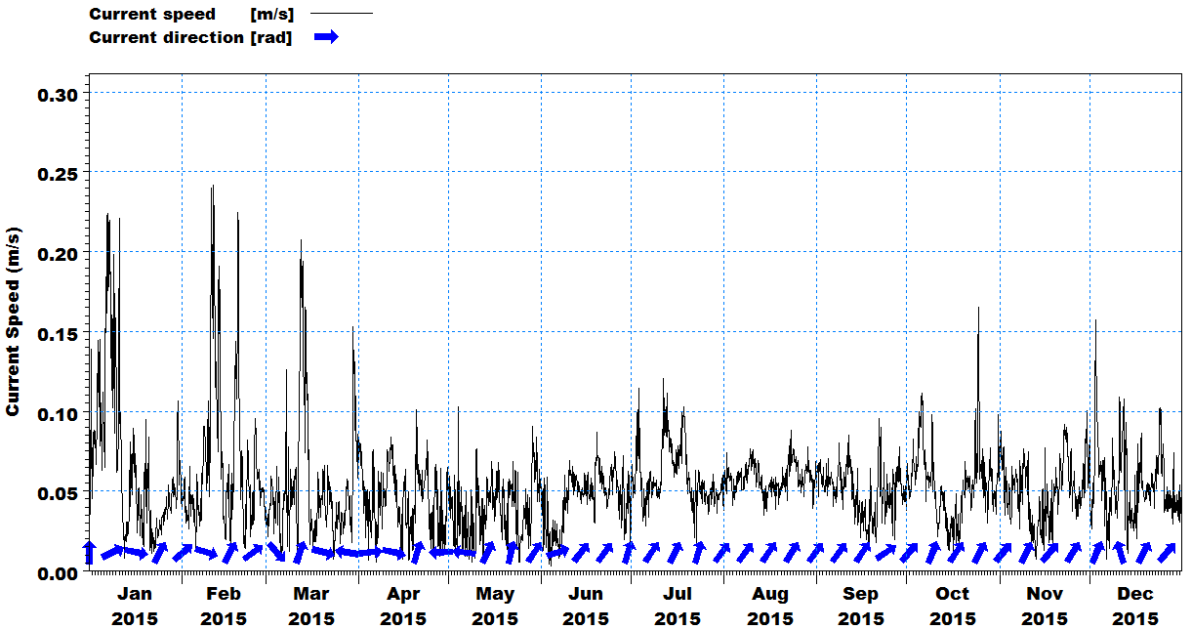

Figure 6.5: Time series of current speeds at point t2 marked in Figure 6.4

6.2 MIKE 21 Spectral Wave (SW)

The model calculates the distribution of wave heights, wave periods, mean wave directions and spreading of waves. It also calculates radiation stresses which drive the longshore current. These results are important to run MIKE 21 ST and LITPACK and will be used further in this study.

Figure 6.6 shows a snapshot of the resulting significant wave heights at certain time in February. In order to check the variation of the significant wave height in front of the seaport, time series was extracted at the point illustrated in Figure 6.6. The time series is presented in Figure 6.7. It can be seen that the highest significant wave heights take place in January and February. This makes sense because the highest wave heights in the northern Hemisphere take place in January and February due to winter storms. The mean significant wave height for the whole year is about 0.4m and the maximum significant wave height is 2.2m.

Looking at the fetch length, one may argue that the resulting significant wave heights from the simulations are too low. This may be explained by the low input wind speeds and the assumption of constant wind speed through the entire domain.

Figure 6.8 shows a snapshot of the resulting peak periods at certain time in February. In order to check the variation of wave period in front of the seaport, time series was extracted at the point illustrated in Figure 6.6. These time series is presented in Figure 6.9. It can be seen that waves are short and the mean T_p for the whole year is about 5.7 second.

Figure 6.10 shows a snapshot of the radiation stresses (S_{yy}) at certain time in February. In order to check the variation of the radiation stresses (S_{yy}) in front of the seaport, time series was extracted at the point illustrated in Figure 6.6. These time series is presented in Figure 6.11. It can be seen that the highest radiation stresses take place in January and February. This is logical since the highest wave heights are in January and February. The radiation stresses play a vital role in various coastal phenomena, such as wave-induced set-up, undertow and the generation of surf-beats.

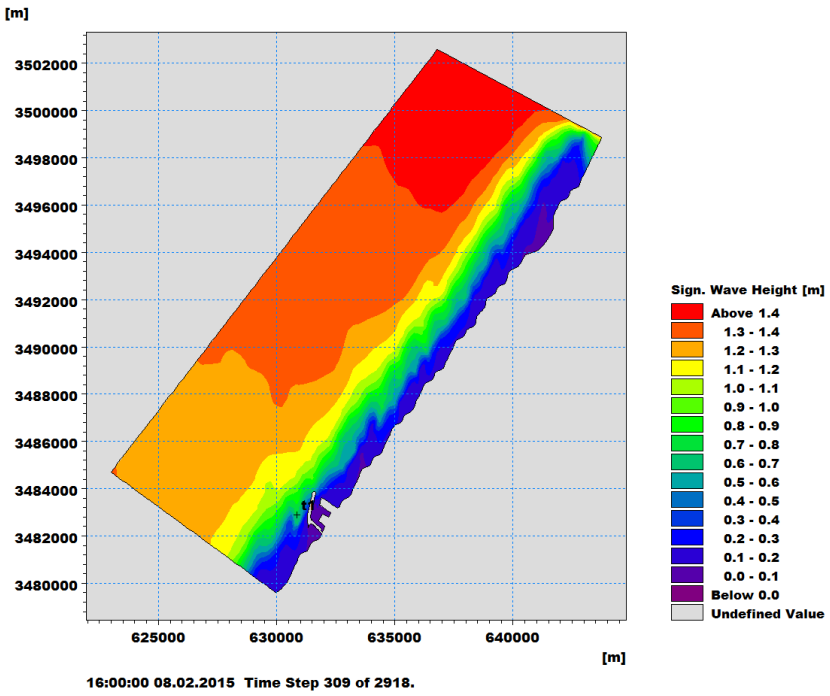

Figure 6.6: Map of the significant wave height (H_s)

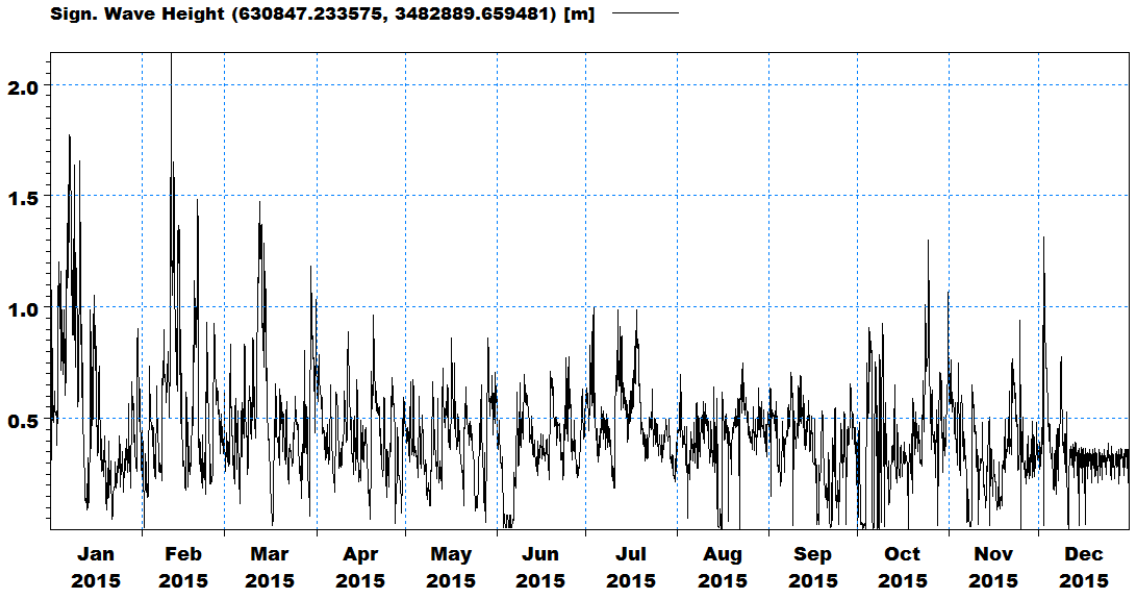

Figure 6.7: Time series of the significant wave height at the point marked in Figure 6.6

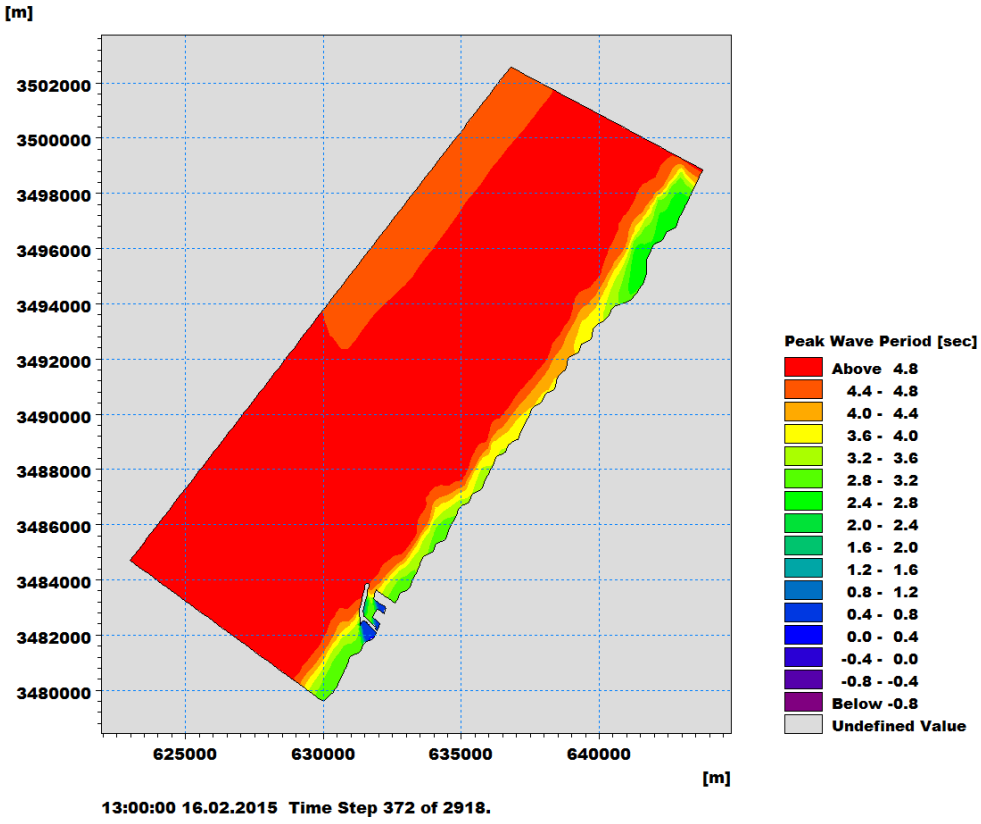

Figure 6.8: Map of the peak period

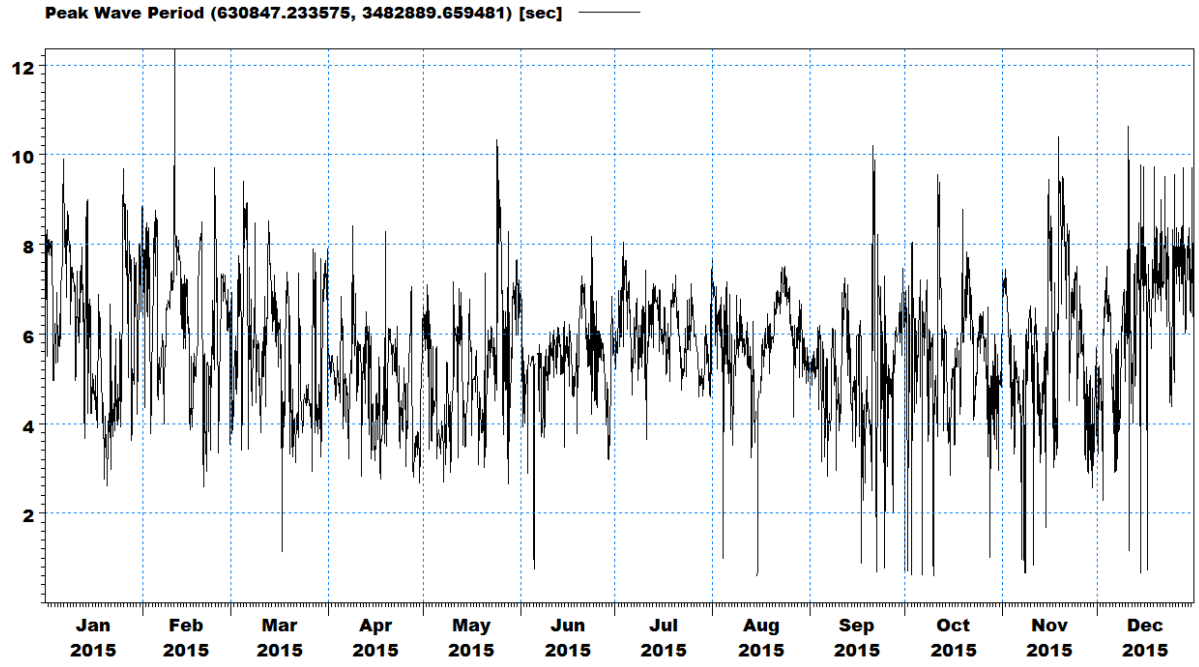

Figure 6.9: Time series of wave period at the point marked in Figure 6.6

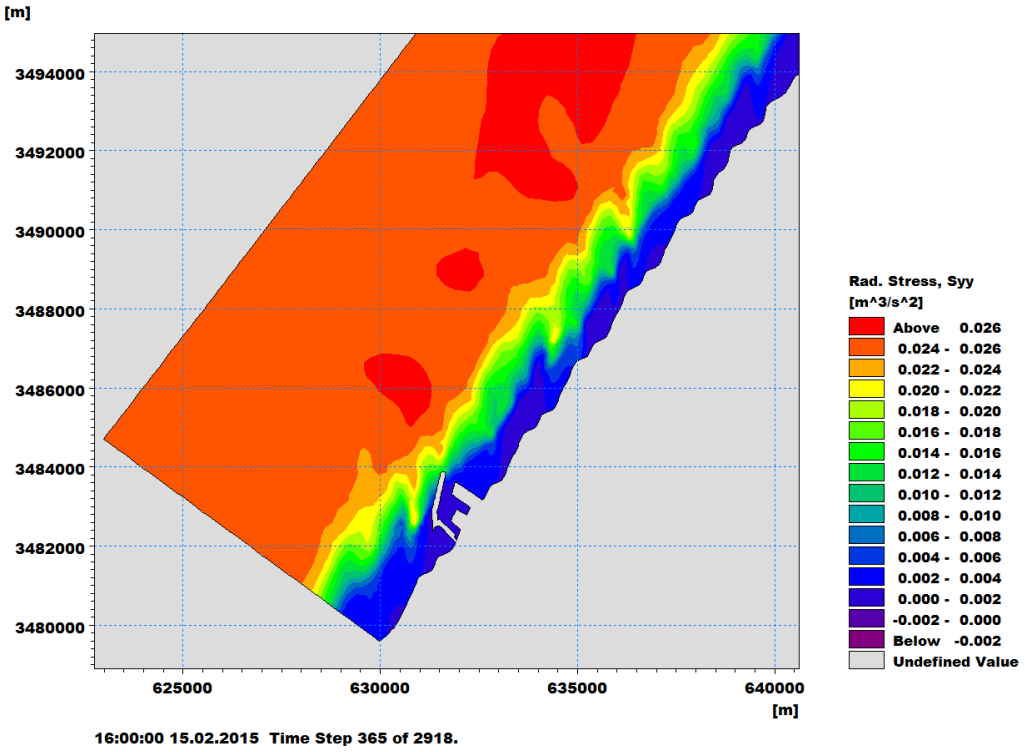

Figure 6.10: Map of the radiation stress, S_{yy}

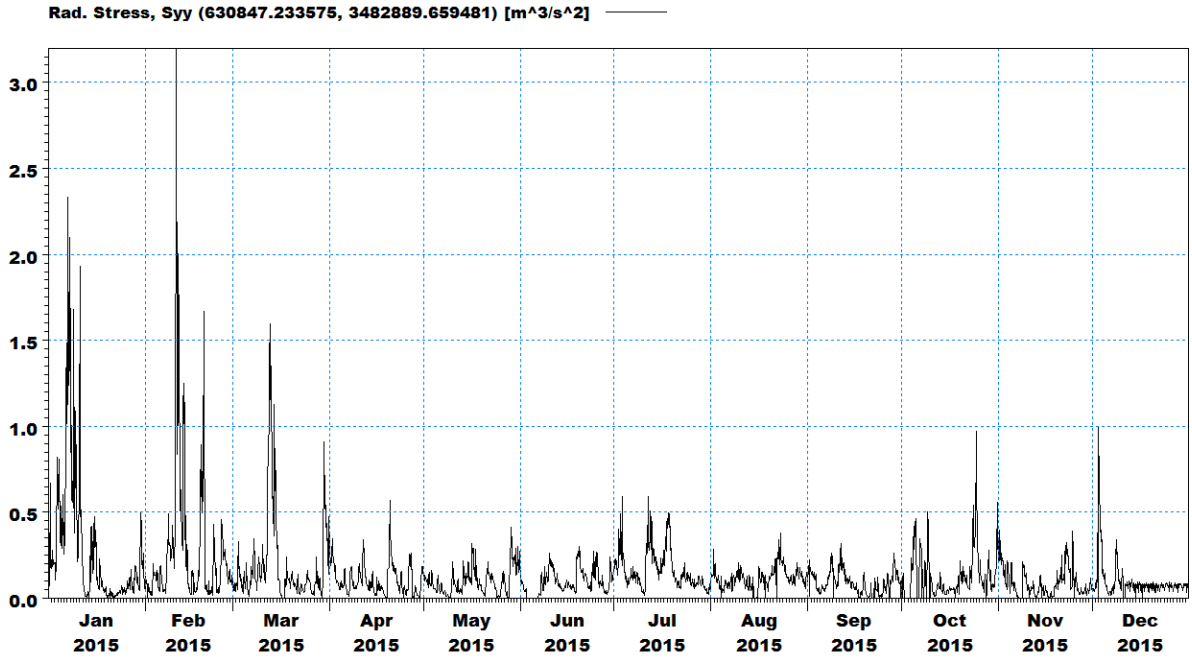

Figure 6.11: Time series of radiation stress, S_{yy} at the point marked in Figure 6.6

6.3 MIKE 21 Sediment Transport (ST)

6.3.1 Development of Bed Level

The development of the bed level along Line 1 and Line 2 are shown in Figure 6.13 and Figure 6.14, respectively. It is seen from Figure 6.13 that the bed level does not change significantly in front the entrance of the proposed seaport. This is good to maintain the nautical depth for ships for longer time in the entrance channel. However, when time goes on the bed level change will increase requiring dredging in the long run. Figure 6.14 shows also that the bed level starts to change considerably seaward of point t3 in the sheltered area ahead of the breakwater. The pattern along Line 2 changes from erosion to accretion to erosion again.

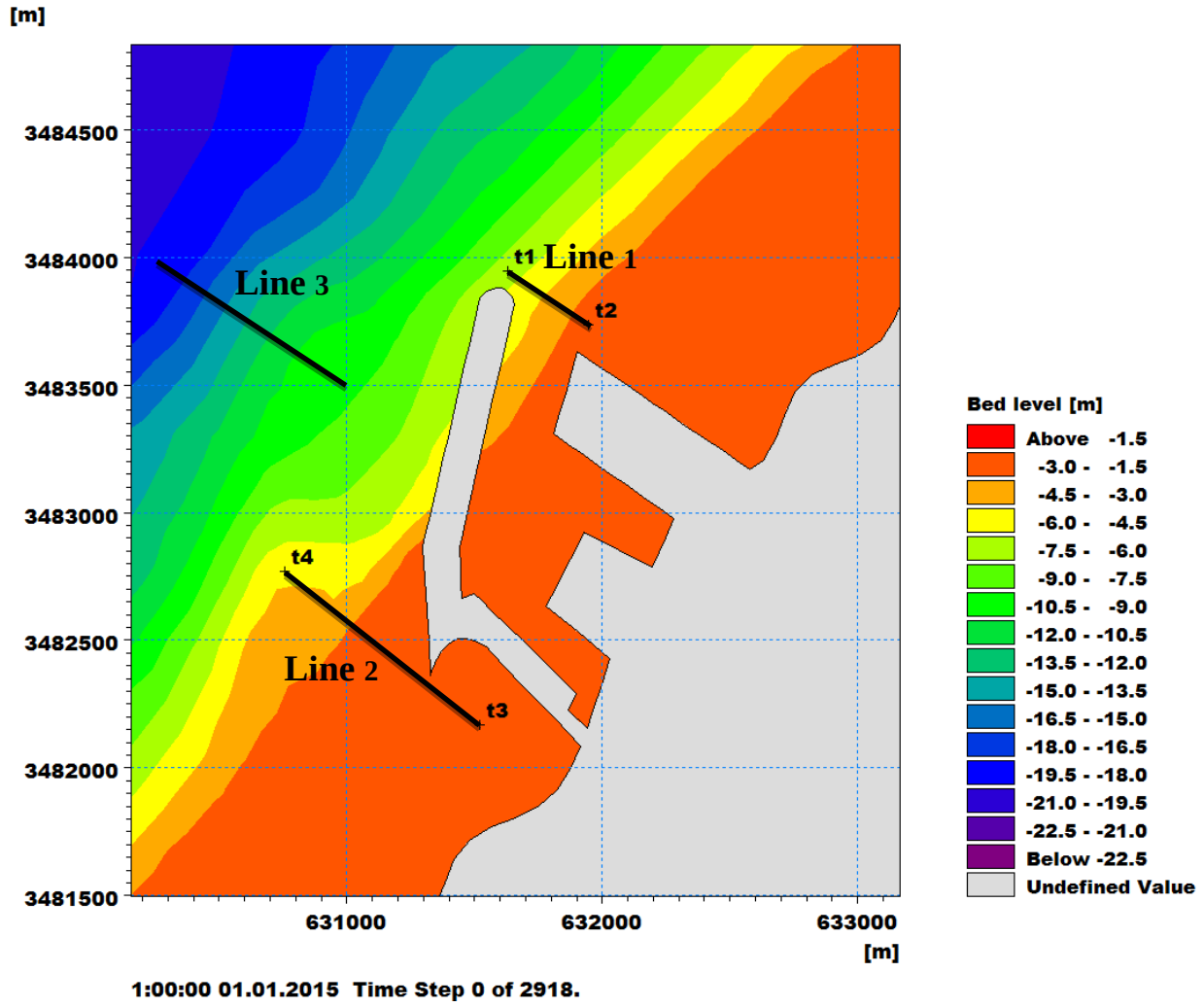

Figure 6.12: Position of extraction lines

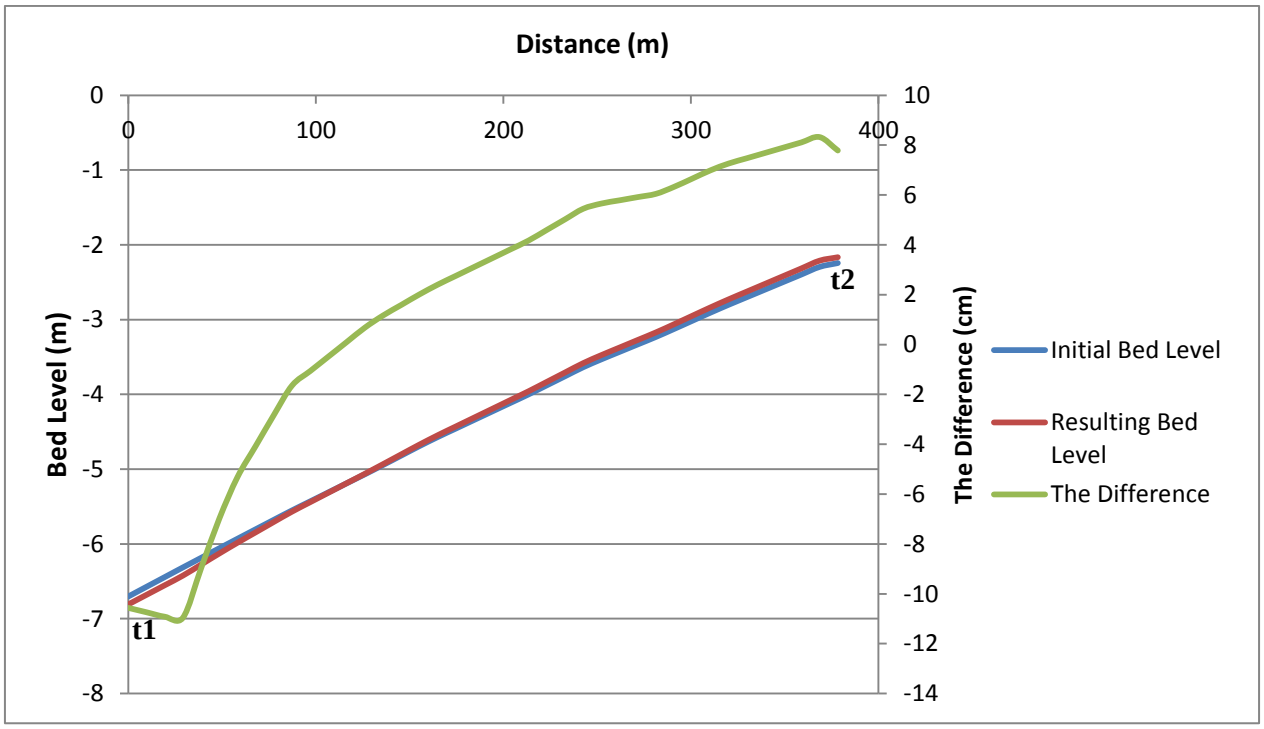

Figure 6.13: Bed level along Line 1: before and after simulation for one year

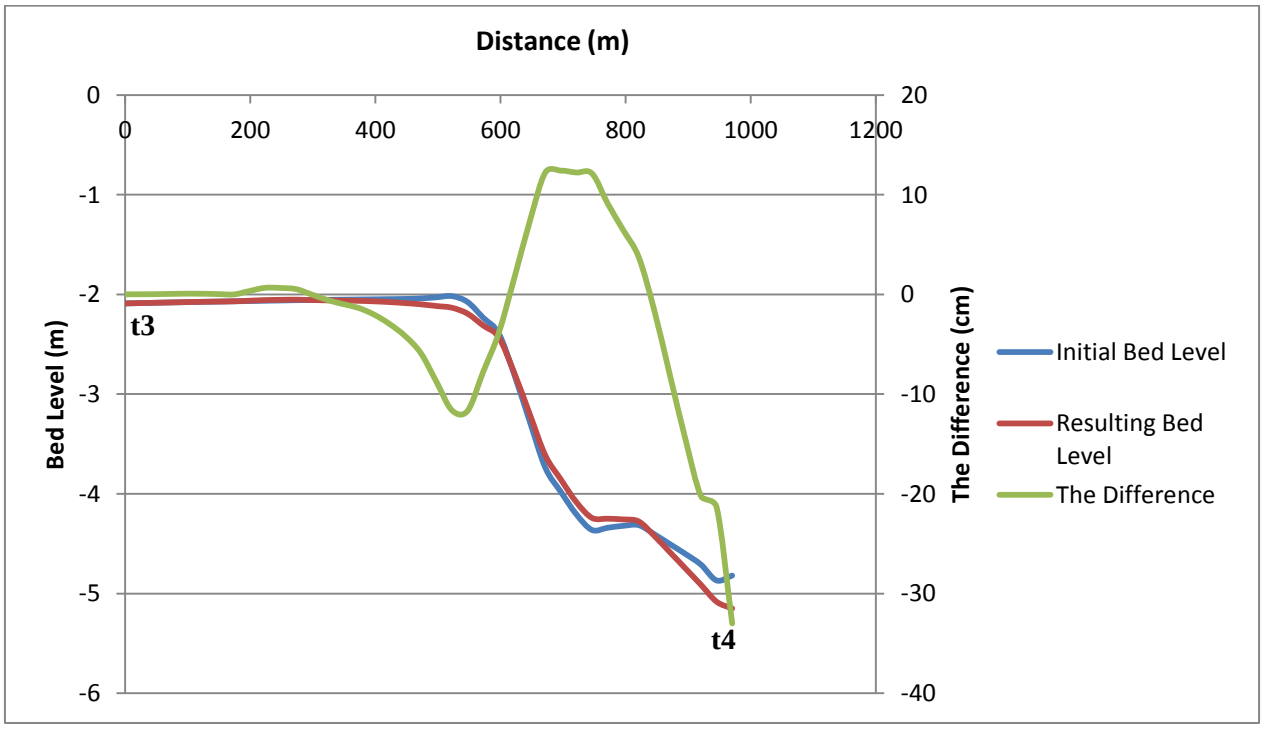

Figure 6.14: Bed level along Line 2: before and after simulation for one year

Figure 6.15 shows the magnitude of the bed level at the midpoint of line 1 illustrated in Figure 6.12. The pattern of sediment transport at this point is accumulation with almost no change in June, August and December. It increases gradually by 2.8 cm during the whole year.

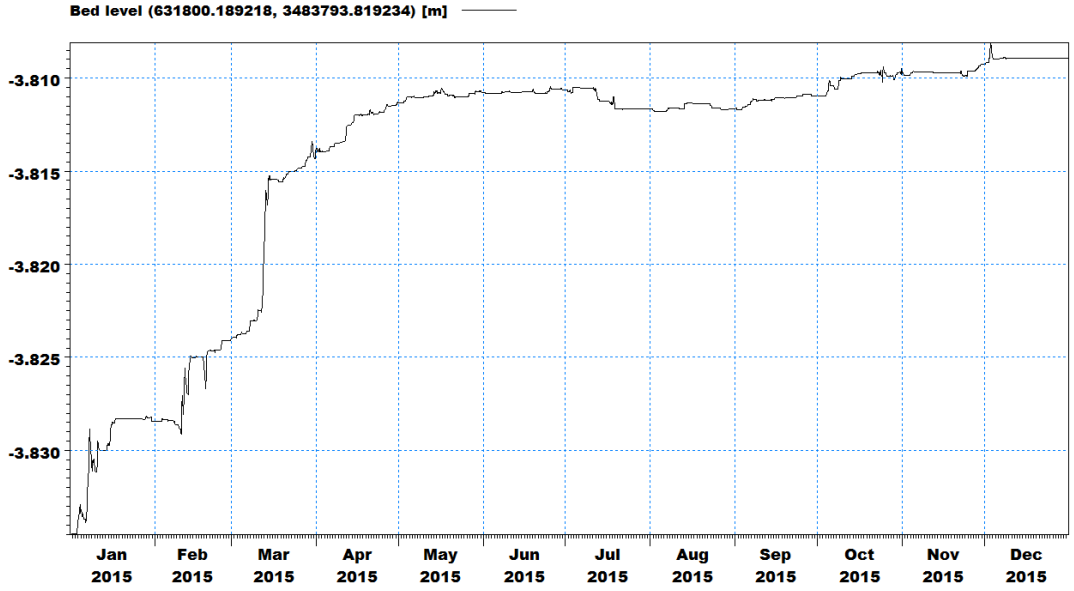

Figure 6.15: Bed Level throughout the year 2015 at the middle point of Line 1 illustrated in Figure 6.12

Figure 6.16 shows the magnitude of the bed level at the point t4 marked at Line 2 in Figure 6.12. The pattern of sediment transport at this point is erosion throughout the entire year. It decreases almost by the same rate during the entire year resulting in a total erosion of 37 cm.

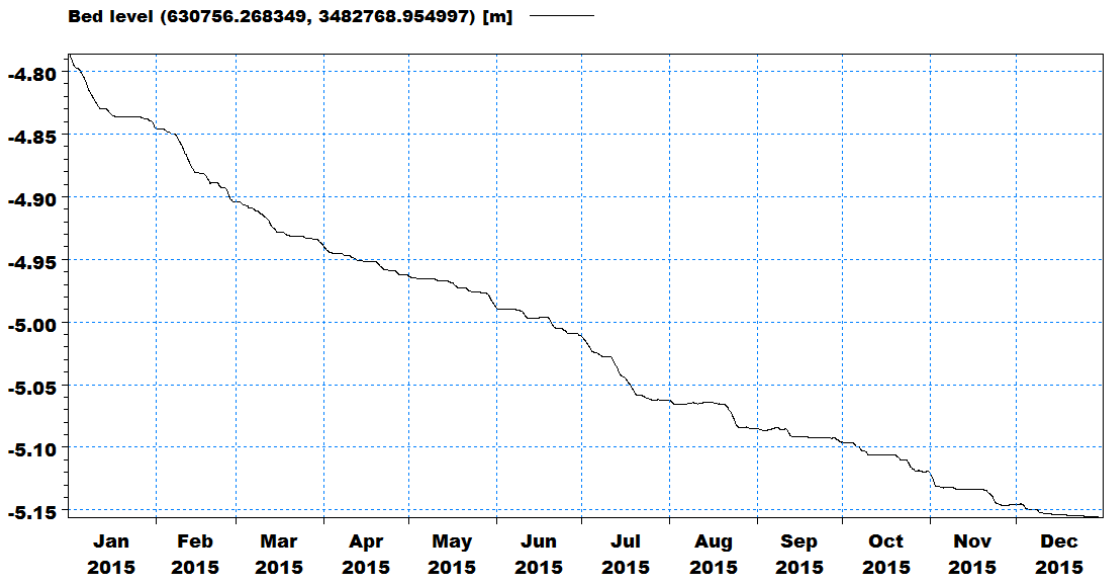

Figure 6.16: Bed Level throughout the year 2015 at point t4 marked at Line 2 in Figure 6.12

MIKE 21 ST Model was also run for the case that there is no seaport in order to compare the bed level changes with the case that the seaport is constructed. Figure 6.17 shows the development of the bed level along Line 3 shown in Figure 6.12 for two cases. In the case that the seaport is not present accretion takes place along the line. On the other hand, erosion takes place along the line in the case that the seaport is available. This indicates that the seaport has an impact on the morphological changes which are described in the next sections

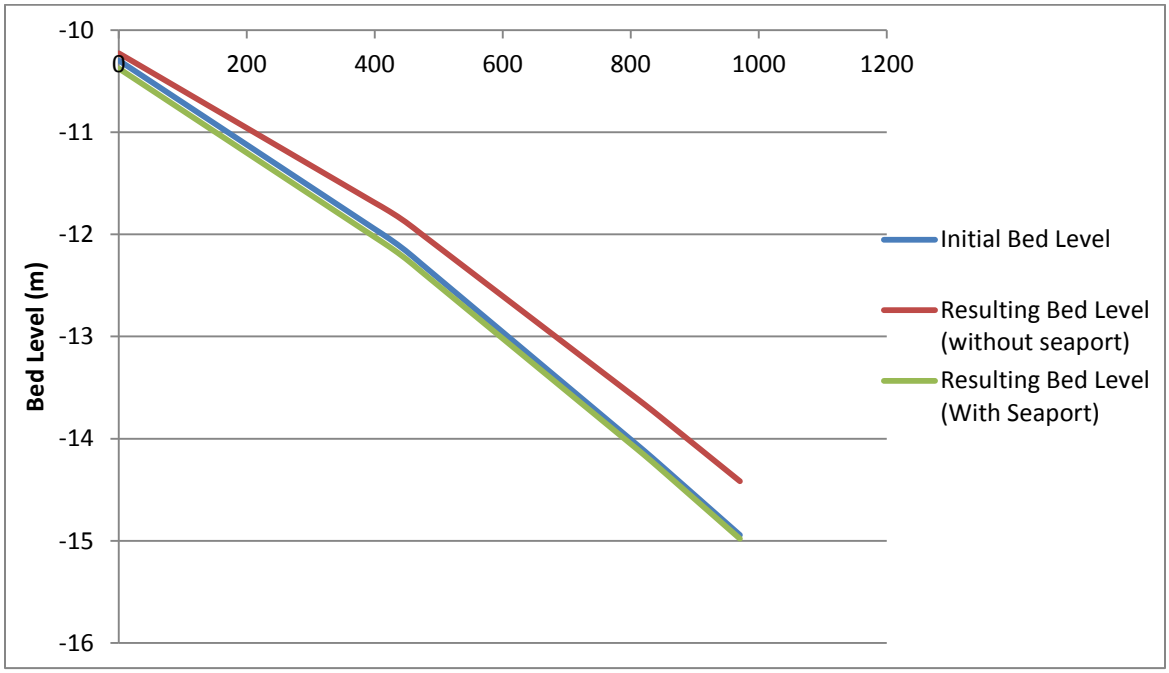

Figure 6.17: The development of the bed level along Line 3 shown in Figure 6.12

6.3.2 Bed Level Change Rate

In order to check the tendency of sediment transport in the vicinity of the seaport, a plot of the bed level change rate at two different times, November and December, is shown in Figure 6.18 and Figure 6.19 respectively. It can be seen that accumulation of sand will appear inside the seaport basin, in the seaport navigation channel and in the sheltered area ahead of the breakwater. On the other hand, erosion will take place behind the terminal at the North. The seaport navigation channel has to be accessible for ships. Therefore, the predicted process of sediment transport necessitates dredging the seaport navigation channel in the future to maintain its navigable depth.

Scour will take place at the tip of the breakwater. This means that breakwater designer should incorporate scour protection into the design to keep the breakwater stable.

It can be seen that accretion takes place close to erosion zones. This makes sense because when the flow erodes some sediment, it will slow down. Consequently, the sediment carrying capacity of water will decrease and accretion of sediment will take place. The rate of bed level change is not very high which means that the impact of the seaport on the bed level is not adverse in the short term but mitigation measures should be taken in the long run.

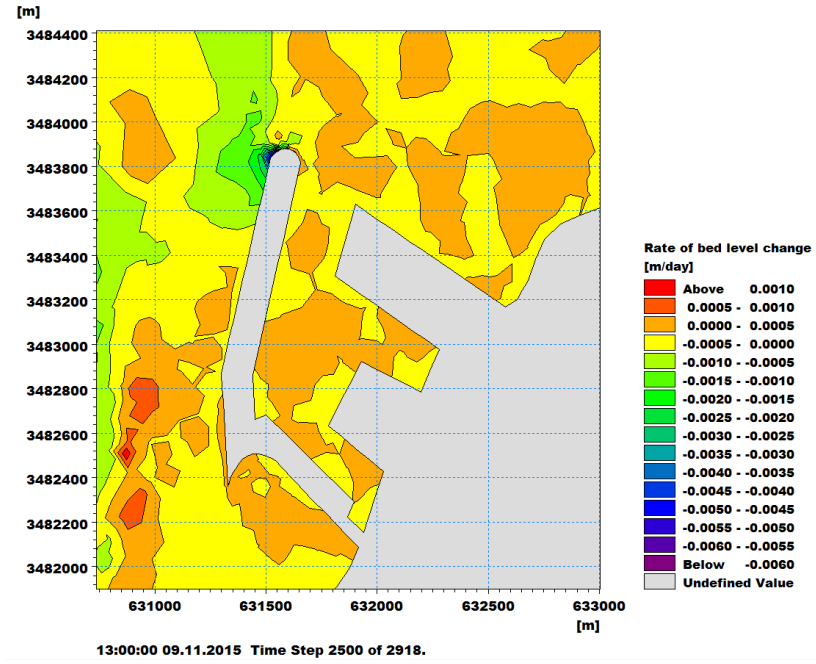

Figure 6.18: Bed level change rate in November 2015

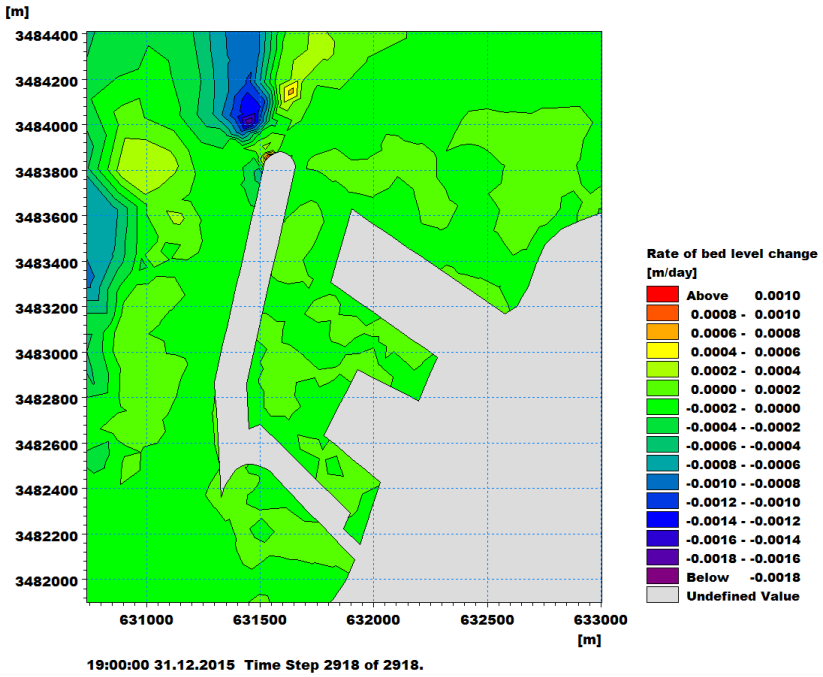

Figure 6.19: Bed level change rate at the end of the simulation period

6.4 LITDRIFT

LITDRIFT model was applied to calculate shoreline sediment transport. In the following paragraphs, the results of the LITDRIFT model are presented. It is stressed that littoral drift calculations could be improved once more accurate data is collected from the area of interest. The gird space used in the cross-shore profile is 10m and the hydraulic bed roughness is assumed to be constant along the profile.

Figure 6.20 illustrates the cross-shore distribution of littoral sediment drift. The main part of littoral sediment transport takes place inside the 2.2 m water-depth contour because the longshore current is driven primarily by breaking waves and concentrated in the surf zone.

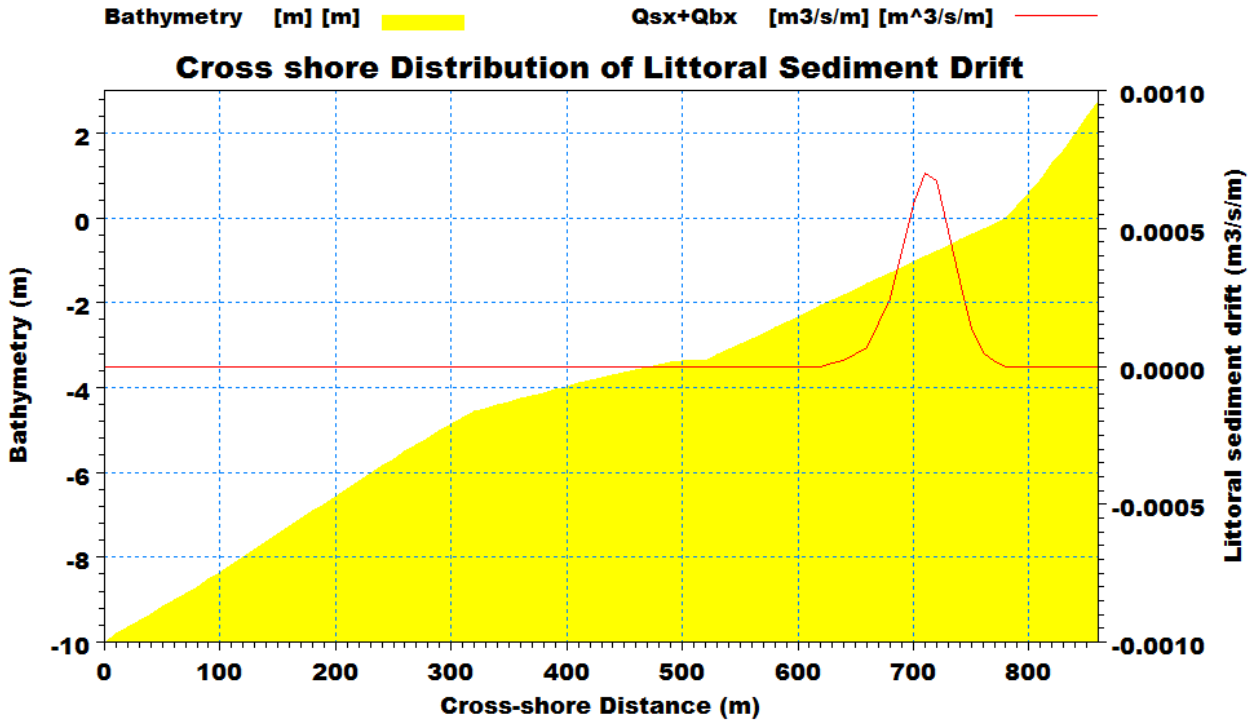

Figure 6.20: Cross-shore distribution of littoral sediment drift

6.4.1 Sediments Blocked by the Seaport

Figure 6.21 shows the accumulated sediment transport across the profile, starting from the shoreline. The total longshore sediment transport is about 0.039 m^3/s. Since the breakwater is not vertical on the shoreline, the overall length of the breakwater cannot be used in estimating the amount of trapped sediment. Instead, the shadow length of the breakwater is used, 690 m. It is assumed that the breakwater efficiency of blocking is 100 percent. The breakwater extends from grid number 78 to 9 (grid size of 10 m) in the model. Figure 6.21 shows the accumulated

transport rate at grid number 9 which will be blocked by the breakwater. This results in a blocked accumulated littoral transport of 0.039 m^3/s which means that the breakwater has the ability to block the total longshore sediment transport. The yearly blocked material is 1.23×10^6 m^3/year.

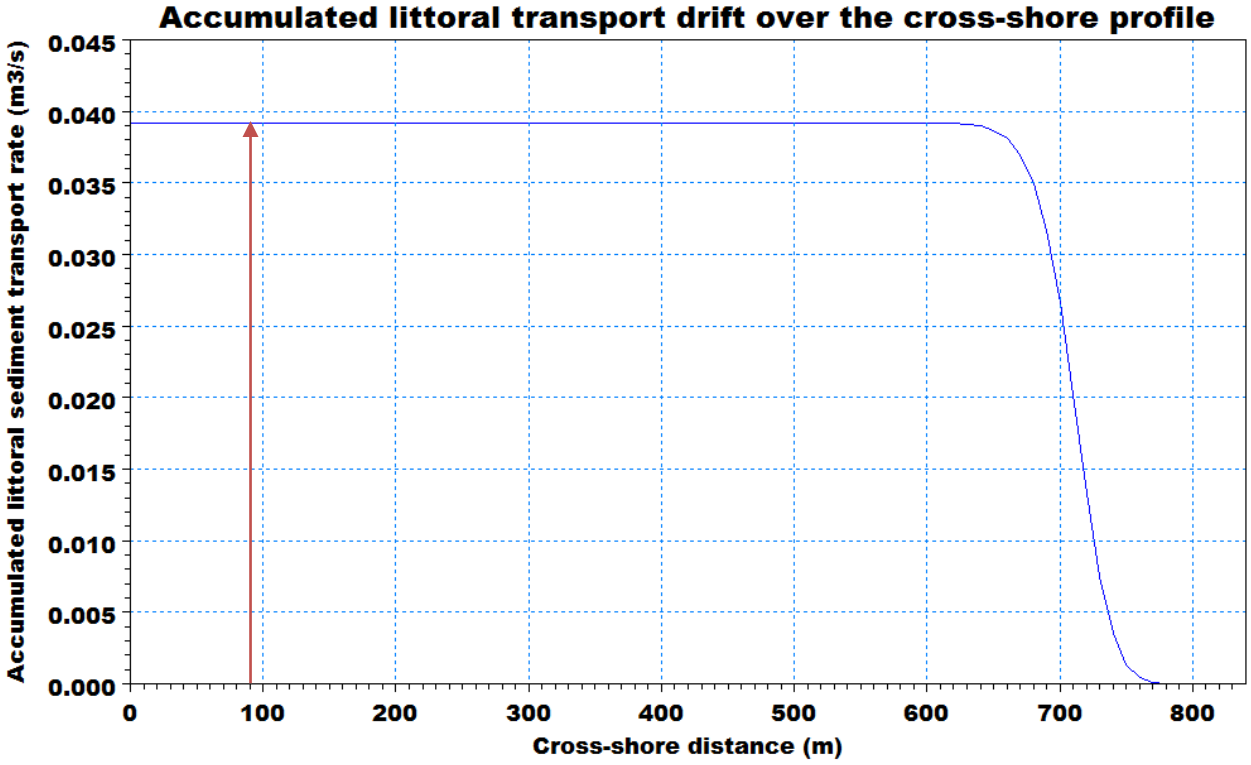

Figure 6.21: Accumulated littoral transport drift over the cross-shore profile

6.4.2 Sensitivity Analysis Using Bed Roughness

In reality, a cross-shore transect of the coast will have a varying bed roughness that is based on the grain size, grain shape, and mainly whether or not bed forms are present. However, the bed roughness will vary over time as waves and currents will transport sediment and alter the position and organization of bottom sediment.

In practice, the question of whether or not to consider a fixed or grain-size dependent bed roughness depends on the amount of available data and the application. Sediment data collected in the field may be limited to one or two samples in the submerged part of the profile, close to shore. Therefore, in most practical cases, it makes sense to use a constant bed roughness along the profile rather than make more complex assumptions. The LITDRIFT manual mentions that the bed roughness is the basic calibration parameter (DHI, 2012d).

Results and Discussion

Prediction of bed roughness value is crucial in the calculation of sediment transport. There are several formulas in literature based on d_{50} for estimating the value of the bed roughness parameter. A sensitivity analysis is performed using four values of bed roughness as follows:

- Constant bed roughness of 0.004m
- Nikuradsse (1993): $K_s = 10*d_{50}$
- Soulsby (1997): $K_s = 2.5*d_{50}$
- DHI: $K_s = 30*d_{50}$

Figure 6.22 shows the accumulated littoral transport drift along the cross shore profile using the four values described above. It is clear that the accumulated littoral transport decreases as the bed roughness increases. An increased bed roughness increases the shear stress felt by the flow, which increases the Shields parameter and thus the sediment transport. However, increased roughness interferes with the flow velocity, slowing it down which decreases the shear stresses and resulting transport. Therefore, changing the bed roughness has two competing impacts. However, the impact on the velocity dominates.

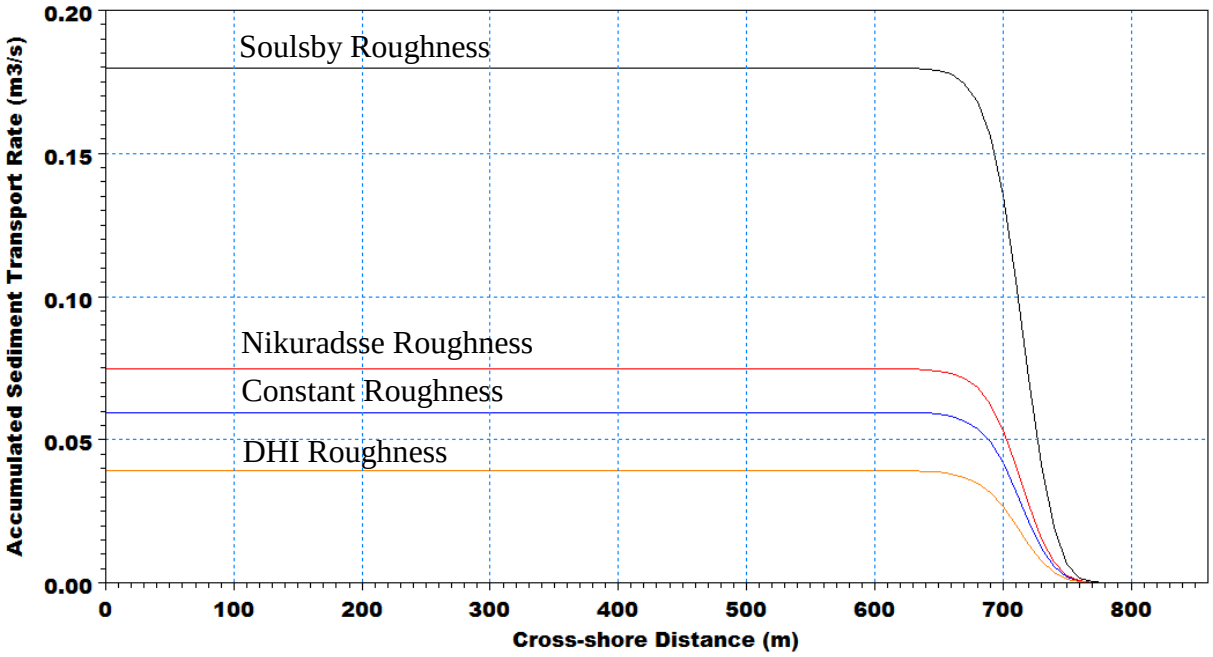

Figure 6.22: Comparison of accumulated littoral transport drift along the cross shore profile

One with a good sense of the longshore transport rate at a particular site can use Figure 2.1 to narrow down the list of alternative roughness values to use. Based on personal communication with a coastal engineer worked in DHI consultants, experts of LITPACK recommend bed roughness of (25-30)×d_{50} to be used for beach modeling using LITPACK. The coastal erosion

within Gaza Strip, combined with the sand consumption for building purposes is about $1.5x10^6$ m^3/year (Zviely & Klein, 2003). Assuming that 18% of sand erosion is due to sand quarried from the beach, this shows that 1.23×10^6 m^3/year is trapped by hard structures. This is in line with the result obtained in the case of using bed roughness of $30\times d_{50}$ as shown in Figure 6.21. Therefore, constant bed roughness of $30\times d_{50}$ is used in the further simulations.

6.5 LITLINE

LITLINE was used to simulate the effect of the seaport on the coastline and to evaluate shoreline evolution. The model is formulated based on the one-line theory of coastline evolution, wherein the entire coastline is schematized as a single line which moves horizontally as a result of accretion or erosion. It calculates the coastline position using hydrodynamic inputs, sediment characteristics, and gradients in sediment transport caused by obstructions or other sources and sinks.

The model was run for different simulation periods: 1 year, 3 year, 5 years, 8 years and 10 years. Figure 6.23 shows the coast line shape after a year from constructing the seaport. It can be seen that accumulation of sediments will take place updrift of the seaport (ahead of the breakwater). On the other hand, sediment erosion will take place downdrift of the seaport (behind the terminal). These results are in line with the results obtained from MIKE 21 ST as was presented earlier.

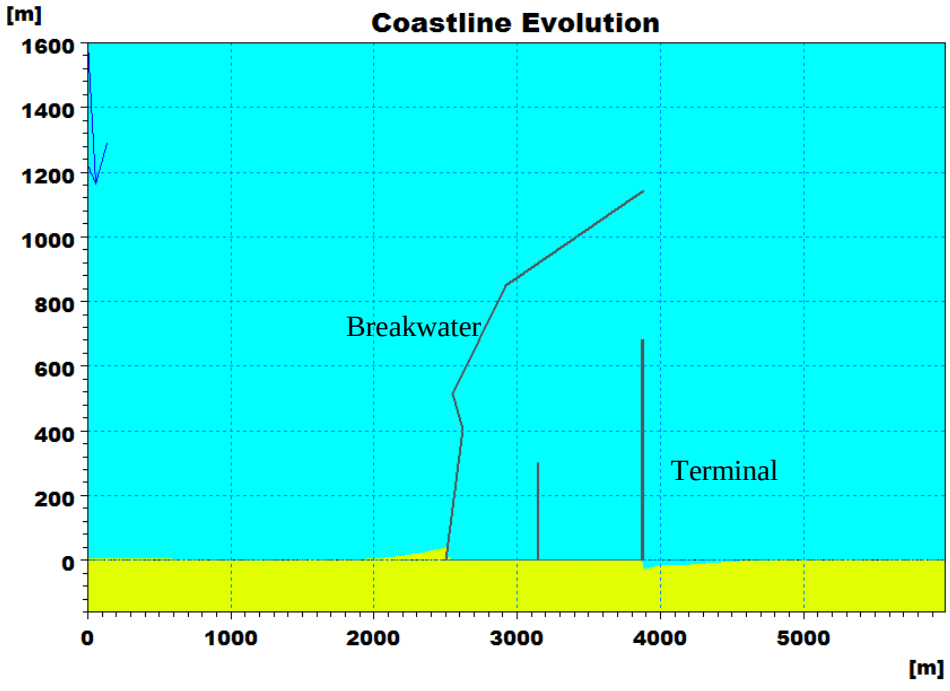

Figure 6.23: LITLINE Model graphic results after a year

The final coastline shape of each simulation period is illustrated in Figure 6.24. The trend of coastline evolution is the same after each period. However, the amount of sand accretion and erosion will increase in time. This means that mitigation measures are needed to maintain the existing beach alignment prior to the construction of the seaport. For instance, sand accumulated updrift of the seaport can be transferred along the effected shore by sediment bypass system.

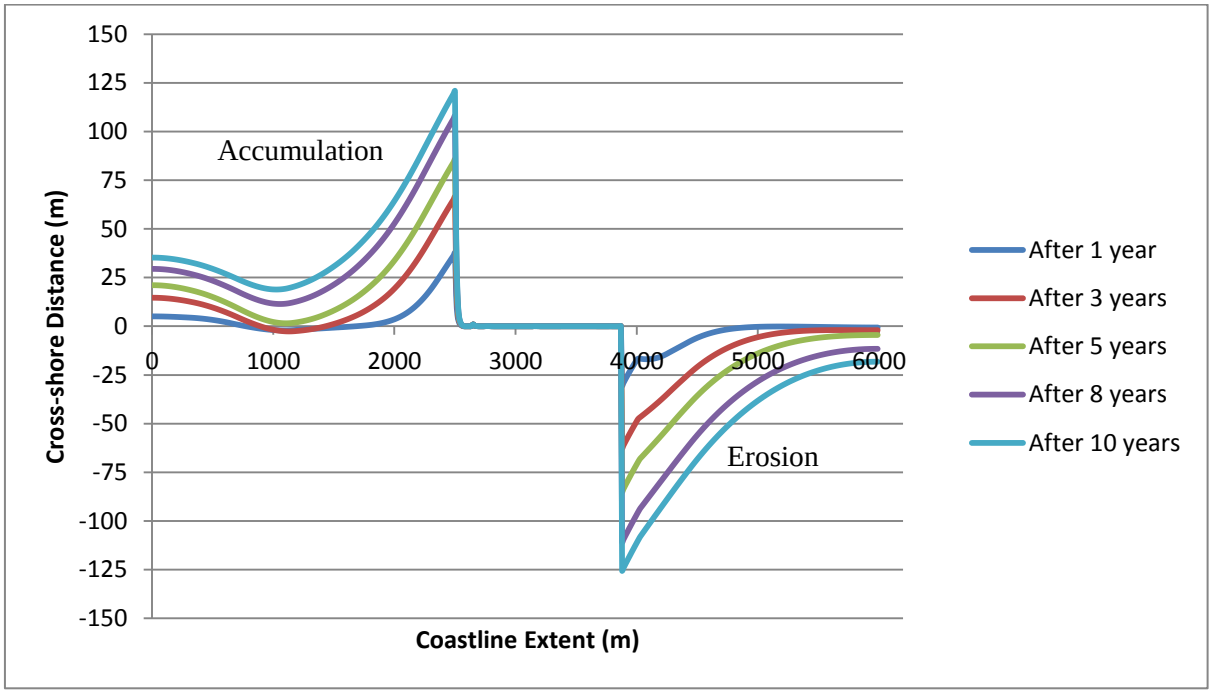

Figure 6.24: Coastline evolution in the future

6.5.1 Sensitivity Analysis

Sensitivity analysis was performed in order to study the influence of each parameter on longshore sediment transport. Eight parameter combinations were prepared, simulated and compared. Two bed roughness calculations were used: $2.5*d_{50}$ and $30*d_{50}$. The wave height was varied between 0.7 m and 1.4 m. The wave period was also varied between 6 seconds and 8 seconds. Table 6.1 shows the eight parameter combinations.

Table 6.1: Parameter combinations simulated in LITLINE

Case #	Bed Roughness (m)	Wave Height (m)	Wave Period (s)
Case 1	$K_s=2.5*d_{50}$	0.7	6
Case 2	$K_s=2.5*d_{50}$	0.7	8
Case 3	$K_s=2.5*d_{50}$	1.4	6
Case 4	$K_s=2.5*d_{50}$	1.4	8
Case 5	$K_s=30*d_{50}$	0.7	6
Case 6	$K_s=30*d_{50}$	0.7	8
Case 7	$K_s=30*d_{50}$	1.4	6
Case 8	$K_s=30*d_{50}$	1.4	8

The final coastline position for all cases is plotted in Figure 6.25. The results show a broad variation in accretion volume updrift of the seaport and the amount of erosion downdrift.

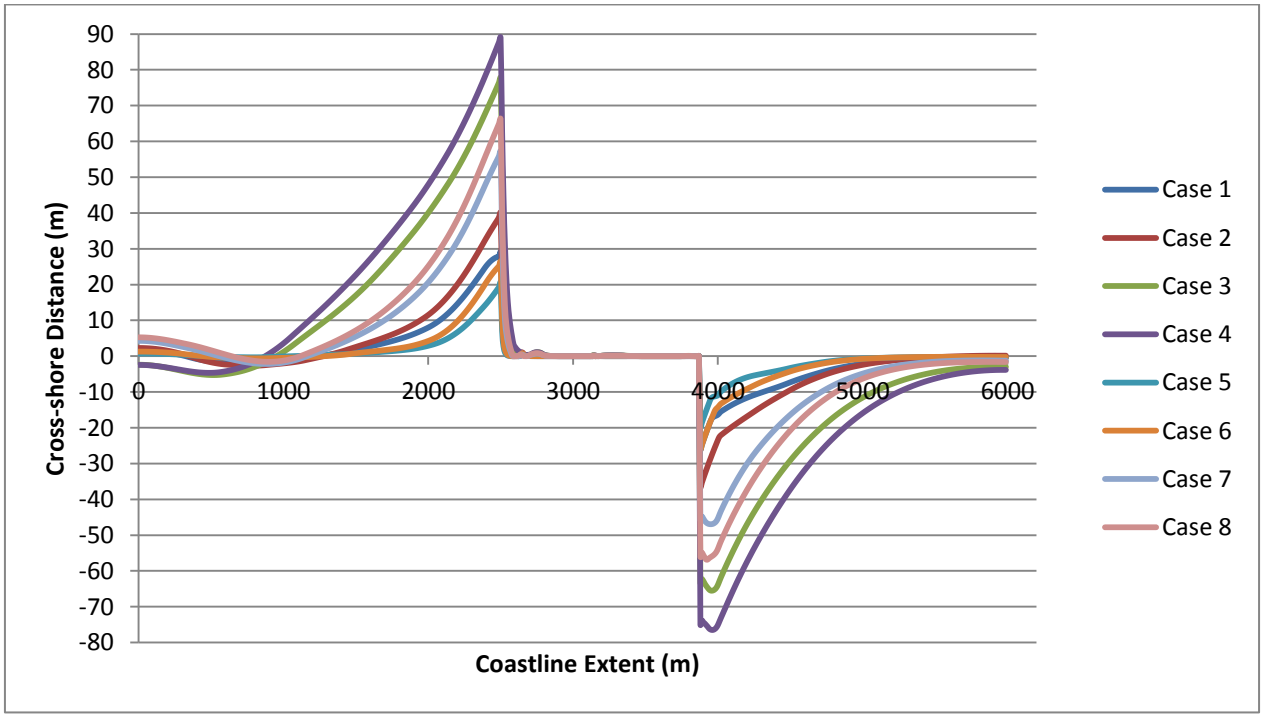

Figure 6.25: Coastline position after a year

Table 6.2 lists the maximum retreat and accretion of the coastline for the eight cases. Figure 6.26 depicts the definition of maximum retreat and maximum accretion.

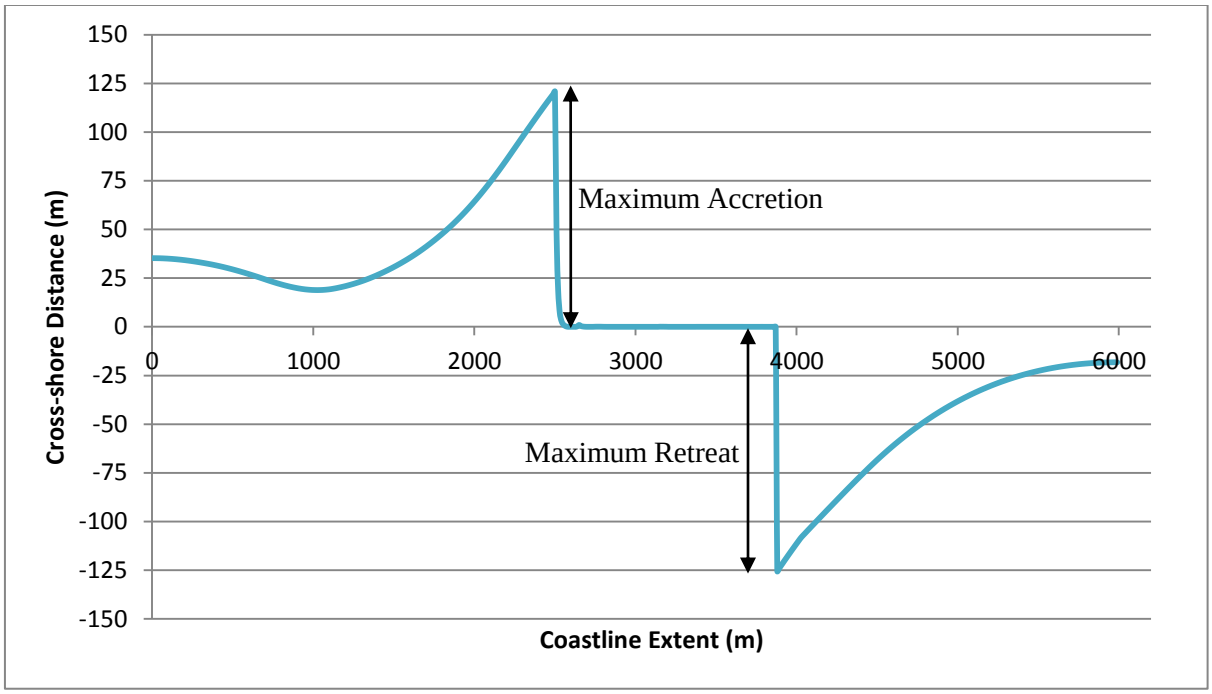

Figure 6.26: Definition of maximum retreat and maximum accretion

Table 6.2: Maximum retreat and accretion of coastline over one year period

Case #	Max Retreat (m)	Max Accretion (m)
Case 1	26.06	29.04
Case 2	36.58	40.09
Case 3	65.52	77.75
Case 4	76.50	89.04
Case 5	19.84	20.57
Case 6	26.00	26.40
Case 7	46.95	57.23
Case 8	56.84	66.29

The influence of a larger wave height results in a larger maximum retreat and a larger maximum accretion as shown by Cases 3 and 4 as well as 7 and 8. This makes sense because littoral drift is directly proportional to the wave height to the power of 2.5. There will be more sand transport and therefore more will be blocked by the seaport. In order to make the comparison easier, the results of case 1 and case 3 are plotted alone in Figure 6.27.

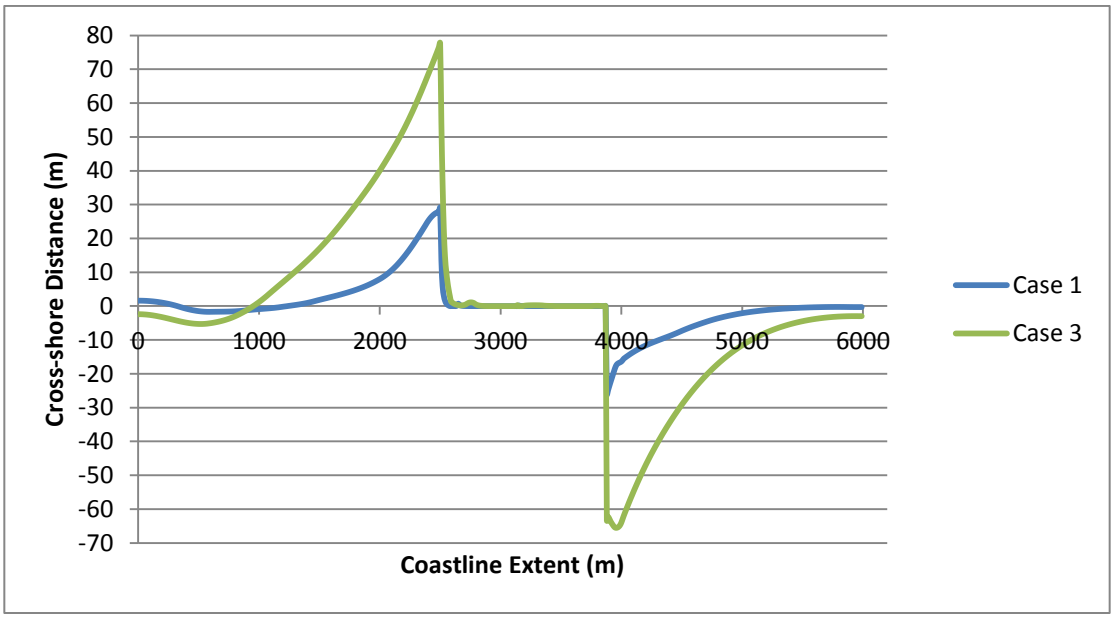

Figure 6.27: Comparison of shoreline evolution over a year using different wave heights

The longer wave periods seems to increase both the maximum retreat and the maximum accretion, as shown by Cases 2 and 4 as well as 6 and 8. This makes sense because longer waves have the same effect on sediment transport as wave height. Sediment transport is directly proportional to the square of wave period (Kamphuis, 2002). In order to make the comparison easier, the results of case 1 and case 2 are plotted alone in Figure 6.28.

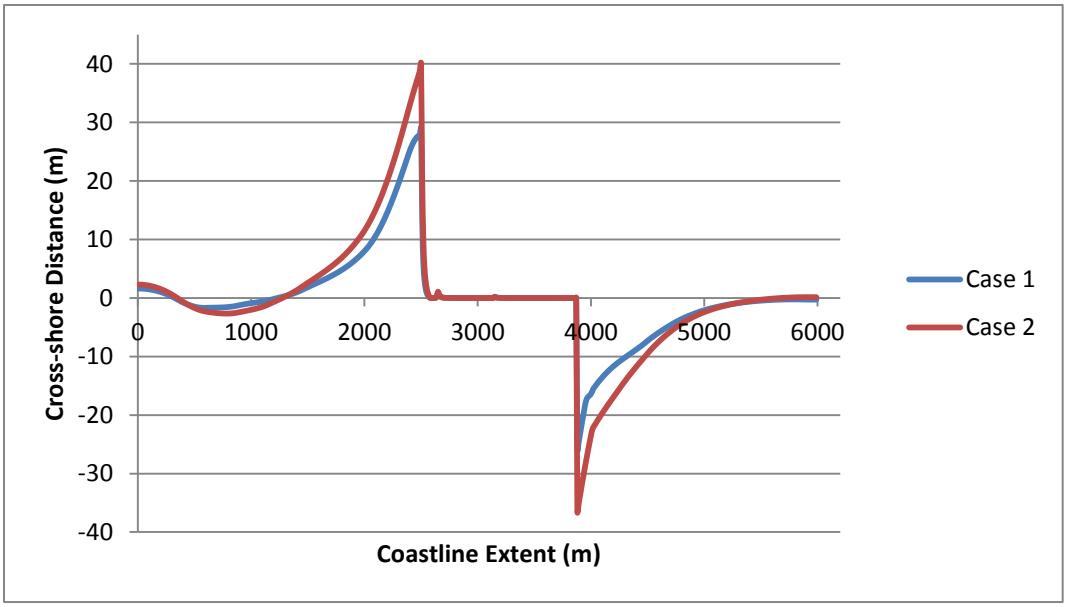

Figure 6.28: Comparison of shoreline evolution over a year using different peak periods

Increasing the bed roughness seems to decrease both the maximum retreat and the maximum accretion, as shown by Cases 5 and 6 as well as 7 and 8. This makes sense because increased bed roughness interferes with the flow velocity, slowing it down which decreases the shear stresses and resulting sediment transport. In order to make the comparison easier, the results of case 1 and case 5 are plotted alone in Figure 6.29.

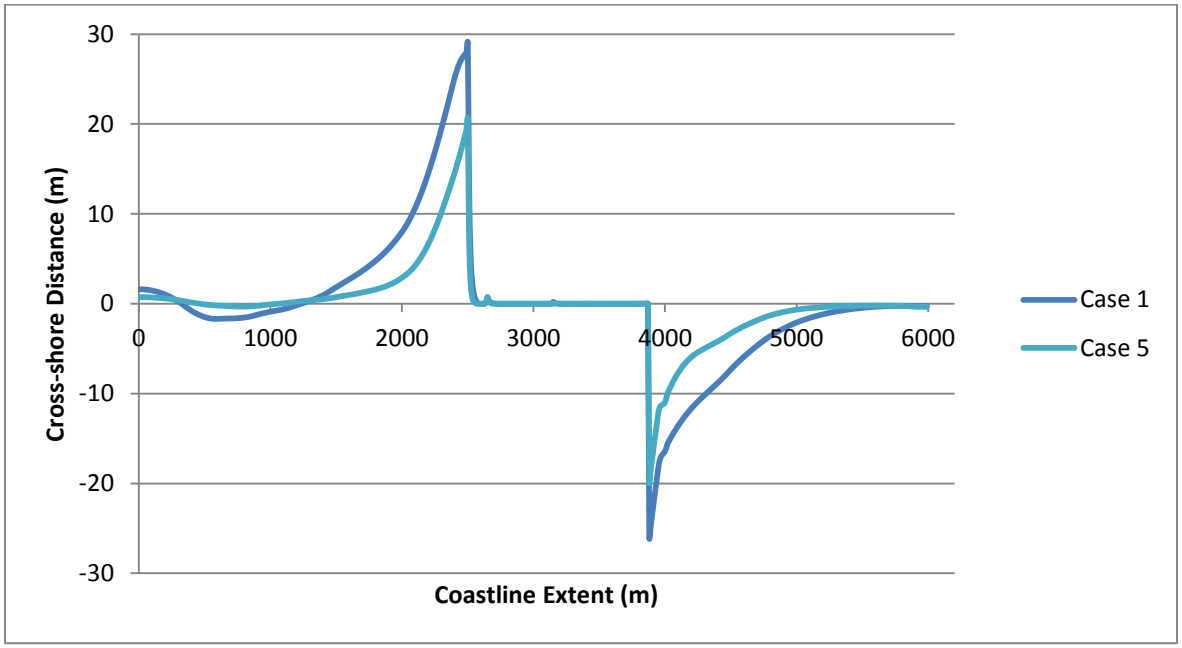

Figure 6.29: Comparison of shoreline evolution over a year using different bed roughness

6.5.2 Validation of Results

In order to validate the results of LITLINE, some field data would be needed. The results of this study cannot be validated since the seaport is not built yet. Nevertheless, once the seaport is built, aerial photographs taken every 10 days can shed light on the coastline development. It is also a better idea to simulate a multi-year coastline development since aerial photographs can more easily capture larger changes in the coastal alignment.

7 Conclusion and Recommendations for Future Work

7.1 Conclusion

Throughout this study, the effect of the proposed Gaza Seaport on the morphology of the coast of Gaza was predicted. The effect of the seaport on the morphology was investigated with the incorporation of the numerical models, MIKE 21 and LITPACK, developed by DHI.

Two dimensional sediment transport computations were carried out using MIKE 21 for the pre- and post-seaport construction stage to study the morphological impact of the proposed seaport on the coast of Gaza. The results reveal that the morphological development of the bathymetry around the seaport is different in the two cases. The main focus was on the morphological change in the case with a seaport. The results show that sediment accumulation will take place inside the seaport basin, in the seaport navigational channel and updrift of the seaport (ahead of the seaport). On the other hand, sediment erosion will take place downdrift of the seaport (behind the seaport) and scour will take place at the tip of the breakwater.

Mathematical modeling, LITPACK, was applied to predict the shoreline evolution for the proposed seaport. The LITDRIFT model of the LITPACK software showed annual littoral sediment transport of 1.23×10^{6} m^3 by adjustment of the cross section profile. The main part of littoral sediment transport takes place inside the 2.2 m water-depth contour. The LITLINE model of the LITPACK software predicted the shoreline morphological evolution after 1 year, 3 years, 5 years, 8 years and 10 years from the construction of the seaport.

The LITPACK results show sound agreement with the results obtained from MIKE 21 in terms of accretion and erosion zones. The results of prediction shoreline evolution reveal that shoreline accretion and erosion increase in time and mitigation measures are needed to maintain the natural longshore movement of sediments. Sand accumulated due to blocking longshore sand transport generated by constructing the seaport should be transferred along the shore to maintain the existing beach alignment prior to the seaport construction. In addition to the impact of the proposed seaport, the patterns of erosion/accretion reveal that incident waves drive northward alongshore currents that move sand away from the south towards the north.

A sensitivity analysis using four different values of bed roughness was performed by LITDRIFT. The results of the analysis show that the accumulated littoral transport drift decreases as the bed roughness increases. Another sensitivity analysis using different combinations of wave height, wave period and bed roughness was performed by LITLINE to study the effect of each parameter on the coastline evolution based on evaluating the maximum accretion and the maximum retreat. The results reveal that the influence of a larger wave height and a longer wave period result in a larger maximum retreat and a larger maximum accretion. In contrast, the influence of increased bed roughness results in a less maximum retreat and a less maximum accretion.

7.2 Limitations of Study and Recommendations for Future Work

Absence of sufficient field data is a major limitation of this study. This limitation makes it necessary to assume certain parameters in the model and makes model calibration and validation difficult. Consequently, there is a scope of further improvement of the model for the site of interest. Future work is recommended to take the following aspects into consideration:

- The used field wind data seems low and questionable compared to global wind data at some neighbouring locations and it was assumed to be constant through the local model domain. The simulation can be improved by using better measured wind data at several locations in the model domain.
- Wave climate was kept the same along the northern and southern boundaries of the model. Wave measurements should be taken at the boundaries for future works.
- Calibration of the sediment transport model should be performed with a detailed field survey containing data regarding wave climate, wind parameters, current parameters and water levels at the site of interest.
- Once the seaport is built, calibration of coastline evolution model should be performed using aerial photographs illustrating the coastline evolution.
- Bed roughness and bottom friction were assumed and kept constant in the simulations. Sediment diameter (d_{50}) was also kept constant along the cross shore profile. Thus, field survey at the coast should be done to estimate these parameters well.
- The bathymetry obtained from MIKE C-MAP was constant along the first 200m seaward from the shoreline so it was corrected based on old field survey obtained in 1986. Further work should be based on new field bed level survey done around the seaport.

- Continuous bed level survey to a certain depth illustrating the evolution of the nearshore bathymetry can help in calibrating the sediment transport model.
- The environmental impact of the proposed Gaza Seaport was beyond the scope of the current study. Therefore, it is recommended to include it in further work since it is of importance. Furthermore, economic feasibility should be done to assess the overall feasibility of the construction of the seaport.

8 References

Ackers, P., and White, W. (1973). Sediment Transport: New Approach and Analysis. *Journal of the Hydraulics Division*, ASCE, 99.

Ali, M. (2002). The Coastal Zone of Gaza Strip-Palestine Management and problems. *Presentation for MAMA first kick-off meeting*, 2.

Bagnold, R. A. (1966). An approach to the sediment transport problem from general physics. *US Geol. Surv. Prof. Paper*, 422, 231-291.

Bayram, A., Larson, M., Hanson, H. (2007). A new formula for the total longshore sediment transport rate. *Coastal Engineering*, 54, 700-710.

Bijker, E.W. (1969). Littoral Drift as a Function of Waves and Current. *Delft Hydraulics Laboratory*, 58. Delft, The Netherlands.

Bosboom, J. and Stive, M. (2015). *Coastal Dynamics I*. VSSD, Delft, The Netherlands.

Destroyed Gaza Seaport: Why Doesn't Dutch Government Demand Compensation from Israel? (2010, September). Retrieved May 23, 2016, from http://alternativenews.org/archive/index.php/features/economy-of-the-occupation/2840-destroyed-gaza-seaport-why-doesnt-dutch-government-demand-compensation-from-israel-2840

DHI. (2007). *MIKE 21 ST: Non-Cohesive Sediment Transport Module: User Guide*.

DHI. (2012a). *MIKE 21 & MIKE 3 FLOW MODEL FM: Hydrodynamic and Transport Module: Scientific Documentation*. Hørsholm, Denmark: MIKE BY DHI.

DHI. (2012b). *LITPACK: An integrated modelling system for littoral processes and coastline kinetics: Short Introduction and Tutorial.* Hørsholm, Denmark: MIKE BY DHI.

DHI. (2012c). *LITLINE: Coastline evolution: LITLINE USER GUIDE*. Hørsholm, Denmark: MIKE BY DHI.

DHI. (2012d). *LITDRIFT: Longshore current and littoral drift: LITDRIFT user guide.* Hørsholm, Denmark: MIKE BY DHI.

DHI. (2012e). *MIKE C-MAP: Extraction of World Wide Bathymetry Data: User Guide.*

DHI. (2012f). *MIKE 21 SW: Spectral Waves FM Module: User Guide.*

DHI. (2012g). *LITSTP: Nearshore sediment transport in currents and waves: LITSTP User Guide. Horsholm*, Denmark: Mike by DHI.

DHI. (2013). *MIKE 21 & MIKE 3 FLOW MODEL FM: Hydrodynamic Module: Short Description.* Hørsholm, Denmark: MIKE BY DHI.

DHI. (2015). *MIKE 21 Wave Modelling, MIKE 21 Spectral Waves FM: Short Description*. Hørsholm, Denmark: MIKE BY DHI.

References

DHI. (2016). MIKE 21. Retrieved June 04, 2016, from https://www.mikepoweredbydhi.com/products/mike-21

Einstein, H. A., & Krone, R. B. (1962). Experiments to determine modes of cohesive sediment transport in salt water. *Journal of Geophysical Research, 67(4),* 1451-1461.

Engelund, F. and Hansen, E. (1976). *A Monograph on Sediment Transport in Alluvial Channels.* Nordic Hydrology *7*, 293-306.

Engelund, F. and Hansen, E.(1972). *A Monograph on Sediment Transport in Alluvial Streams.* Teknisk forlag, Copenhagen.

Frijlink, H.C. (1952). Discussion des formules de debit solide de Kalinske, Einstein et Meyer – Peter et Mueller compte tenue des mesures recentes de transport dans les rivieres Neerlandaises. *2me Journal Hydraulique Societe Hydraulique de France*, Grenoble, 98-103.

Gaza Strip. (2015). Retrieved April 29, 2016, from http://www.worldabc.xyz/Gaza_Strip

Hasselmann K. (1974). On the spectral dissipation of ocean waves due to white capping, *Bound. Layer Meteor., 6*, 107-127.

Horikawa, K. (1988). *Nearshore dynamics and coastal processes: Theory, measurement, and predictive models*. Tokyo: University of Tokyo Press.

Inman, D. L., Zampol, J. A., White, T. E., Hanes, B. W., Waldorf, B. W., and Kastens, K. A. (1981). Field measurements of sand motion in the surf zone. *Proceedings of 17th International Conference on Coastal Engineering, ASCE, New York,* 1215-1234.

Janssen, P. A. E. M., Lionello, P., & Zambresky, L. (1989). On the interaction of wind and waves. *Philosophical Transactions of the Royal Society of London. Series A, Mathematical and Physical Sciences, 329(1604),* 289-301.

Kalinske, A. A. (1947). Movement of sediment as bed load in rivers. *Transactions, American Geophysical Union, 28,* 615-620.

Kaminsky, G.M. and N.C. Kraus. (1993). Evaluation of depth-limited wave breaking criteria, *Proc. of 2nd Int. Symposium on Ocean Wave Measurement and Analysis*, New Orleans, 180-193.

Kamphuis, J. W. (1991). Alongshore sediment transport rate. *Journal of Waterways, Port, Coastal and Ocean Engineering, ASCE, 117(6),* 624-641.

Kamphuis, J.W. (2002). Alongshore Transport Rate of Sand. In *Proceedings of 28th ICCE*, 2478-2490. Cardiff.

Komar, P. D., and Inman, D. L. (1970). Longshore sand transport on beaches. *Journal of Geophysical Research 75(30),* 5514-5527.

Komen, G. J., Cavaleri, L., Donelan, M., Hasselmann, K., Hasselmann, S., & Janssen, P. A. E. M. (1996). *Dynamics and modelling of ocean waves*. Cambridge University Press.

References

Kraus, N. C., Isobe, M., Igarashi, H., Sasaki, T. O., and Horikawa, K. (1982). Field experiments on longshore transport in the surf zone. *Proceedings of 18th International Conference on Coastal Engineering, ASCE,* 969-988. New York.

Life in the Gaza Strip. (2014). Retrieved April 29, 2016, from http://www.bbc.com/news/world-middle-east-20415675

Lilly, D. K. (1989). The length scale for sub-grid-scale parameterization with anisotropic resolution. *In Annual Research Briefs, 1,* 3-9.

Longuet-Higgins, M. S., & Stewart, R. W. (1964). August. Radiation stresses in water waves; a physical discussion, with applications. In *Deep Sea Research and Oceanographic Abstracts, 11(4),* 529-562.

Meyer-Peter, E., & Müller, R. (1948). Formulas for bed-load transport. In *Proceedings of the 2nd Meeting of the International Association for Hydraulic Structures Research,* 39-64.

Miche, M. (1944). Mouvements Ondulatories de la Mer en Profondeur Constante ou Décroissante, Ann. Ponts Chauss., 25-28,131-164,270-292 and 369-406.

Miedema, S. (2015). *Introduction Dredging Engineering.* VSSD, Delft, The Netherlands.

Miller, H. C. (1999). Field measurements of longshore sediment transport during storms. *Coastal Engineering, 36,* 301-321.

Nielsen, P. (1979). *Some basic concepts of wave sediment transport*. Kongens Lyngby, Denmark: Technical University of Denmark.

Nikuradse, J. (1933). *Laws of flow in rough pipes.* VDI Forschungsheft, 361.

Palestinian National Authority, Ministry of Environmental Affairs. (2001). *Gaza Coastal and Marine Environmental Protection and Management Action Plan.*

Perlin, A. and E. Kit. (1999). Alongshore sediment transport on Mediterranean coast of Israel. *Journal of waterway, port, coastal, and ocean engineering, 125(2),* 81-83.

Rottner, J. (1959). A formula for bed-load transportation. *Houille Blanche, 14 (3),* 285–307.

Ruessink, B.G., D.J.R. Walstra, and H.N. Southgate. (2003). Calibration and verification of a parametric wave model on barred beaches. *Coastal Eng*., 48, 139-149.

Shields, A. (1936). *Application of Similarity Principles and Turbulence Research to Bedload Movement,* California Institute of Technology, Pasadena (translated from German).

Shore Protection Manual. (1984). U.S. Army Engineer Waterways Experiment Station, 4th Ed., U.S. Government Printing Office, Washington, D.C.

Smagorinsky, J. (1963). General circulation experiments with the primitive equations: i. The basic experiment. *Monthly weather review, 91*(3), 99-164.

Smaling, D. (1996). *Gaza Sea Port* (Master's thesis). Delft University of Technology.

References

Soulsby, R.L (1997). *Dynamics of Marine Sands. Thomas Telford, London, 249.*

Tide Times for Ashkelon. (2016). Retrieved July 05, 2016, from http://www.tide-forecast.com/locations/Ashkelon/tides/latest

Van Rijn, L. C. (1984). Sediment transport, part I: bed load transport. *Journal of hydraulic engineering*, *110*(10), 1431-1456.

Wang, P., Ebersole, B. A., and Smith, E. R. (2002). Longshore sand transport – initial results from large-scale sediment transport facility. ERDC/CHL CHETNII-46, U.S. Army Engineer Research and Development, enter, Vicksburg, MS. http://chl.erdc.usace.army.mil/

Ward, K. (2014). *A Prospected Study for Development of Berths Facility Services (Loading and Unloading) Of Gaza Seaport Using Simulation Techniques* (Master's thesis). Islamic University-Gaza.

Wright L.D and Thom G. (1977). Coastal depositional landforms: a morphodynamic approach. *Progress in Physical Geography 1*, 412-159.

ZVIELY, D. and KLEIN, M. (2003). The environmental impact of the Gaza Strip coastal constructions. *Journal of Coastal Research*, 19(4), 1122-1127. West Palm Beach (Florida), ISSN' 0749-0208.

Zyserman, J.A. and Fredsøe, J. (1992). *Inclusion of the Effect of Graded Sediment in a Deterministic Sediment Transport Model*. MAST G6M-Coastal Morphodynamics Final Workshop, Abstracts-in-depth. Pisa, Italy.